2016

# Development And Application Of Foraminiferal Carbonate System Proxies To Quantify Ocean Acidification In The California Current

Emily B. Osborne
*University of South Carolina*

# Development and Application of Foraminiferal Carbonate System Proxies to Quantify Ocean Acidification in the California Current

by

Emily B. Osborne

Bachelor of Science
College of Charleston, 2012

---

Submitted in Partial Fulfillment of the Requirements

For the Degree of Doctor of Philosophy in

Marine Science

College of Arts and Sciences

University of South Carolina

2016

Accepted by:

Robert C. Thunell, Major Professor

Claudia Benitez-Nelson, Committee Member

Michael Bizimis, Committee Member

Howie D. Scher, Committee Member

Leslie R. Sautter, Committee Member

Cheryl L. Addy, Vice Provost and Dean of the Graduate School

# DEDICATION

I dedicate my dissertation to a group of people who have unconditionally loved and supported me throughout this process and throughout my life. Tim for being so loving and patient while making me feel like the coolest gal in the universe. I'm so glad you found me in that introductory geology lab at CofC. My dad, for being my first teacher and inspiring my scientific curiosity at a young age. Let's make the world a better place in which to live, together! My mom for being the most patient listener and for always being eager to learn more about my scientific world. Your love for me is unparalleled and keeps me in constant awe of you. My big sister, Whitney, for always making me laugh and living in an alternate Osborne sister universe with me. Without each of you, this work would not have been possible.

# ACKNOWLEDGEMENTS

First and foremost, I have to acknowledge my *fantastic* advisor, Bob Thunell. It has been such an honor and pleasure being your student. You have helped me grow so much as a scientist, writer and individual. I am so lucky that you chose me to be part of your lab. Also, thank you for trying to teach me the English language and usually making me laugh/cry in the process. Accordingly, I have to also thank my amazing undergraduate advisor who gently guided me into the world of forams and encouraged me to follow in her footsteps at USC, Leslie "Doc" Sautter. A HUGE thanks to my amazing officemates who have become close friends, Natalie Umling, Brittney Marshall and Dominika Wojcieszek (and Jessica Holm as an honorary officemate) for making the last 4.5 years so much fun. Having you gals in the office and traveling all over the world with you guys has made for some amazing and lasting memories. I love you girls! An extra special shout out to Gnat, aka. my school wife, I could not have maintained sanity without you. Also thank you to all of the many, amazing graduate school friends who have come and gone during my time and USC you all made this process so much more fun! A special thank you to Wayne Buckley for spending many chilly hours with me in the CEMS lab, teaching me to be an analytical chemist. Of course, the chemistry would not have been possible without the huge help from Michael Bizimis. And last but not least, thank you to Eric Tappa, the omniscient one of the MSRL lab. I don't know what the lab (or I) would do without you.

# ABSTRACT

The oceanic uptake of anthropogenic carbon has mitigated climate change, but has also resulted in a global average 0.1 decline in surface ocean pH over 20$^{th}$ century known as ocean acidification. The parallel reduction in carbonate ion concentration ([$CO_3^{2-}$]) and the saturation state of seawater ($\Omega$) has caused many major calcium carbonate-secreting organisms such as planktonic foraminifera to exhibit impaired calcification. We develop proxy calibrations and down core records that use calcification and geochemical characteristics of planktonic foraminifera as proxies for the marine carbonate system. This study focuses specifically on the surface ocean chemistry of the California Current Ecosystem (CCE), which has been identified as a region of rapidly progressing ocean acidification due to natural upwelling processes and the low buffering capacity of these waters. The calibration portion of this study uses marine sediments collected by the Santa Barbara Basin (SBB), California sediment-trapping program located in the central region of the CCE. We calibrate the relationships of *Globigerina bulloides* calcification intensity to [$CO_3^{2-}$] and the B/Ca ratios of *G. bulloides*, *Neogloboquadrina dutertrei* and *Neogloboquadrina incompta* shells to $\Omega$ calcite using *in situ* measurements and model simulations of these independent variables. By applying these proxy methods to down core, our records from the SBB indicate a 20% reduction in foraminiferal calcification since ~1900, translating to a 35% decline in [$CO_3^{2-}$] in the CCE over this period. Our high-resolution calcification record also reveals a substantial interannual to decadal modulation of ocean acidification in the CCE related to the sign of Pacific Decadal

Oscillation and El Niño Southern Oscillation. In the future we can expect these climatic modes to both enhance and moderate anthropogenic ocean acidification. Based on our historic record, we predict that if atmospheric $CO_2$ reaches 540 ppm by the year 2100 as predicted by a conservative $CO_3$ pathway, $[CO_3^{2-}]$ will experience a net reduction of 55%, resulting in at least a 30% reduction in calcification of planktonic foraminifera that will likely be mirrored by other adversely affected marine calcifiers.

# TABLE OF CONTENTS

# LIST OF TABLES

# LIST OF FIGURES

# CHAPTER 1

## CALCIFICATION OF THE PLANKTONIC FORAMINIFERA *GLOBIGERINA BULLOIDES* AND CARBONATE ION CONCENTRATION: RESULTS FROM THE SANTA BARBARA BASIN[1]

[1] Osborne, E.B., Thunell, R.C., Marshall, B.J., Holm, J.A., Tappa, E.J., Benitez-Nelson, C., Cai, W-J. and Chen, B. (2016), *Paleoceanography* 31, doi:10.1002/2016PA002933. Reprinted with permission of publisher.

## 1.1 ABSTRACT

Planktonic foraminiferal calcification intensity, reflected by shell wall thickness, has been hypothesized to covary with the carbonate chemistry of seawater. Here we use both sediment trap and box core samples from the Santa Barbara Basin to evaluate the relationship between the calcification intensity of the planktonic foraminifera species *Globigerina bulloides*, measured by area density (μg/μm$^2$), and the carbonate ion concentration of seawater ([$CO_3^{2-}$]). We also evaluate the influence of both temperature and nutrient concentration ([$PO_4^{3-}$]) on foraminiferal calcification and growth. The presence of two *G. bulloides* morphospecies with systematically different calcification properties and offset stable isotopic compositions were identified within sampling populations using distinguishing morphometric characteristics. The calcification temperature and by extension calcification depth of the more abundant "normal" *G. bulloides* morphospecies was determined using $\delta^{18}O$ temperature estimates. Calcification depths vary seasonally with upwelling and were used to select the appropriate [$CO_3^{2-}$], temperature and [$PO_4^{3-}$] depth measurements for comparison with area density. Seasonal upwelling in the study region also results in collinearity between independent variables complicating a straightforward statistical analysis. To address this issue, we use additional statistical diagnostics and a down core record to disentangle the respective roles of each parameter on *G. bulloides* calcification. Our results indicate that [$CO_3^{2-}$] is the primary variable controlling calcification intensity while temperature influences shell size. We report a modern calibration for the normal *G. bulloides* morphospecies that can be used in down core studies of well preserved sediments to estimate past [$CO_3^{2-}$].

## 1.2 INTRODUCTION

Planktonic foraminifera are ubiquitous microzooplankton that secrete calcium carbonate ($CaCO_3$) shells that comprise up to 80% of the calcite preserved in seafloor sediments [*Schiebel,* 2002]. Fossil shells of foraminifera preserved in marine sediments have been used for a wide variety of paleoclimate applications that have greatly enhanced our understanding of past oceanic and climatic conditions. Due to the relatively short life span of planktonic foraminifera (~ 1 month), their shells represent a brief snapshot of surface ocean conditions during their time of calcification [*Bé,* 1977]. It is generally accepted that surface ocean carbonate ion concentration ($[CO_3^{2-}]$) plays a key role in the calcification of planktonic foraminifera with the level of response varying among species [e.g., *Spero et al*., 1997; *Bijma et al*., 1999, 2002; *Barker and Elderfield,* 2002; *Mekik and Raterink,* 2008; *Moy et al.,* 2009; *Marshall et al.,* 2013]. The calcification intensity of planktonic foraminifera, or the amount of calcite deposited relative to shell size, reflects both the efficiency (effort to precipitate calcite under varying environmental conditions) and rate (how much calcite is added over time) of calcification during an individual's lifespan [*Weinkauf et al.,* 2016]. Calcification intensity of fossil foraminiferal shells can be estimated using morphometric characteristics such as weight, size and area.

Initial morphometric observations of shells grown in culture and their relationship to carbonate chemistry indicate that the species *Orbulina universa* produced a 37% higher shell mass at elevated $[CO_3^{2-}]$ (600 μmol $kg^{-1}$) relative to that of individuals grown in ambient seawater $[CO_3^{2-}]$ (170 μmol $kg^{-1}$) [*Spero et al.* 1997; *Bijima et al.,* 1999, 2002]. Subsequently, *Barker and Elderfield* [2002] found that the size-normalized shell

weights (SNSW), which are more reflective of shell thickness rather than size, from a series of core-top samples varied systematically with latitude. The authors found that SNSW decreased with increasing latitude due increased $CO_2$ solubility and declining [$CO_3^{2-}$] associated with decreasing temperature *[Barker and Elderfield*, 2002]. A down core study in the Southern Ocean observed that SNSW of post-industrial-age foraminiferal shells from surface sediments were 35% lower than Holocene-age shells and attributed this difference to increasing anthropogenic $CO_2$ and declining [$CO_3^{2-}$] during the last two centuries [*Moy et al*., 2009]. A recent sediment trap study highlighted the importance of the shell weight size-normalization technique and described a new size-normalization method, area density, which resulted in a highly significant relationship with [$CO_3^{2-}$] for two species of tropical planktonic foraminifera [*Marshall et al.,* 2013].

While considerable effort has gone into developing foraminiferal geochemical proxies for carbonate system variables [e.g., *Sanyal et al.,* 1996; *Yu et al.,* 2007; *Foster et al.,* 2008; *Henehan et al.,* 2013; *Rae et al.,* 2011; *Allen et al.,* 2011, 2012], relatively less emphasis has been placed on developing morphometric-based techniques [e.g., *Spero et al.,* 1997; *Bijma et al.,* 1999, 2002; *Barker and Elderfield,* 2002; *Marshall et al.,* 2013]. In this regard, SNSW estimates of foraminiferal calcification intensity have great potential for serving as a quantitative measure for past [$CO_3^{2-}$]. SNSW analyses also require minimal analytical instrumentation and therefore can easily be measured in many laboratories. Because SNSW measurements are non-destructive, foraminifera used for this purpose can be used for geochemical analyses, thus providing tandem proxy records on a single sample population.

The development of proxy methods for estimating carbonate system parameters is needed since observational records are limited to the last 20-30 years [e.g. *Takahashi et al.,* 1982; *Bates et al.,* 2014]. Such methods could provide an indirect means for estimating how marine calcifiers and the marine carbonate system have responded to carbon perturbations on both short (decadal to century) and long time-scales (millennial). These records would be instrumental in understanding how the marine carbonate system will respond to future increases in ocean acidification associated with various projected $CO_2$ scenarios. This study establishes a means to reconstruct past [$CO_3^{2-}$] by providing an empirical relationship between *Globigerina bulloides* calcification intensity and ambient [$CO_3^{2-}$] that can be applied to well-preserved marine sediments.

### 1.2.1 Variables Influencing Growth and Calcification

The calcification and growth of planktonic foraminifera have been linked not only to seawater [$CO_3^{2-}$], but also to variables such as temperature and nutrient concentration [e.g. *Bé et al.,* 1973; *Spero et al.,* 1997; *Aldridge et al.,* 2012]. It has been suggested that a unique combination of these factors comprises a species-specific set of "optimal growth" conditions that result in a stress-induced, reduced calcification response when these environmental conditions are not satisfied [*de Villers et al.,* 2004]. However, several tests of the optimal growth hypothesis failed to find a link between either the absolute abundance of a given species, which would hypothetically occur under that species' optimal growth conditions, or the calcification intensity of those individuals [*Beer et al.,* 2010; *Weinkauf et al.,* 2013; *Weinkauf et al.,* 2016]. Rather, a study using Mediterranean sediment samples indicated that the calcification of four species of planktonic foraminifera responded passively to changes in seawater properties, such as

[$CO_3^{2-}$], as opposed to a physiologic response brought about by stress from unfavorable conditions [*Weinkauf et al.,* 2013]. Despite being unable to identify the specific environmental factors that controlled calcification response for each of these species, the results of this work were consistent with carbonate chemistry being the primary control on calcification [*Weinkauf et al.,* 2013]. Furthermore, another study evaluated foraminiferal calcification change over a deglaciation (Marine Isotope Stages 6-7) and noted that *Globigerinoides ruber* and *G. bulloides* showed very similar calcification responses despite having very different ecological requirements and therefore optimal growth conditions. Rather, these changes were linked to $pCO_2$ and the carbonate saturation of seawater [*Gonzalez-Mora et al.,* 2008].

Temperature has been cited as a control of foraminiferal shell size, with larger shells growing in warmer waters [*Bé et al.,* 1973; *Hecht,* 1976; *Schmidt et al.,* 2004; *Lombard et al.,* 2009], where [$CO_3^{2-}$] is also generally high. In order to differentiate the influence of these variables, a culture study by *Lombard et al.* [2010] maintained constant temperature and varied [$CO_3^{2-}$], and observed that foraminifera (*Orbulina universa* and *Globigerinoides sacculifer*) had a significant increase in shell weight with no significant change in shell size in response to elevated [$CO_3^{2-}$]. This result corroborated earlier observations of lower SNSW associated with the Holocene relative to SNSW during the Last Glacial Maximum when temperatures were colder and [$CO_3^{2-}$] was higher [*Barker and Elderfield,* 2002]. While previous results indicate that [$CO_3^{2-}$] is the predominant factor controlling calcification intensity, some research has suggested that temperature does perhaps play an important role in calcification rate, which is inherently related to calcification intensity. A study of eight modern planktonic foraminifera species found

that increased temperature resulted in an increase in calcification rate across all species [*Lombard et al.,* 2009]. *de Villers* [2004] also concluded that optimum temperatures were an important factor in foraminiferal calcification rates measured by SNSW. Contrary results from a culturing study by *Manno et al.* [2012] indicated that increased temperature resulted in no net change in *Neogloboquadrina pachyderma* (sinistral) calcification rate. Rather, this study found that a decline in pH, and by extension [$CO_3^{2-}$], resulted in a significant decline in calcification rate even in cultures where temperature was elevated simultaneously.

Due to the fact that previous results indicate that shell size is influenced by temperature, size-normalization of shell weights is essential for creating a metric that best constrains calcification intensity [e.g. *Barker and Elderfield,* 2002; *Lombard et al.,* 2010; *Beer et al.,* 2010]. Sieve-based weights (SBW), measurement-based weights (MBW) and area density (AD) are examples of such methods. SBW measurements are made on a narrow size-range (~50 µm) by sieving and measuring the mean weight of a pool of individuals to calculate an average weight for the sample population [*Broecker and Clark,* 2001]. MBW more effectively accounts for shell size by normalizing sieve-based weights with a mean diameter or silhouette area parameter [*Barker and Elderfield,* 2002]. However, both of these size-normalizing methods are confined to examination of a narrow size-fraction of sediments, thereby potentially limiting the number of individuals available for analysis [see *Marshall et al.,* 2013 for a review]. Area density overcomes this limitation by using an individual rather than a population approach, allowing for a broad size-fraction to be used and maximizing the number of individuals available per sample [*Marshall et al.,* 2013]. The area density method uses an individual weight and

silhouette area measured for each shell and normalizes individual weights prior to taking the population mean. Although time consuming, the area density method effectively captures the intrinsic natural variability of biological samples, particularly at the individual level that would otherwise be lost when measuring bulk weights. Furthermore, since there is no size-fraction restriction for the AD method, a larger number of individuals is typically available for analysis, thus generating a more robust estimate of the sample population. Importantly, the area density method has also proven to be the most effective size-normalization technique, which is important in calcification intensity studies such as this one [*Beer et al.,* 2010b; *Marshall et al.,* 2013].

While temperature and [$CO_3^{2-}$] have been the primary variables considered in foraminiferal calcification studies, some research indicates that nutrient concentration may also influence foraminiferal calcification. A North Atlantic study of the species *G. bulloides* suggests that high concentrations of nitrate ($NO_3^-$) and phosphate ($PO_4^{3-}$) have adverse effects on calcification of this species [*Aldridge et al.,* 2012]. Previous research on corals and coccolithophores has observed a decline in calcification as a result of high nutrient concentrations, which is attributed to adsorption of calcium hydrogen phosphate ($CaHPO_4$) onto the calcite surface blocking growth cites for crystallization [*Kinsey and Davies,* 1979; *Paasche and Brubank,* 1994; *Lin and Singer,* 2006]. Conversely, the results of a sediment trap study in the Cariaco Basin (Venezuela) indicate that nutrients are not a key factor controlling calcification intensity of two planktonic foraminiferal species (*G. ruber* and *G. sacculifer*) and that covariation between [$CO_3^{2-}$] and nutrient concentrations can result in spurious correlations between foraminiferal calcification intensity and nutrient concentration [*Marshall et al.,* 2013].

## 1.3 Regional Setting: The Santa Barbara Basin

This study utilizes *G. bulloides* shells preserved in marine sediments (both sediment trap and sediment core) and hydrographic data collected off the California Margin in the Santa Barbara Basin (SBB). *Globigerina bulloides* is a species that often dominates the foraminiferal flux in the SBB [*Kincaid et al.,* 2000] and has been used commonly in down-core paleoceanographic reconstructions for this basin [e.g. *Hendy and Kennett,* 1999; *Friddell et al.,* 2003; *Pak et al.,* 2004; *Pak et al.,* 2012]. It is a symbiont-barren spinose foraminifera found in transitional to subpolar waters and is frequently found in association with upwelling regimes [*Bé et al.,* 1977; *Hemleben et al.,* 1989].

The SBB is an approximately 100 km long, ~600 m deep east-west trending basin extending from Point Conception to the greater Los Angeles area (Figure 1). There are north and south bounding continental shelves, with the Channel Islands forming the southern bound of the basin. Sills at the eastern and western mouths of the basin (200 meters and 400 meters, respectively) restrict water exchange between the basin and the open ocean. Limited influx of oxygenated water coupled with high productivity rates result in anoxic conditions in the deepest part of the basin producing ideal conditions for the preservation of annually laminated or varved sediments [*Reimers et al.,* 1990; *Thunell et al.,* 1995]. Prevailing southward winds result in Ekman-induced upwelling in the basin that typically peaks during the spring to early summer months and relaxes during the fall and winter [*Hendershot and Wiant,* 1996]. Seasonal upwelling produces a wide range of [$CO_3^{2-}$], temperature and nutrient values, making this an ideal setting for examining the influence of each of these variables on calcification (Supporting information Figure S1).

## 1.4 Materials and Methods

### 1.4.1 Sediment Trap and Sediment Core Samples

The University of South Carolina has maintained a sediment trap time-series in the deepest portion of the SBB (34˚14'N, 120˚02'W, ~580 m water depth; Figure 1) from 1993-present [*Thunell; et al.,* 1995, 2007; *Thunell,* 1998]. McLean Mark VII-W automated sediment traps equipped with 0.5 $m^2$ funnel openings are deployed for 6-month periods and samples are collected continuously on a bi-weekly basis. Sample bottles are buffered and poisoned with a sodium azide solution prior to deployment. Sediment samples are split using a McLean four-head rotary splitter and usually refrigerated in sodium borate buffered deionized water to prevent dissolution of carbonates prior to sample use. This study utilizes sediment trap material collected from 2007-2010, a period when water column carbonate system variables were measured on water samples collected near the SBB sediment trap mooring by the Plumes and Blooms Program.

Additionally, a 0.5 meter box-core collected in 2012 near the sediment trap mooring (34˚13'N, 119˚58'W, 580 m water depth; Figure 1) was used to supplement our sediment trap observations. Radiogenic isotopes of lead ($^{210}$Pb) and cesium ($^{137}$Cs) were used to develop an age model for the box-core (Supporting information Text 1) using a high purity germanium well detector [*Moore,* 1984]. Radioisotope activities indicate an average sedimentation rate of 0.43 cm $yr^{-1}$; and an average mass accumulation rate of 5.84 g $cm^2$ $yr^{-1}$ (Supporting information Figure S2). Using these age constrains we

estimate that the 0.5 meter core extends back to ~1895 and the uppermost sediments contained in the core represent the year ~2006.

A 1/16 split of each sediment trap sample and roughly 3 grams of box-core sediment were used for foraminiferal analyses; if insufficient material was available from the sediment trap sample an additional 1/16 split was used. Despite the high organic matter content typically found in sediment trap samples, previous tests demonstrated that an oxidative treatment of the samples (buffered 30% $H_2O_2$ for 45 min) yielded statistically identical area density values to that of untreated samples [*Marshall et al.* 2013]. Therefore it was deemed unnecessary to oxidatively clean sediment trap samples prior to area density analysis. Both trap and core sediments were washed using borate buffered deionized water through a 125 μm sieve and dried in a 40˚C oven prior to analyses.

### 1.4.2 Hydrographic Measurements

Monthly hydrographic measurements are made along a transect in the SBB by the Plumes and Blooms Program (http://www.icess.ucsb.edu/PnB/PnB.html), with one of the sampling stations (Station 4; 34˚15'N, 119˚54'W) located adjacent to the sediment trap mooring (Figure 1). From 2007-2010 total alkalinity (TA) and total dissolved inorganic carbon (DIC) measurements were also made at Station 4 on 25 monthly cruises that took place over a 40 month period (Supporting Information Text S2). Water samples used for TA and DIC analyses were collected at depths of 0, 5, 10, 20, 30, 50, 75, 100, 150, and 200 meters.

The CO2Sys program (Version 2.1) originally by Lewis and Wallace [1998]

(CO2SYS.BAS) and modified by *Pierrot et al.* [2006] was used to estimate unknown seawater marine carbonate system variables. This program uses two "master" carbonate system variables (TA, DIC, pH and $pCO_2$) to estimate the remaining unknown variables at a set of given input conditions (e.g. temperature, salinity and pressure). For the time period associated with the sediment trap samples (2007-2010), [$CO_3^{2-}$] is estimated using *in situ* measurements of TA and DIC from the SBB. Supplementary CTD and bottle data from Plumes & Blooms Station 4 including salinity, temperature, pressure, phosphate concentration ([$PO_4$]) and silicate concentration ([$SiO_4$]) are used as input conditions for these calculations. For the sediment core portion of the study, $pCO_2$ and TA are used as mater variables. We assume a constant TA of 2250 µmol $kg^{-1}$ based on the mean measured surface TA measured in the SBB from 2007-2010. Seawater $pCO_2$ is derived according to Henry's Law using atmospheric $CO_2$ measurements from the Mauna Loa Time-Series [1960-present; http://www.esrl.noaa.gov/gmd/ccgg/trends/]/] and temperature, salinity and pressure dependent solubility coefficients ($K_0$) following the formulation of *Weiss* [1974]. Measured sea surface temperature from the SBB (1955-present; 34° 24.2' N, 119° 41.6' W") and salinity from the Scripps Pier (1916-present; 32° 52.0′ N, 117° 15.5′ W) measured as a part of the Shore Stations Program (http://shorestations.ucsd.edu/shore-stations-data/) were used to determine time-specific $K_0$ values and as input conditions for our down core calculations. The dissociation constants ($K_1$ and $K_2$) determined by *Mehrbach et al.* [1973] and refit to the seawater scale by *Dickson and Millero* [1987] were used as constants for our CO2Sys carbonate system calculations. The $HSO_4$ and $B(OH)_3$ dissociation constant ($K_{SO4}$ and $K_B$, respectively) according to *Dickson et al.* [1990] and the boron concentration and

chlorinity relationship determined by *Lee et al.* [2010] were used for our calculations

### 1.4.3 Area-Normalized Shells Weights: The Area Density Method

A total of 82 sediment samples (39 sediment trap and 43 sediment core) are included in our area density analysis. We use a combination of upper and lower sediment trap samples ($n$=32) that coincide with the 25 TA and DIC sampling periods (2007-2010) for our modern area density sediment trap calibration (Table 1.1). Lower trap samples (~450 m depth) were available for 22 of the 25 carbonate chemistry sampling periods, while upper trap samples (~150 m depth) were available for ten of these periods. The upper sediment trap was added to the SBB sediment trap mooring in 2009 allowing for both upper and lower sediment trap samples to be analyzed for eight of the TA and DIC sampling periods. An additional 7 sediment trap samples from months when no water column carbonate chemistry data is available were analyzed to produce a full annual-cycle of area density measurements from December 2009-December 2010.

*Globigerina bulloides* shells were systematically picked from the >125 µm size fraction of each sediment sample using a gridded tray. The >125 µm size fraction was chosen because *G. bulloides* smaller than this range likely represent individuals that have not reached the adult stage [*Berger,* 1971; *Peeters et al.*, 1999]. On average shell diameters from sediment trap and core samples range from 200-400 µm in size. Atypical *G. bulloides* shells with abnormally large and thin final chambers or individuals with over-sized apertures where the final chamber is not fully sutured to the test were excluded from our analyses due to the effect these morphologic features have on shell area. Careful

attention was paid to selecting individuals that were free of visible clay particles or organic matter that could potentially bias shell weights.

SNSW was measured using the area density method described in detail by *Marshall et al.* [2013]. Following this method, individual shells were weighed in a copper weigh boat using a high precision microbalance (Mettler Toledo XP2U; ±0.43 µg) in an environmentally controlled weigh room and then photographed umbilical side up using a binocular microscope (Zeiss Stemi 2000-C) fitted with a camera (Point Grey Research Flea3 1394b). Photos were uploaded to a microscopic imaging program (Orbicule Macnification 2.0) to measure the length of the longest shell diameter (Feret diameter) and the 2-D surface area or silhouette area of each shell. This program uses RGB images to calculate a region of interest by outlining the imaged shell to estimate a pixel 2-D area. Pixel measurements are converted to lengths (µm) and areas ($\mu m^2$) by calibrating an image of a 1 mm microscale taken at the same magnification and working distance as shell photos. Individual weights were then divided by their corresponding areas and the mean area density value was calculated for each sample population (equation 1). Mean area density values are most representative of the population calcification intensity and by extension ambient calcification conditions, and were the focus of our calibration and statistical analyses. Ideally 40 individuals were included in each sample population in order to minimize measurement standard error ($SE = \sigma/\sqrt{n}$). Due to the asymptotic nature of area density standard error, we would argue that a sample size of 30-40 individuals represents a high level of confidence (Supporting information Figure S3).

$$\textit{Area Density}\ (\mu g/\mu m^2) = \textit{Individual Weight}\ (\mu g)/\textit{Individual Area}\ (\mu m^2) \qquad (1)$$

### 1.4.4 Stable Isotope Analysis

Approximately 70µg (15-30 individuals) of *G. bulloides* from each sample used for area density analyses were pooled to measure $\delta^{18}O$ (Table 1.2). The foraminifera were cleaned for 30 minutes in 3% $H_2O_2$ followed by a brief sonication and acetone rinse. Isotopic analyses were carried out on an Isoprime isotope ratio mass spectrometer equipped with a carbonate preparation system. The long-term standard reproducibility is 0.07‰ for $\delta^{18}O$. Results are reported relative to Vienna Pee Dee Belemnite (V-PDB). Because the $\delta^{18}O$ of foraminifera reflects both seawater temperature and the $\delta^{18}O$ of seawater ($\delta^{18}O_w$), accounting for any variations in $\delta^{18}O_w$ is essential to properly estimating temperature. The $\delta^{18}O_w$ varies as a function of salinity and therefore a $\delta^{18}O$:salinity relationship typically is used to determine $\delta^{18}O_w$; here we use a $\delta^{18}O$:salinity relationship that was determined specifically for the Southern California Bight (equation 2). Measured sea surface salinity from Plumes and Blooms (Station 4) and the SIO Pier time-series (1916-Present) are used, respectively, for sediment trap and sediment core estimates of $\delta^{18}O_w$. The use of measured surface salinity as opposed to assuming constant salinity for the down core record was particularly important in calculating $\delta^{18}O_w$ and the resulting temperature estimates. Scaling to V-PDB from Standard Mean Ocean Water (SMOW) of estimated $\delta^{18}O_w$ was done by subtracting 0.27‰ [*Hut, 1987*]. $\delta^{18}O$ calcification temperatures were calculated using a culture-derived temperature relationship (equation 3) developed within the Southern California Bight region for *G. bulloides* (12-chambered shells) [*Bemis et al.*,1998].

$$\delta^{18}O_{water} = 0.39 * (\text{Salinity}) - 13.23 \quad (2)$$

$$T(^{\circ}C) = 13.2 - 4.89 * (\delta^{18}O_{calcite} - \delta^{18}O_{water}) \quad (3)$$

## 1.5 Results and Discussion

### 1.5.1 Comparison of Sediment Trap and Sediment Core Area Density Measurements

Assessing the potential for dissolution of foraminiferal shells within the water column and on the seafloor is of utmost importance when using foraminiferal shell weights as a water column proxy. For a total of eight sampling periods from 2009-2010, samples from both trap depths were available for area density analysis and are used to assess similarities and differences of area density and morphometric measurements recorded at each sampling depth. A comparison of measurements from each depth was used to determine if dissolution impacts foraminiferal shells as they settle through the water column and a comparison of sediment trap and sediment core measurements is used to assess the potential for seafloor dissolution.

Observations by *Milliman et al.* [1999] suggest that 60-80% of $CaCO_3$ particles dissolve in the upper 500-1,000 m of the water column despite being well above the lysocline. The mechanism driving water column dissolution is not well understood and has not been replicated by either *in situ* [*Thunell et al.*, 1981] or modeling studies [*Jansen et al.*, 2002]. Estimates for the Pacific Ocean north of 20˚N indicate that the depth of the calcite saturation horizon can range from 200 to 1000 meters with a mean of 600 meters water depth (Feely et al., 2004). Water column measurements of TA and DIC from 2007-2010 in the SBB were used to assess calcite saturation. Although water column measurements are limited to 0-400 meters, these data indicate supersaturated values

(1.25) at 400 meters and suggest that supersaturation also exists at the basin bottom (600 meters water depth; Supporting information Figure S4). The preservation of unfragmented assemblages of foraminifera and the occasional presence of aragonite thecosome pteropods that are highly susceptible to dissolution are physical evidence that preservation of calcite in the SBB is not an issue. Shell features that are typically used as indicators of dissolution, such as reduced spine bases and formation of cracks [*Dittert and Henrich,* 2000], are not observed in trap or core sediments.

For the eight sampling periods where both upper and lower trap samples were measured, the mean area density values determined for each depth are within two standard errors of each other (Figure 2). Independent t-tests indicate that there is no significant difference in the area density population means for six of eight sampling periods ($p$ 2-tail >0.05), while there is a moderately different sample mean recorded for a single sampling period ($p$ 2-tail= 0.02; 9/25/09) and a significant different sample mean for one sampling period ($p$ 2-tail <0.001; 10/8/10). These results indicate that generally there is no difference in area density between the two sampling depths suggesting that there is no significant dissolution occurring within the SBB water column.

We also compare shell weights, diameters and area densities between the sediment trap and the seafloor sediments to assess post-depositional dissolution. If significant dissolution is occurring on the seafloor in SBB we would expect to see differences in shell morphometric characteristics in the sediment trap samples versus the seafloor samples. While the lack of temporal overlap between sediment trap (2007 to 2010) and down core measurements (1985-2005) is not ideal for such a comparison, measurements from each of these populations indicate a similar range in weight and size.

Independent t-tests were conducted to statistically determine if the weight, diameter and area density of shells collected by the trap and in the core are significantly different. These results indicate there is no significant difference in shell size preserved in trap and seafloor sediments ($p$ >0.05). However, there is a moderately significant difference in shell weight ($p$ >0.01) and highly significant difference in area density ($p$ <0.001). The results of this comparison indicate that overall higher weights and area density values are observed in core sediments relative to trap sediments. We attribute these offsets to higher [$CO_3^{2-}$] and increased calcification intensity over the 100-year down core sampling period relative to the more recent sediment trap sampling period (See section 4.6 for discussion on [$CO_3^{2-}$] change over this interval).

### 1.5.2 *GLOBIGERINA BULLOIDES* MORPHOSPECIES

Studies of *G. bulloides* small subunit ribosomal RNA (SSU rRNA) indicate high cryptic diversity with a total of seven distinct genotypes [*Darling et al.,* 2008]. Genetic studies of *G. bulloides* from the SBB and the greater Southern California Bight have identified the presence of two of these genotypes that represent two distinct morphospecies [*Darling et al.,* 2000]. The most dominant genotype, IId, is found in abundance throughout the year, while a rare genotype, IIa, that is found commonly at high latitudes, is present during cool periods in the SBB [*Darling et al*., 1999; *Darling et al.,* 2000; *Darling et al.,* 2003]. It was speculated that the IIa individuals were a heavily calcified *G. bulloides* morphotype that has previously been observed in the Southern California Bight [*Darling et al*., 2003]. *Sautter and Thunell* [1991] first identified a heavily calcified "encrusted" morphotype of *G. bulloides* that is enriched in $^{18}O$ during peak upwelling (April) in the San Pedro Basin, located just south of the SBB. *Hendy and*

*Kennett* [2000] also identified an abundant small and thickly calcified *G. bulloides* morphotype in glacial sediments from the SBB. Bemis *et al.* [2002] applied a $\delta^{18}O$ temperature relationship derived for normal *G. bulloides* to these encrusted glacial specimens and found that they yielded unreasonably cold temperature estimates.

Due to the fact that species- and morphospecies-specific calcification responses have been documented in foraminifera, it is important to determine if more than one *G. bulloides* morphospecies exists in our sample populations and if these morphospecies calcify differently. Since both genetic observations and isotopic analyses of *G. bulloides* morphospecies within the SBB indicate two distinct forms, it is likely that these morphospecies also calcify differently [*Bemis et al.,* 2002; *Darling et al.,* 2003]. To assess if calcification varies between "encrusted" (IIa) and "normal" *G. bulloides* (IId), we examined weight-area and area density-diameter relationships of individuals included in our study. *Marshall et al*. [2015] demonstrated that cryptic species of *Orbulina universa* can be identified using this technique and highlighted significant differences in calcification between morphospecies in the Cariaco Basin, Venezuela.

If the calcification differs between morphospecies we would expect the slopes and intercepts of their weight-area regressions to be different. We would also expect to see a distinct grouping of morphotype populations when area density is regressed against shell diameter with the encrusted individuals likely plotting in the higher area density range. This assessment indicates that the encrusted *G. bulloides* morphotype is present in our samples and does in fact calcify differently from the normal morphotype. The weight-area relationship of the less abundant encrusted morphotype has a slightly higher intercept and a steeper slope (Supporting information Figure S5). Encrusted individuals

identified by our weight-area analyses were also identified using area density-diameter relationships, with the encrusted individuals plotting in the upper area density range. Accordingly, these morphometric relationships were used to identify encrusted individuals and we exclude them from our normal sample populations.

The normal *G. bulloides* morphospecies dominates all sample populations with typically fewer than two encrusted individuals in each sample. However, during winter and peak upwelling periods the abundances of encrusted individuals increase and comprise as much as 15-25% of the *G. bulloides* population. The association of the encrusted *G. bulloides* with cooler conditions is not surprising due to the fact that this genotype is found typically in polar regions [*Darling et al.*, 2003]. For a limited number of samples there were enough individuals of the encrusted form to compare mean area densities between the two morphospecies. The difference between normal and encrusted populations is illustrated by plotting mean area density versus mean size-normalized shell weight (mean sample weight/mean sample diameter) (Figure 3). The encrusted morphospecies consistently have a higher weight and area density range due to the more heavily calcified nature of their shells.

It is important to note that not all encrusted individuals identified by our weight-area analyses were visually distinct using a light microscope. A closer evaluation of surface texture and pore density of the two morphotypes using a scanning electron microscope (SEM) reveals a decreased pore density and more rigid surface structure of encrusted compared to normal *G. bulloides* (Figure 4). While previous studies have suggested that encrusted *G. bulloides* are rare in the Southern California Bight, possibly due to the difficulty of visual distinction between the morphospecies, our results indicate

that this morphospecies is more abundant than previously thought. Frequency distributions of individual morphometric measurements (shell diameter, weight, 2-D area and area density) from the entire sediment trap dataset for normal ($n$ = 1,108) and encrusted ($n$ = 77) *G. bulloides* were used to identify characteristic features of each morphospecies (Supporting information Figure S6). These data indicate that the morphospecies are similarly sized, although encrusted individuals are slightly smaller in terms of diameter and 2-D area and are typically heavier although the ranges in weights between morphospecies overlap making this a non-diagnostic characteristic. The difference in area density distributions between morphospecies is the most diagnostic feature for differentiating the normal and encrusted morphospecies. Based on this assessment, the combination of a weight and size measurement is the best morphological means to confidently differentiate between normal and encrusted *G. bulloides*. This method, as opposed to SEM analyses that require sample coating, is particularly useful if individuals will be used later for geochemical analyses.

### 1.5.3 $\delta^{18}$-O Derived Calcification Depths

Previous sediment trap and plankton tow studies have verified that the $\delta^{18}O$ of *G. bulloides* is a reliable indicator of the seawater temperature at which individuals calcified [*Curry and Matthews,* 1981; *Ganssen and Sarnthein,* 1983; *Kroon and Ganssen,* 1988; *Sautter and Thunell,* 1991b; *Thunell et al.,* 1999]. While we assume that the $\delta^{18}O$ value for multiple shells represents the mean temperature and depth at which each population of individuals calcified, there are limitations to this assumption. Single-specimen $\delta^{18}O$ results have shown that a considerable range of $\delta^{18}O$ can exist within a single sample population and this variability has been attributed to differences in depth habitats,

bioturbation of sedimentary sequences, and possibly vital effects [*Killingley et al.,* 1981; *Ganssen et al.,* 2011]. A statistical assessment by *Schiffelbein and Hills* [1984] examined the relationship between the number of specimens used in a $\delta^{18}O$ analysis and measurement precision, and recommended 20+ individuals for high confidence in bulk $\delta^{18}O$ measurements [*Schiffelbein and Hills*, 1984]. We used on average 20 individuals per $\delta^{18}O$ analysis in order to maximize confidence in our $\delta^{18}O$ values while preserving enough material to duplicate measurements. Another important consideration when using $\delta^{18}O$ to estimate calcification depth is that the $\delta^{18}O$ signature of foraminiferal calcite is a composite representation of various depth/calcification habitats throughout the life cycle of that individual. Although the exact depth habitats and timing of ontogenic stages are not well constrained, it is generally thought that juvenile planktonic foraminifera calcify in shallower water depths and that the majority of foraminiferal calcite is formed at greater depths within the water column during the final adult and terminal life stages [e.g. *Hemleben et al.,* 1989]. Lastly and perhaps most importantly for our study, bulk isotopic analyses may also include cryptic morphospecies. In our case the inclusion of encrusted *G. bulloides* that have a documented offset in their stable isotopic composition from the normal morphospecies can result in a $\delta^{18}O$ measurement that is a mixture of significantly different $\delta^{18}O$ end member values.

The oxygen isotopic composition of 15-30 individuals of *G. bulloides* was used to determine a mean calcification temperature (Table 1.2; Equation 3) and by extension a mean calcification depth for each sediment trap sample. The depth of calcification was determined by comparing each population mean $\delta^{18}O$ calcification temperature to a time equivalent CTD temperature profile to determine the depth of that temperature.

Anomalously high $\delta^{18}O$ (>0.80‰) from several winter and peak upwelling sampling periods were the first indication that $^{18}O$-enriched encrusted individuals were included in some samples. A subsequent examination of weight-area relationships of the *G. bulloides* populations included in our initial stable isotope analyses supported this hypothesis. Duplicate measurements were made on sample populations that excluded encrusted individuals that were identified by morphometric analyses. For example, a stable isotope measurement on a sample from an upwelling period that included encrusted individuals had a $\delta^{18}O$ value of 0.66‰, equating to a calcification temperature of 8.2˚C and an unreasonable calcification depth of greater than 200 meters. A duplicate measurement made on a strictly normal population from the same sample yielded a $\delta^{18}O$ of -0.58‰, equating to a 14.3˚C calcification temperature and a 20 meter calcification depth. Morphometric analyses were used to identify and exclude initial $\delta^{18}O$ results from samples that included encrusted individuals. Duplicate $\delta^{18}O$ measurements where then made on strictly normal populations of *G. bulloides* from these samples. The stable isotope results indicate that normal *G. bulloides* calcifies over a range of temperatures and depths over the course of the three-year time-series ($n$ = 45). $\delta^{18}O$ values range from 0.4 to -0.9‰, with a mean of -0.20‰.

Normal *G. bulloides* $\delta^{18}O$ temperatures estimated using Equation 2 indicate a mean calcification temperature for *G. bulloides* of 12.5˚C, with a range of 10-16˚C. This range is in good agreement with the previously established preferred temperature range (11-16˚C) for *G. bulloides* in this region [*Sautter and Thunell,* 1991a]. These results indicate that *G. bulloides* calcifies over a broad range of water depths (0-75 m), with a mean calcification depth of 40 meters during the study period that loosely follows the

12.5 ˚C isotherm. The range in calcification temperatures and depths is not surprising due to the fact that *G. bulloides* is a surface-mixed layer species whose depth habitat is influenced by seasonal upwelling and vertical migration of the thermocline and chlorophyll maximum [*Prell and Curry,* 1981; *Hemleben et al.,* 1989; *Sautter and Thunell,* 1991a and 1991b]. Previous studies in upwelling regions have found *G. bulloides* at depths ranging from near the sea surface [*Thiede,* 1983; *Kroon and Ganssen,* 1988] to below the thermocline [*Fairbanks et al.,* 1982]. Low $\delta^{18}O$ during upwelling suggests shoaling of the *G. bulloides* depth habitat during these periods. Generally, depth habitats and calcification temperatures tend to be deeper and cooler, respectively, prior to upwelling with a shift to shallower depths and warmer temperatures at the onset of upwelling (Figure 5).

Due to the range of $\delta^{18}O$-determined calcification depths and the large surface to depth change in $[CO_3^{2-}]$, temperature and $[PO_4^{3-}]$, the water column measurements were carefully selected to best reflect *in situ* calcification conditions before pairing with area density measurements. We use the $\delta^{18}O$-derived calcification depth to select the applicable water depth measurement (0, 5, 10, 20, 30, 50, 75 m). For three samples from an unusually strong upwelling period in early 2008, the very small sample sizes (smaller shells and lower abundances) did not allow for duplicate measurements to exclude encrusted individuals. Original $\delta^{18}O$ values indicate calcification temperatures less than 9˚C and calcification depths well over 100 meters. Encrusted individuals were identified using morphometric analyses and removed from the mean area density value for each of these samples and the depth of the 12.5˚C isotherm (mean calcification temperature) was instead used to assign a calcification depth.

### 1.5.4 Area Density Annual Cycle

Due to the discontinuous nature of the available carbonate chemistry data and the sediment trap samples selected for the area density:[$CO_3^{2-}$] calibration, seven additional sediment trap samples were measured to complete one full annual cycle of area density measurements from December 2009 to December 2010. Fourteen sediment trap samples were used to generate this continuous annual cycle of normal *G. bulloides* area density. Nine out of fourteen samples had more than one encrusted individual, these individuals were removed from the normal population and are examined separately in our time-series analysis. The Pacific Fisheries Upwelling Index (PFEL; http://www.pfeg.noaa.gov/products/PFEL; 33˚ N, 119˚ W), which is based on sea surface windstress, is used as an indicator of upwelling strength in SBB.

The highest area density values for both the normal and encrusted *G. bulloides* occur during winter months, when upwelling is weakest, and the lowest area density values generally occur during spring through early summer, when upwelling is strongest (Figure 6). We attribute the inverse relationship observed between *G. bulloides* area density and upwelling strength to the introduction of low [$CO_3^{2-}$] deep-waters to the sea surface during periods of increased upwelling. The exact timing of changes in upwelling recorded by the PFEL index are reflective of sea surface conditions, while *G. bulloides* is responding to changes in upwelling that occur at varying depths within the water column. Generally, the $\delta^{18}O$-derived calcification depth of normal *G. bulloides* remains around 40-50 meters with the exception of upwelling. During peak upwelling in March the calcification depth shoals to the surface mixed layer and when upwelling weakens in April the calcification depth deepens to 25 meters. Because TA and DIC measurements

were not made continuously over this interval, we use measured temperature and oxygen concentration from the Plumes and Blooms and CalCOFI datasets to estimate [$CO_3^{2-}$] using an empirical relationship relating these two variables [*Alin et al.,* 2012]. Changes in [$CO_3^{2-}$] agree well with the seasonal trends observed in both normal and encrusted area densities (Figure 6). SEM images of final chamber shell wall cross sections taken of similarly sized individuals from a peak upwelling and non-upwelling period clearly illustrate differences in shell wall thickness associated with low and high [$CO_3^{2-}$] conditions, respectively (Figure 6 A, B).

We also evaluated how abundances of encrusted and normal *G. bulloides* vary in relation to seasonal hydrographic changes in the SBB. The number of encrusted and normal individuals was determined for a 1/16th split of each sample, with the maximum number of individuals picked from any sample being 40 (Figure 6). Four consecutive sediment trap samples extending from late April to late June had fewer than 40 normal *G. bulloides* in a split, with the lowest number of individuals (13) occurring in April, coinciding with the lowest temperatures and strongest upwelling (Figure 6). Interestingly, the timing of the lowest normal *G. bulloides* abundances do not coincide with the lowest area densities. Several other studies have also indicated that calcification intensity and abundance of *G. bulloides* are not always linked, weakening the optimal growth hypothesis proposed by *de Villers* [2004; *Beer et al.,* 2010; *Weinkauf et al.,* 2013]. The lack of synchroneity between lowest abundance, which would hypothetically coincide with the species' non-optimal growth conditions and lowest calcification intensity instead suggests that *G. bulloides* calcification is responding abiotically to changes in its

calcification environment as proposed by *Weinkauf et al.* [2013], while abundance is responding to favorable ecological conditions.

While *G. bulloides* has generally been identified as an "upwelling indicator", peak abundances of the normal morphospecies in the SBB are inversely related to upwelling strength. These observations suggest that normal *G. bulloides* thrive when the mixed layer is deep, the water column is well stratified and there is a well-defined chlorophyll maximum. Such conditions exist during the non-upwelling periods in the fall and winter months in the SBB. Like normal *G. bulloides,* the encrusted form was also found in highest abundance during winter months but also reappears briefly during peak upwelling in late May. Peak abundances of the encrusted morphospecies also occur during non-upwelling periods, but there is also a considerable secondary pulse of encrusted individuals that coincides with peak upwelling, indicating that this morphospecies thrives in low temperature conditions.

There were enough encrusted individuals to evaluate the stable oxygen and carbon isotopic composition of this morphospecies from four samples used in the area density time-series. Encrusted samples are consistently enriched in both $^{13}C$ and $^{18}O$ relative to values determined for time-equivalent normal individuals. Our analyses indicate that on average there is a 0.5‰ and a 1.0‰ offset between the $\delta^{18}O$ and $\delta^{13}C$, respectively. However, there is considerable variability in offsets, particularly for $\delta^{18}O$. Therefore, due to the limited number of observations ($n$=4) these average offsets should be considered with caution. When the normal $\delta^{18}O$-temperature calibration is applied to encrusted samples, the resulting temperature estimates are up to 2˚C colder than those for

the normal individuals, resulting in calcification depth estimates that differ by nearly 100 meters.

### 1.5.5 Regression Analyses

A series of regression analyses (simple, multiple and hierarchical) were conducted using SPSS statistical software (IBM) to test the correlations between water column variables (*in situ* $[CO_3^{2-}]$, temperature and $[PO_4^{3-}]$) and normal *G. bulloides* mean shell area density (Appendix A; Text S3). Statistical analyses were also used to evaluate covariance among the independent variables themselves and to weigh the influence of each predictor variable on calcification intensity. Values for each independent variable were determined using the $\delta^{18}O$-derived calcification depths for each sample (described in section 4.3).

Simple linear regressions (SLR) indicate that *G. bulloides* area density correlates significantly with all three of the predictor variables ($[CO_3^{2-}]$ $R^2$= 0.80, Temperature $R^2$= 0.70 and $[PO_4^{3-}]$ $R^2$= 0.54); with the highest correlation coefficients observed between area density and $[CO_3^{2-}]$ and temperature (Supporting Information Table S1). SLR between the independent variables themselves also indicate that significant correlations exist between the variables; temperature is positively correlated with $[CO_3^{2-}]$ and $[PO_4^{3-}]$ is negatively correlated with $[CO_3^{2-}]$ and temperature (Supporting information Figure S7). Because the SBB is influenced by seasonal upwelling, it is not surprising that the predictor variables co-vary, thus complicating a straightforward SLR approach. During early spring and summer months upwelling results in low temperature waters depleted in $[CO_3^{2-}]$ and enriched in nutrients being brought to the surface, resulting in collinearity

amongst these environmental variables (Supporting information Table S2). In fact, Multiple linear regression (MLR) statistics were used to quantify further the redundancy between the collinear independent variables using a stepwise multiple regression. By using a variable that is unrelated to the dependent variable, in this case mean shell area, the shared variance between two independent variables can be estimated. Using this method, we estimate that temperature and [$CO_3^{2-}$] are 86% redundant, while [$PO_4^{3-}$] and [$CO_3^{2-}$] are 65% redundant in our dataset (Supporting information Table S3).

Due to the strong collinearity that exists between the independent variables used in this study, a number of statistical tests were conducted in attempt to disentangle these relationships. The issue of collinearity can be resolved by replacing measured values with calculated residual values. This approach was used in a series of stepwise hierarchal regressions analyses to model the influence of each predictor variable (Supporting information Table S4). The results of the four models indicate that [$PO_4^{3-}$] is not an important predictor variable while temperature and [$CO_3^{2-}$] are excellent predictors of area density. Although the results of our tests consistently suggest that [$CO_3^{2-}$] is more significantly related to area density than temperature, the tight collinearity that exists between these two independent variables (86% shared variance) resulted in very similar outcomes of our statistical tests. The covarying nature of temperature and [$CO_3^{2-}$] during our study period makes it nearly impossible to confidently distinguish their respective influences using only statistical tests. This highlights the need for an alternative approach to decouple the respective roles of these variables on *G. bulloides* calcification intensity.

### 1.5.6 Decoupling Temperature and $[CO_3^{2-}]$

We chose to further evaluate the influence of temperature and $[CO_3^{2-}]$ on *G. bulloides* calcification intensity using a down core sediment record. As a result of increasing atmospheric $CO_2$ during the last 100 years, surface water $[CO_3^{2-}]$ has been declining as a result of ocean acidification [e.g., *Gruber et al.*, 2012], while temperature has been increasing as a result of the greenhouse effect [e.g., *Field et al.*, 2006]. Thus, long-term trends in temperature and $[CO_3^{2-}]$ are effectively decoupled during the last century as opposed to being tightly positively correlated as in our sediment trap study period. We use sea surface temperature data from the SBB (1955-present; 34° 24.2′ N, 119° 41.6′ W), sea surface salinity data from the Scripps Pier (1916-present; 32° 52.0′ N, 117° 15.5′ W), measured atmospheric $CO_2$ (1958-present; Mauna Loa), and assume a constant total alkalinity (2250 µmol $kg^{-1}$) to quantitatively estimate how $[CO_3^{2-}]$ has changed over the last century in our study region (Table 1.3; Appendix A; Text S4). The inverse trends between temperature and $[CO_3^{2-}]$ over this interval in our study region provide an opportunity to independently evaluate the influences of these variables on the calcification of *G. bulloides* (Figure 7).

Area density, shell diameter and $\delta^{18}O$ measured on normal *G. bulloides* from the SBB box core are compared to the hydrographic time-series of temperature and $[CO_3^{2-}]$ (Figure 7). *Globigerina bulloides* $\delta^{18}O$ decreases over the sediment core and indicates roughly a 2˚C warming, which is in good agreement with *in situ* measurements of temperature from the SBB (Supporting information Figure S8). Shell diameter increases while area density decreases over the 100 year down core dataset. There is a significant and positive correlation between $\delta^{18}O$-derived temperature and mean shell diameter ($R^2$=

0.40, $p$ <0.001). More importantly, there is an insignificant and negative correlation between temperature and area density ($R^2$= 0.11, $p$= 0.03). The correlation between temperature and diameter supports previous observations that shell size is predominantly controlled by ambient temperature [e.g. *Schmidt et al.,* 2004; *Lombard et al.,* 2010]. The anticorrelation between temperature and area density indicates that correlations in our sediment trap observations are due simply to the collinearity between temperature and $[CO_3^{2-}]$ during that study interval.

We use the linear regression between area density and $[CO_3^{2-}]$ from our sediment trap observations (Figure 9) to estimate $[CO_3^{2-}]$ from the down core area density values. A comparison of area density-$[CO_3^{2-}]$ estimates to calculated surface $[CO_3^{2-}]$ (1960-2005) indicates considerable agreement between these records (Figure 8). Overall both datasets indicate a similar long term declining trend although the $[CO_3^{2-}]$ estimated from area density measurements are generally lower, which is likely due to the fact that *G. bulloides* is not recording sea surface conditions. The increased variability observed in the proxy record is likely a product of calculated $[CO_3^{2-}]$ values not appropriately accounting for shifts in upwelling (Supporting information Figure S9). The proxy $[CO_3^{2-}]$ error represents the standard error of the estimate associated with our regression relationship and is typically within error of the calculated $[CO_3^{2-}]$.

### 1.5.7 Final results and comparison to previous work

While both temperature and $[PO_4^{3-}]$ could play some mediating role in calcification intensity, our hierarchical regression models and down core results indicate that these variables are secondary to $[CO_3^{2-}]$. In particular, the down core data indicate

that calcification temperature affects shell size while [$CO_3^{2-}$] is the dominant control on calcification intensity of *G. bulloides*. Based on our sediment trap observations, the relationships that exists between area density and [$CO_3^{2-}$] for the normal and encrusted *G. bulloides* morphospecies are best described by linear relationships (Table 1.4; Figure 9). The regression for encrusted *G. bulloides* is based on a limited number of observations and therefore has a low level of certainty. Due to the significant offset observed between *G. bulloides* morphospecies calcification intensity observed in this study, these calibration equations should be applied with caution to other *G. bulloides* morphospecies. While the normal *G. bulloides* (genotype IIb) occurs over a range of sea surface temperatures (10-19 ˚C) during both upwelling and non upwelling periods it has not yet been observed in the Atlantic Ocean [*Darling et al.,* 2003]. Therefore our normal *G. bulloides* area density calibration may not be suitable for Atlantic morphotypes [*Stewart*, 2000; *Kucera and Darling*, 2002].

The results of our work agree well with several previous studies that have cited [$CO_3^{2-}$] as the dominant factor influencing *G. bulloides* calcification [*Barker and Elderfield*, 2002; *Gonzalez-Mora et al.,* 2008; *Moy et al.,* 2009]. The commonality amongst these previous studies is that they were all conducted using sediment core-top and down core records, making this the first sediment trap study to directly assess the relationship between *in situ* [$CO_3^{2-}$] and *G. bulloides* calcification. Another recent sediment trap study in the North Atlantic (Madeira Basin), where there are negligible changes in [$CO_3^{2-}$], evaluated the response of *G. bulloides* calcification intensity to temperature and productivity and also observed no significant response of SNSW to these variables [*Weinkauf et al.,* 2016]. A laboratory culture that exposed *G. bulloides* to

varying [$CO_3^{2-}$] found no conclusive influence on shell weight but this is likely due to the fact that these weight measurements were not size-normalized and that calcite added during culturing cannot be separated from pre-cultured calcite [*Spero et al.*, 1997].

While our results agree with much of the previous work on *G. bulloides* calcification, they also contrast with two studies that link *G. bulloides* calcification to nutrient concentration. Results from an Arabian Sea plankton tow (0-60 m) study suggested that the relationship observed between *G. bulloides* MBW and [$CO_3^{2-}$] ($R^2$= 0.4) was not the product of a causal relationship and recommended investigating the influence of other environmental variables on calcification [*Beer et al.*, 2010a]. In a follow up study, both SBW and MBW of *G. bulloides* (150-200 µm and 200-250 µm) from a North Atlantic plankton tow indicated a significant negative correlation with nutrient concentration leading the authors to suggest that increased nutrient content of seawater inhibits *G. bulloides* calcification [*Aldridge et al.*, 2012]. As in the SBB, nutrient concentration ([$PO_4^{3-}$ and [$NO_3^-$]) and [$CO_3^{2-}$] are closely linked in the North Atlantic ($R^2$= 0.72 and 0.82, respectively; *Aldridge et al.*, 2012) making it difficult to determine the extent to which each variable affects calcification intensity. It is also important to note that surface plankton tows (0-60 m) were used to collect the individuals used in both of these studies and therefore possibly contain a range of pre-adult ontogenic stages that would complicate shell weight analysis. Specifically, the authors indicate that some individuals from this study had not completed calcification of their final chamber [*Aldridge et al.*, 2012]. Further, our work highlights the importance of pairing SNSW with ambient calcification conditions rather than simply surface conditions. This is

particularly important for *G. bulloides* as its depth of calcification appears to be strongly related to the depth of the thermocline, which can vary significantly seasonally.

Several species-specific area density calibrations have been developed for tropical species using sediment trap samples from the Cariaco Basin [*Marshall et al.,* 2013] providing a direct comparison to our area density results. Despite the differences in $[CO_3^{2-}]$ ranges between studies, this comparison clearly indicates that strong inter-species differences exist and highlights the considerable offset even between *G. bulloides* morphospecies (Figure 10). The slopes of the symbiont-bearing species (*G. sacculifer* and *G. ruber*) are notably steeper than those recorded for symbiont-barren *G. bulloides* morphospecies. Some studies have suggested that the calcification in symbiont and non-symbiont bearing species may respond differently to changes in carbonate chemistry. Species that harbor photosynthetic symbionts such as *G. ruber* and *G. sacculifer* have the ability to convert $HCO_3^-$ to $CO_3^{2-}$ via pH regulation thereby increasing ambient $[CO_3^{2-}]$ and enhancing a microenvironment for calcification [*Jørgensen et al.,* 1985; *Rink et al.,* 1998]. For this reason *Aldridge* et al. [2012] suggested that due to a lack of symbionts *G. bulloides* exhibit a larger change in shell weights [*Barker and Elderfield,* 2002] as compared to *G. ruber* [*de Moel et al.,* 2009] since the Last Glacial Maximum. The inter-species comparison of area density calibrations suggests the opposite; symbiont-bearing species respond more dramatically to changes in $[CO_3^{2-}]$ relative to the non-symbiont bearing species. In order to fully assess the differences between the calcification intensity of symbiont-bearing and -barren foraminifera and $[CO_3^{2-}]$, calibrations should be developed for additional foraminifera species.

## 1.6 CONCLUSIONS

Our results indicate that the calcification intensity of the planktonic foraminifera *G. bulloides* is significantly related to the ambient [$CO_3^{2-}$] making it an ideal species for reconstructions of surface ocean [$CO_3^{2-}$] from well-preserved sediments. The non-destructive nature of the area density method allows for [$CO_3^{2-}$] estimates to be directly coupled with geochemical measurements from a single sample population, which is an exciting prospect for developing multi-proxy climate records. We also identify two cryptic morphospecies of *G. bulloides* that have been previously found in our study region using a combination of morphometric measurements. Due to the significant difference in calcification and offset in the stable isotopes observed between these morphospecies, we suggest using this morphometric technique as a means to identify cryptic species when generating paleo reconstructions using *G. bulloides*.

Table 1.1 Sediment trap sample information and morphometric measurements.

| Trap ID | Sampling Date | *n* | Mean Area Density (µg/µm2) | Area Density 1-sigma | Area Density 2 Standard Errors | Mean Sample Mass (µg) | Mean Sample Diameter (µm) | Mean Sample Area (µm2) |
|---|---|---|---|---|---|---|---|---|
| SBB28 Cup 12 | 9/14/07 | 40 | 5.95E-05 | 9.27E-06 | 2.93E-06 | 4.00 | 320.70 | 69120.88 |
| SBB29 Cup 1 | 10/9/07 | 32 | 6.88E-05 | 7.65E-06 | 2.70E-06 | 3.33 | 282.08 | 47705.31 |
| SBB29 Cup 3 | 11/13/07 | 35 | 6.61E-05 | 8.94E-06 | 3.02E-06 | 3.40 | 289.54 | 51971.62 |
| SBB29 Cup 8 | 2/11/08 | 29 | 5.82E-05 | 1.35E-05 | 5.02E-06 | 2.79 | 264.86 | 43132.23 |
| SBB29 Cup 10 | 3/18/08 | 35 | 5.20E-05 | 1.17E-05 | 3.96E-06 | 3.14 | 295.07 | 51484.82 |
| SBB29 Cup 12 | 4/22/08 | 24 | 6.05E-05 | 9.13E-06 | 3.73E-06 | 3.26 | 292.55 | 52535.93 |
| SBB30 Cup 1 | 5/30/08 | 33 | 6.20E-05 | 1.29E-05 | 4.48E-06 | 3.03 | 276.09 | 48913.89 |
| SBB30 Cup 5 | 6/16/08 | 29 | 7.15E-05 | 1.05E-05 | 3.90E-06 | 2.97 | 253.85 | 41558.00 |
| SBB30 Cup 8 | 7/21/08 | 26 | 6.06E-05 | 1.70E-05 | 6.67E-06 | 2.22 | 240.94 | 44619.51 |
| SBB31 Cup 2 | 4/21/09 | 26 | 5.30E-05 | 1.86E-05 | 7.31E-06 | 1.31 | 191.72 | 28133.93 |
| SBB31Cup 5 | 5/27/09 | 23 | 5.44E-05 | 2.06E-05 | 8.61E-06 | 1.40 | 217.70 | 30139.98 |
| SBB31Cup 7 | 6/26/09 | 33 | 7.64E-05 | 1.08E-05 | 3.74E-06 | 4.05 | 287.50 | 53222.53 |
| SBB31Cup 10 | 7/28/09 | 33 | 7.52E-05 | 1.24E-05 | 4.30E-06 | 3.91 | 269.86 | 48355.76 |
| SBB31 Cup 12 | 8/27/09 | 39 | 7.20E-05 | 9.18E-06 | 2.94E-06 | 4.08 | 292.92 | 56752.28 |
| SBB32T Cup 1 | 9/25/09 | 40 | 6.45E-05 | 6.27E-06 | 1.98E-06 | 5.64 | 384.31 | 88165.28 |
| SBB32T Cup 3 | 10/30/09 | 40 | 5.90E-05 | 7.76E-06 | 2.45E-06 | 5.32 | 389.32 | 90705.17 |
| SBB32T Cup 5 | 11/20/09 | 32 | 6.27E-05 | 1.03E-05 | 3.63E-06 | 4.59 | 347.33 | 73448.54 |
| SBB32T Cup 10 | 2/26/10 | 27 | 7.07E-05 | 6.70E-06 | 2.58E-06 | 5.43 | 358.30 | 76028.01 |
| SBB32B Cup 1 | 9/25/09 | 39 | 6.70E-05 | 7.19E-06 | 2.30E-06 | 6.06 | 383.52 | 253489.77 |
| SBB32B Cup 3 | 10/30/09 | 37 | 6.16E-05 | 9.07E-06 | 2.98E-06 | 5.22 | 372.26 | 85349.99 |
| SBB32B Cup 5 | 11/20/09 | 30 | 6.74E-05 | 8.57E-06 | 3.13E-06 | 4.84 | 345.53 | 73089.22 |
| SBB32B Cup 10 | 2/26/10 | 31 | 7.01E-05 | 1.08E-05 | 3.89E-06 | 4.51 | 325.64 | 67841.72 |
| SBB33T Cup 9 | 7/21/10 | 35 | 5.99E-05 | 9.97E-06 | 3.37E-06 | 4.37 | 334.40 | 70165.72 |
| SBB33T Cup 12 | 8/20/10 | 30 | 6.21E-05 | 7.58E-06 | 2.77E-06 | 5.10 | 367.47 | 82217.40 |
| SBB34T Cup 1 | 9/21/10 | 39 | 5.83E-05 | 5.41E-06 | 1.73E-06 | 5.60 | 392.26 | 96486.26 |
| SBB34T Cup 3 | 10/28/10 | 31 | 5.81E-05 | 4.69E-06 | 1.68E-06 | 5.83 | 392.82 | 96902.16 |
| SBB34T Cup 5 | 11/19/10 | 38 | 5.71E-05 | 1.15E-05 | 3.72E-06 | 4.40 | 352.46 | 77019.80 |
| SBB34T Cup 7 | 12/16/10 | 38 | 5.67E-05 | 7.88E-06 | 2.56E-06 | 4.47 | 355.33 | 77579.35 |
| SBB34B Cup 1 | 9/21/10 | 31 | 5.29E-05 | 7.47E-06 | 2.68E-06 | 4.22 | 363.65 | 79928.89 |
| SBB34B Cup 3 | 10/28/10 | 35 | 5.57E-05 | 7.28E-06 | 2.46E-06 | 5.14 | 385.49 | 89122.85 |
| SBB34B Cup 5 | 11/19/10 | 37 | 5.79E-05 | 9.30E-06 | 3.06E-06 | 4.38 | 348.90 | 74751.42 |
| SBB34B Cup 7 | 12/16/10 | 30 | 6.10E-05 | 9.45E-06 | 3.45E-06 | 4.69 | 357.72 | 78415.93 |

Table 1.2 Stable isotope results, calcification depths and hydrographic data.

| Trap ID | Sampling Date | *n* | $\delta^{18}O$ (‰) | $\delta^{18}O$-Temperature (˚C) | $\delta^{18}O$-Calcification Depth (m) | Depth Specific Carbonate (µmol $kg^{-1}$) | Depth Specific Temperature (˚C) | Depth Specific Phosphate (µmol $kg^{-1}$) |
|---|---|---|---|---|---|---|---|---|
| SBB28 Cup 12 | 9/14/07 | 40 | -0.19 | 12.37 | 26 | 118.49 | 11.70 | 1.22 |
| SBB29 Cup 1 | 10/9/07 | 32 | -0.09 | 11.69 | 55 | 141.78 | 12.00 | 1.13 |
| SBB29 Cup 3 | 11/13/07 | 35 | -0.03 | 11.40 | 57 | 135.66 | 13.00 | 0.82 |
| SBB29 Cup 8 | 2/11/08 | 29 | 0.02 | N/A | N/A | 86.78 | 10.90 | 1.52 |
| SBB29 Cup 10 | 3/18/08 | 35 | N/A | N/A | N/A | 74.21 | 10.10 | 1.68 |
| SBB29 Cup 12 | 4/22/08 | 24 | 0.37 | N/A | N/A | 123.65 | 13.10 | 1.06 |
| SBB30 Cup 1 | 5/30/08 | 33 | 0.08 | 11.87 | 13 | 83.38 | 10.00 | 1.84 |
| SBB30 Cup 5 | 6/16/08 | 29 | 0.05 | 14.22 | 37 | 131.82 | 11.79 | 1.19 |
| SBB30 Cup 8 | 7/21/08 | 26 | -0.59 | 14.32 | 20 | 82.36 | 10.30 | 1.75 |
| SBB31 Cup 2 | 4/21/09 | 26 | -0.06 | 11.92 | 8 | 66.53 | 9.60 | 2.07 |
| SBB31Cup 5 | 5/27/09 | 23 | -0.14 | 12.04 | 15 | 70.02 | 11.03 | 1.70 |
| SBB31Cup 7 | 6/26/09 | 33 | -0.53 | 13.97 | 12 | 154.64 | 14.06 | 0.72 |
| SBB31Cup 10 | 7/28/09 | 33 | -0.38 | 13.12 | 26 | 158.35 | 14.54 | 0.48 |
| SBB31 Cup 12 | 8/27/09 | 39 | -0.55 | 13.83 | 31 | 150.00 | 13.29 | 0.93 |
| SBB32T Cup 1 | 9/25/09 | 40 | -0.28 | 12.55 | 50 | 140.93 | 12.60 | 0.95 |
| SBB32T Cup 3 | 10/30/09 | 40 | -0.01 | 11.14 | 65 | 111.40 | 12.19 | 1.11 |
| SBB32T Cup 5 | 11/20/09 | 32 | -0.25 | 12.17 | 53 | 120.43 | 12.46 | 0.61 |
| SBB32T Cup 10 | 2/26/10 | 27 | -0.27 | 12.08 | 74 | 141.12 | 13.45 | 0.43 |
| SBB32B Cup 1 | 9/25/09 | 39 | -0.91 | 15.62 | 23 | 127.29 | 12.60 | 0.95 |
| SBB32B Cup 3 | 10/30/09 | 37 | -0.65 | 14.24 | 20 | 111.40 | 12.19 | 1.11 |
| SBB32B Cup 5 | 11/20/09 | 30 | -0.36 | 12.74 | 45 | 120.43 | 12.46 | 0.61 |
| SBB32B Cup 10 | 2/26/10 | 31 | -0.32 | 12.35 | 65 | 141.12 | 13.45 | 0.43 |
| SBB33T Cup 9 | 7/21/10 | 35 | 0.15 | 10.52 | 20 | 87.43 | 10.90 | 1.41 |
| SBB33T Cup 12 | 8/20/10 | 30 | 0.01 | 11.23 | 17 | 121.10 | 11.90 | 0.92 |
| SBB34T Cup 1 | 9/21/10 | 39 | -0.62 | 14.11 | 6 | 68.98 | 10.30 | 1.22 |
| SBB34T Cup 3 | 10/28/10 | 31 | -0.62 | 14.08 | 24 | 66.58 | 10.45 | 1.53 |
| SBB34T Cup 5 | 11/19/10 | 38 | -0.24 | 13.01 | 23 | 83.70 | 11.20 | 1.26 |
| SBB34T Cup 7 | 12/16/10 | 38 | -0.04 | 11.20 | 45 | 80.24 | 11.04 | 1.27 |
| SBB34B Cup 1 | 9/21/10 | 31 | -0.28 | 12.44 | 14 | 68.98 | 10.30 | 1.22 |
| SBB34B Cup 3 | 10/28/10 | 35 | -0.47 | 13.37 | 29 | 66.58 | 10.45 | 1.53 |
| SBB34B Cup 5 | 11/19/10 | 37 | -0.08 | 12.21 | 35 | 83.70 | 11.20 | 1.26 |
| SBB34B Cup 7 | 12/16/10 | 30 | 0.15 | 10.24 | 73 | 80.24 | 11.04 | 1.27 |

Table 1.3 Down core calculations of marine carbonate system variables.

| Year | SBB SST (˚C) | SIO SSS (ppt) | TA (mmol/kg-1) | Mauna Loa $CO_2$ (ppm) | Henry's Constant | Calculated $pCO_2$ (matm) | Calculated $[CO_3^{2-}]$ |
|---|---|---|---|---|---|---|---|
| 1955 | 14.83 | 33.61 | 2250 | | 0.038 | | |
| 1956 | 14.96 | 33.63 | 2250 | | 0.038 | | |
| 1957 | 15.76 | 33.59 | 2250 | | 0.037 | | |
| 1958 | 16.54 | 33.55 | 2250 | | 0.036 | | |
| 1959 | 15.52 | 33.69 | 2250 | | 0.037 | | |
| 1960 | 15.80 | 33.66 | 2250 | 316.91 | 0.037 | 298.9 | 187.4 |
| 1961 | 15.40 | 33.69 | 2250 | 317.64 | 0.037 | 299.4 | 185.0 |
| 1962 | 15.18 | 33.68 | 2250 | 318.45 | 0.038 | 300.1 | 183.5 |
| 1963 | 16.38 | 33.69 | 2250 | 318.99 | 0.036 | 301.1 | 189.9 |
| 1964 | 15.58 | 33.83 | 2250 | 319.62 | 0.037 | 301.4 | 185.6 |
| 1965 | 15.82 | 33.59 | 2250 | 320.04 | 0.037 | 301.8 | 186.2 |
| 1966 | 15.71 | 33.61 | 2250 | 321.38 | 0.037 | 303.1 | 185.1 |
| 1967 | 15.79 | 33.56 | 2250 | 322.16 | 0.037 | 303.8 | 185.1 |
| 1968 | 15.36 | 33.64 | 2250 | 323.04 | 0.037 | 304.5 | 182.6 |
| 1969 | 15.62 | 33.63 | 2250 | 324.62 | 0.037 | 306.1 | 183.4 |
| 1970 | 15.12 | 33.61 | 2250 | 325.68 | 0.038 | 306.9 | 180.3 |
| 1971 | 15.18 | 33.62 | 2250 | 326.32 | 0.038 | 307.5 | 180.4 |
| 1972 | 15.84 | 33.69 | 2250 | 327.45 | 0.037 | 308.9 | 183.7 |
| 1973 | 15.32 | 33.76 | 2250 | 329.68 | 0.037 | 310.8 | 180.2 |
| 1974 | 15.39 | 33.69 | 2250 | 330.18 | 0.037 | 311.3 | 180.3 |
| 1975 | 14.92 | 33.70 | 2250 | 331.08 | 0.038 | 311.9 | 177.4 |
| 1976 | 16.39 | 33.73 | 2250 | 332.05 | 0.036 | 313.4 | 185.0 |
| 1977 | 16.49 | 33.72 | 2250 | 333.78 | 0.036 | 315.1 | 184.9 |
| 1978 | 16.55 | 33.44 | 2250 | 335.41 | 0.036 | 316.6 | 184.0 |
| 1979 | 15.75 | 33.41 | 2250 | 336.78 | 0.037 | 317.6 | 179.2 |
| 1980 | 15.91 | 33.41 | 2250 | 338.68 | 0.037 | 319.5 | 179.4 |
| 1981 | 16.53 | 33.63 | 2250 | 340.1 | 0.036 | 321.0 | 182.7 |
| 1982 | 16.04 | 33.57 | 2250 | 341.44 | 0.037 | 322.1 | 179.4 |
| 1983 | 17.22 | 33.44 | 2250 | 343.03 | 0.035 | 324.0 | 184.9 |
| 1984 | 16.66 | 33.58 | 2250 | 344.58 | 0.036 | 325.3 | 181.7 |
| 1985 | 15.80 | 33.61 | 2250 | 346.04 | 0.037 | 326.4 | 176.6 |
| 1986 | 16.09 | 33.50 | 2250 | 347.39 | 0.037 | 327.7 | 177.5 |
| 1987 | 16.12 | 33.49 | 2250 | 349.16 | 0.037 | 329.4 | 177.0 |
| 1988 | 16.01 | 33.58 | 2250 | 351.56 | 0.037 | 331.7 | 175.8 |
| 1989 | 15.24 | 33.59 | 2250 | 353.07 | 0.037 | 332.8 | 171.3 |
| 1990 | 16.66 | 33.58 | 2250 | 354.35 | 0.036 | 334.5 | 178.3 |
| 1991 | 16.00 | 33.52 | 2250 | 355.57 | 0.037 | 335.4 | 174.3 |
| 1992 | 16.74 | 33.39 | 2250 | 356.38 | 0.036 | 336.5 | 177.6 |
| 1993 | 16.77 | 33.40 | 2250 | 357.07 | 0.036 | 337.1 | 177.6 |
| 1994 | 16.05 | 33.42 | 2250 | 358.82 | 0.037 | 338.5 | 173.3 |
| 1995 | 16.52 | 33.37 | 2250 | 360.8 | 0.036 | 340.6 | 174.9 |
| 1996 | 15.74 | 33.58 | 2250 | 362.59 | 0.037 | 341.9 | 170.7 |
| 1997 | 16.89 | 33.65 | 2250 | 363.71 | 0.036 | 343.5 | 176.6 |
| 1998 | 16.76 | 33.59 | 2250 | 366.65 | 0.036 | 346.2 | 174.8 |
| 1999 | 15.08 | 33.66 | 2250 | 368.33 | 0.038 | 347.1 | 165.7 |
| 2000 | 16.60 | 33.67 | 2250 | 369.52 | 0.036 | 348.8 | 173.2 |

| | | | | | | | |
|---|---|---|---|---|---|---|---|
| 2001 | 15.54 | 33.61 | 2250 | 371.13 | 0.037 | 349.9 | 167.1 |
| 2002 | 15.27 | 33.64 | 2250 | 373.22 | 0.037 | 351.8 | 165.1 |
| 2003 | 15.82 | 33.42 | 2250 | 375.77 | 0.037 | 354.4 | 166.7 |
| 2004 | 16.46 | 33.35 | 2250 | 377.49 | 0.036 | 356.3 | 169.3 |
| 2005 | 14.55 | 33.31 | 2250 | 379.8 | 0.038 | 357.6 | 158.8 |
| 2006 | 16.30 | 33.51 | 2250 | 381.9 | 0.036 | 360.4 | 167.5 |
| 2007 | 15.03 | 33.70 | 2250 | 383.76 | 0.038 | 361.6 | 160.9 |
| 2008 | 15.40 | 33.58 | 2250 | 385.59 | 0.037 | 363.5 | 161.9 |
| 2009 | 15.57 | 33.55 | 2250 | 387.37 | 0.037 | 365.2 | 162.2 |
| 2010 | 14.85 | 33.49 | | 389.85 | 0.038 | 367.3 | 157.8 |

Table 1.4 Final calibration equations.

| Data | Y | X | a | b | $R^2$ | p | Std Err Est (AD) | Std Err Est $[CO_3^{2-}]$ |
|---|---|---|---|---|---|---|---|---|
| Normal (*n*=32) | Area Density | $[CO_3^{2-}]$ | 4.19 E-05 | 1.92 E-07 | 0.802 | <0.001 | 3.00E-06 | 15.63 |
| Encrusted (*n*=11) | Area Density | $[CO_3^{2-}]$ | 7.73 E-05 | 1.58 E-07 | 0.658 | 0.002 | 4.00E-06 | 25.40 |

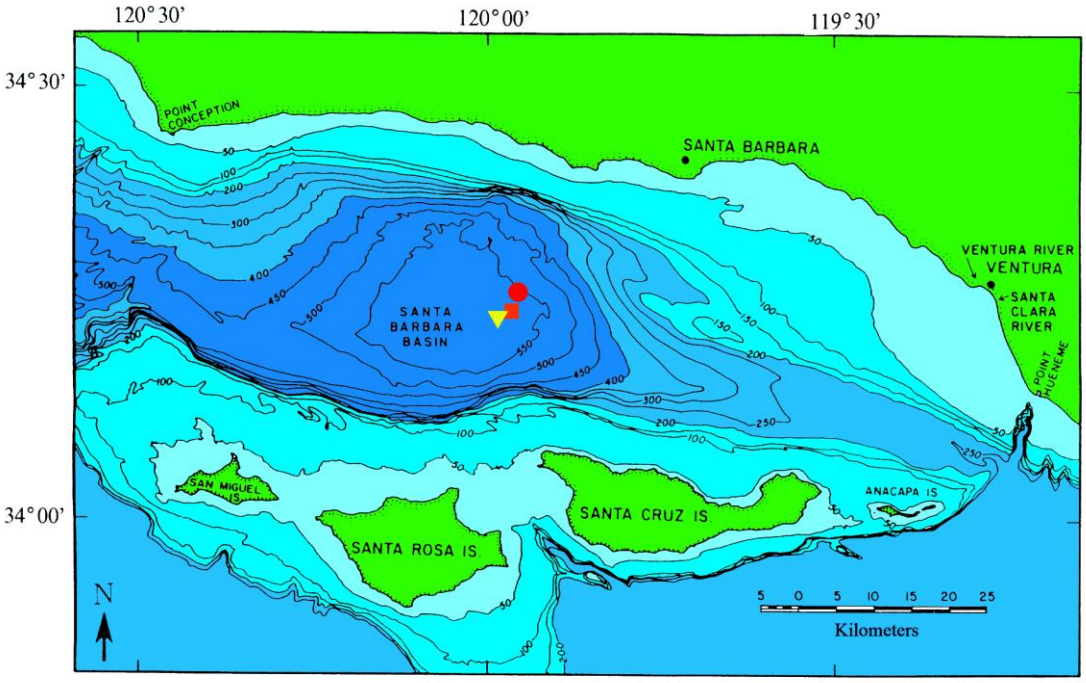


Figure 1.1 Bathymetry of the Santa Barbara Basin with the location of the sediment trap mooring (yellow triangle), Plumes and Blooms Station 4 (orange square) and box-core (red circle).

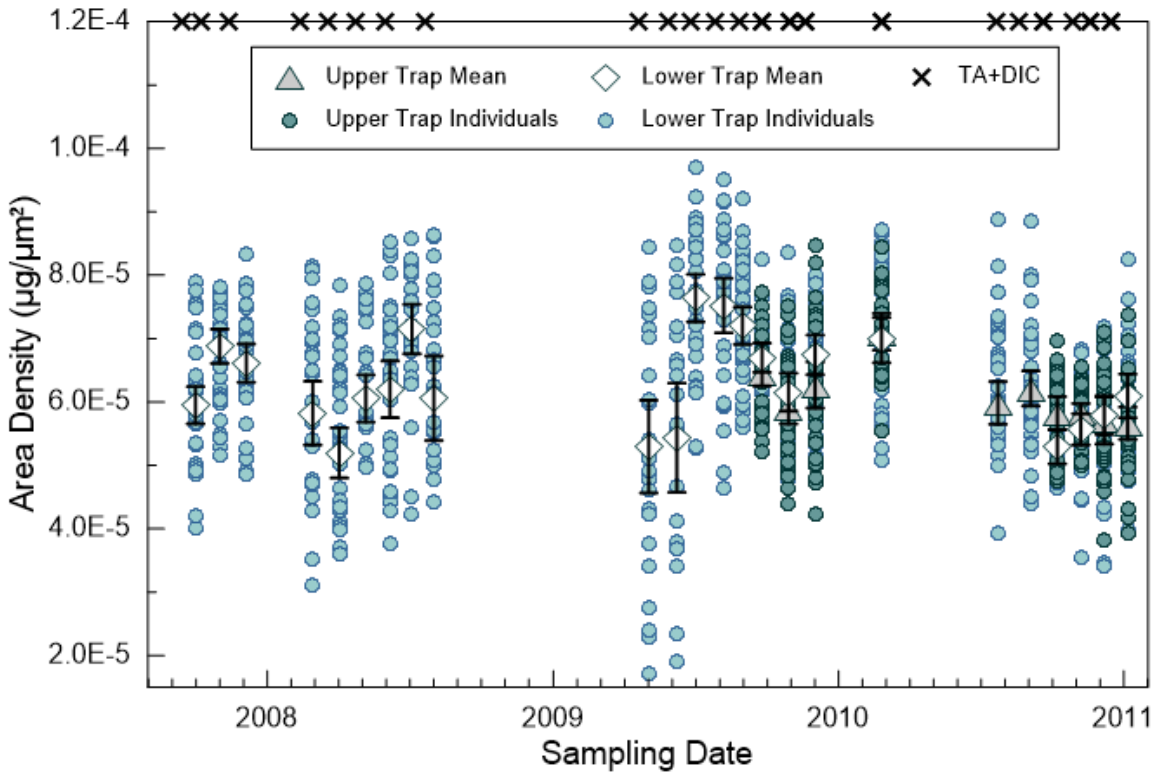


Figure 1.2 Discontinuous time-series of normal *G. bulloides* mean area density from upper (triangles) and lower (diamonds) sediment trap samples and the spread of the individual measurements included in each sample mean (circles). Error bars represent 2 standard errors of the sample means. Hydrographic sampling of TA and DIC are indicated by "X" on the x-axis.

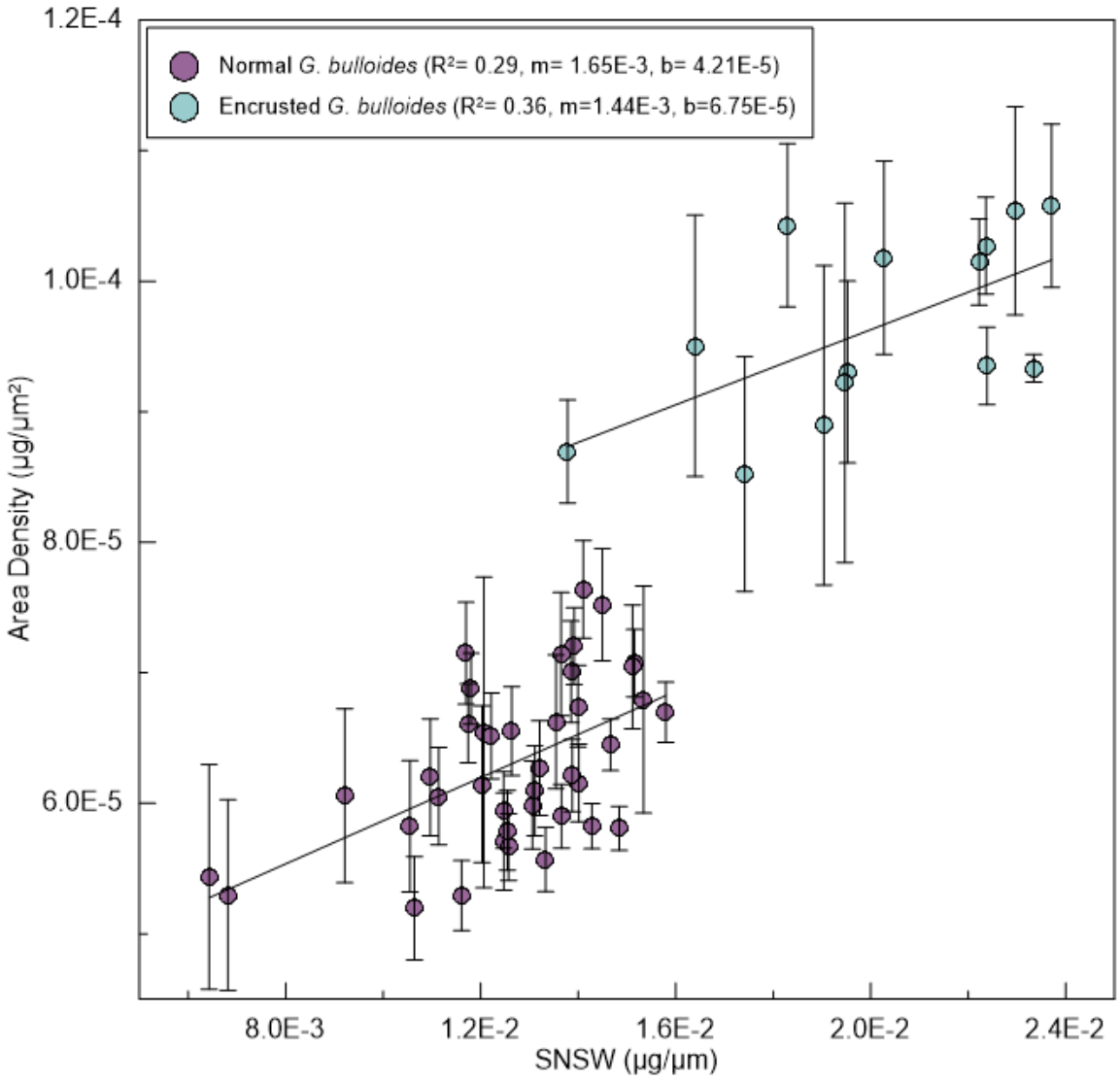


Figure 1.3 Comparison of area density-SNSW of the normal and encrusted morphospecies included in our study. SNSW was determined for each sample by taking the mean sample weight and dividing by mean sample diameter. Error bars represent the 2 standard errors of each sample population ($SE = 2\sigma/\sqrt{n}$).

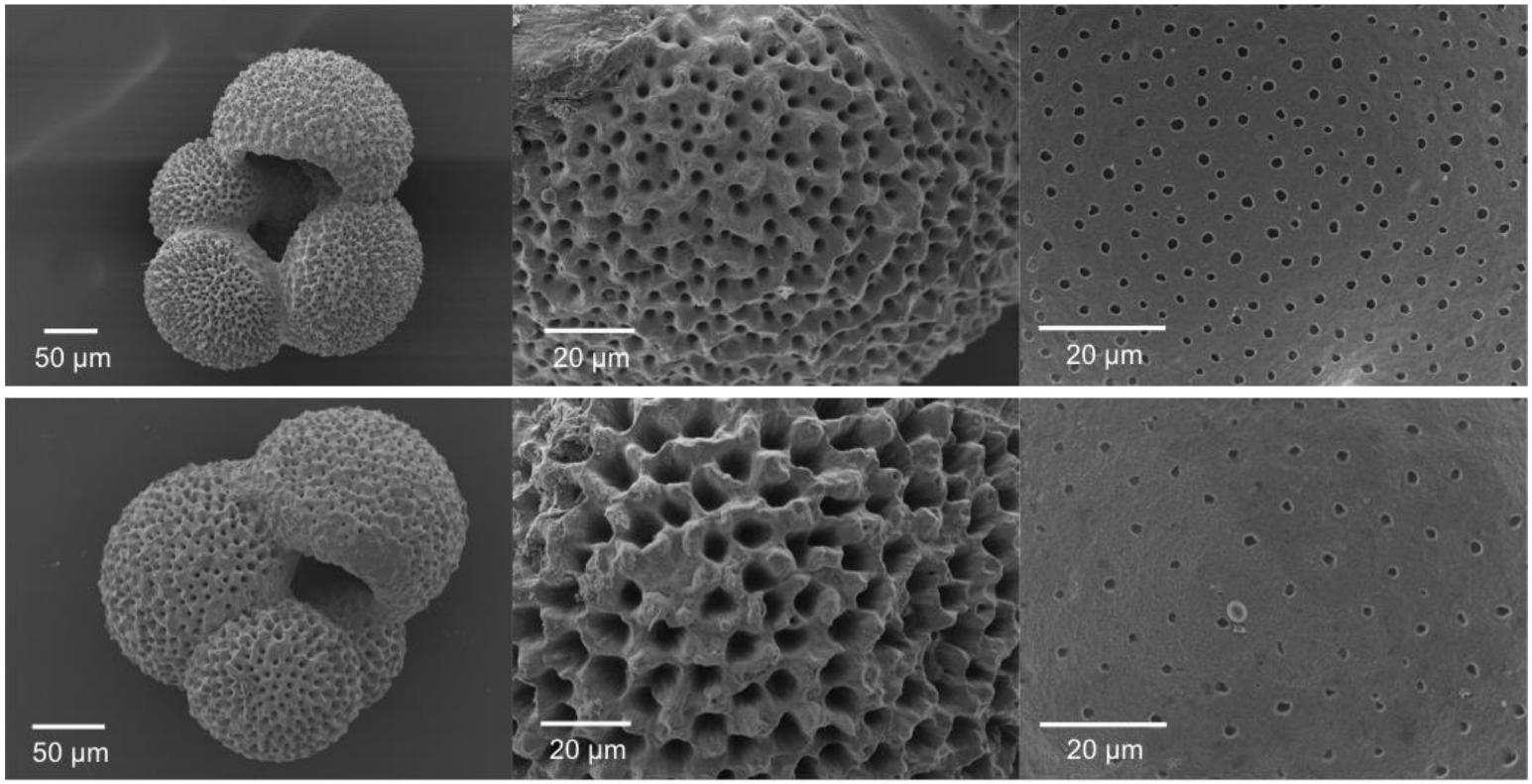


Figure 1.4 SEM images of normal (upper panels) and visually distinct encrusted (lower panels) whole shells, external surface textures and pore density imaged from the inner shell wall.

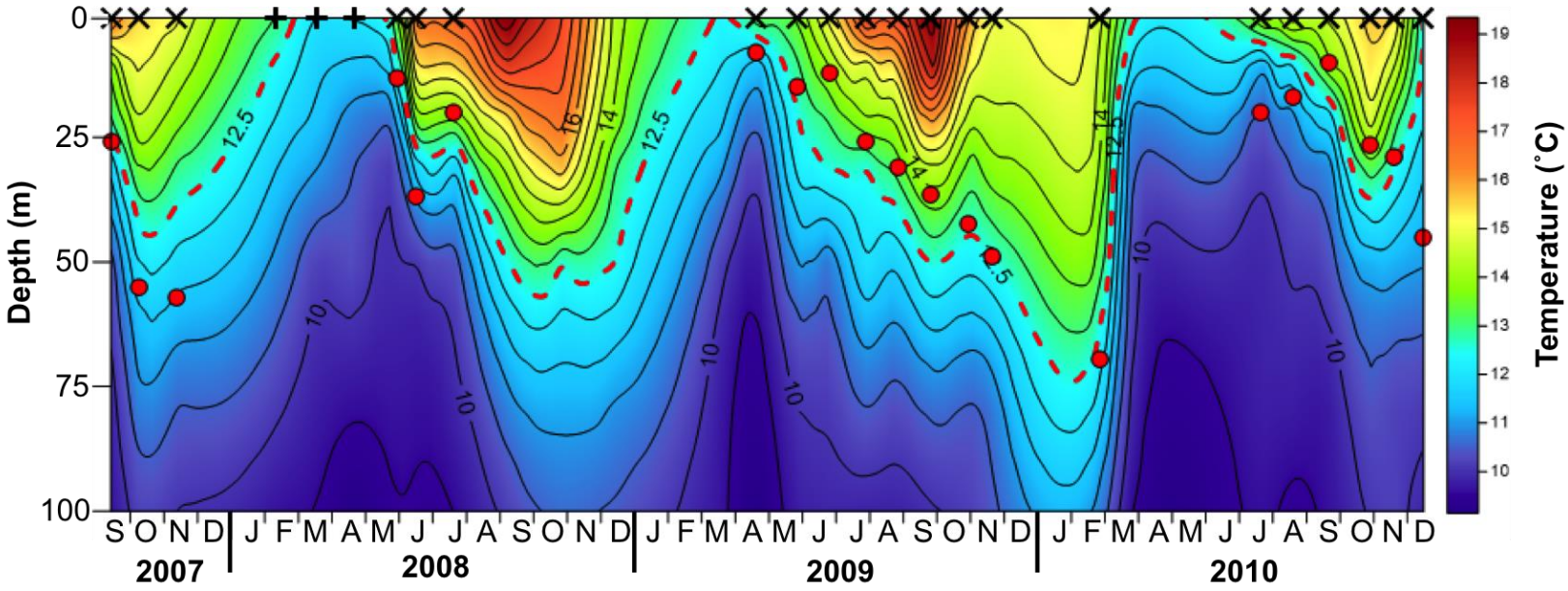


Figure 1.5 *G. bulloides* $\delta^{18}O$ derived calcification depths (red circles) plotted here with contoured measured temperatures (0-100 m) with the 12.5˚C isotherm (dashed red) highlighted as the mean calcification temperature determined for this time-series. This dataset excludes three $^{18}O$ enriched samples from the strong upwelling period in 2008. The dates of coinciding hydrographic data are marked on the upper x-axis as "X" with the three excluded samples marked by a "+".

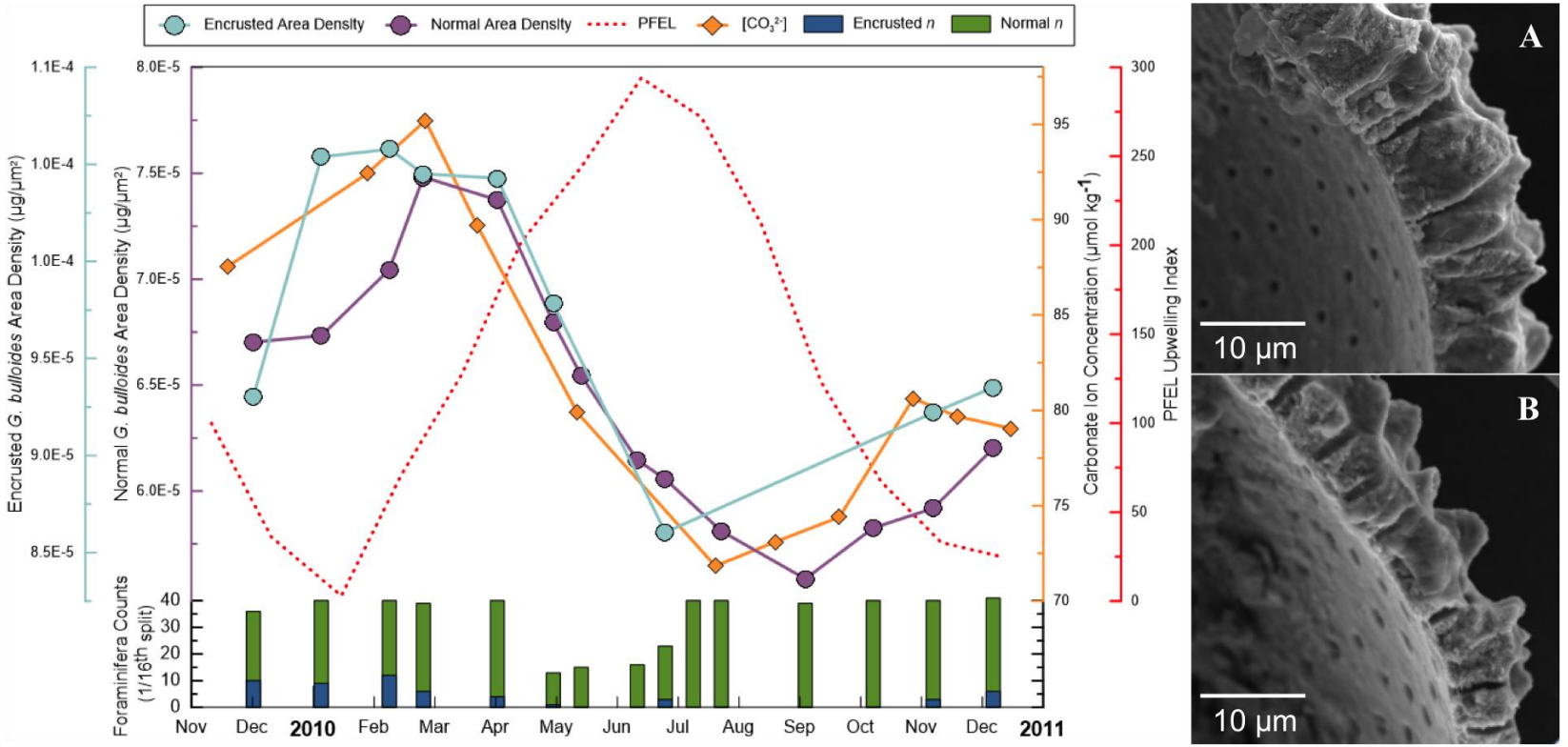


Figure 1.6 Normal and encrusted area density time-series and 1/16th split abundance counts. The Pacific Fisheries Environmental Laboratory upwelling index is plotted as an indicator of upwelling strength and estimates of *in situ* $[CO_3^{2-}]$ determined from measured temperature and oxygen indicate shifts in $[CO_3^{2-}]$ SEM images illustrate the difference in shell wall thickness from a non-upwelling (A) and an upwelling (B) sample.

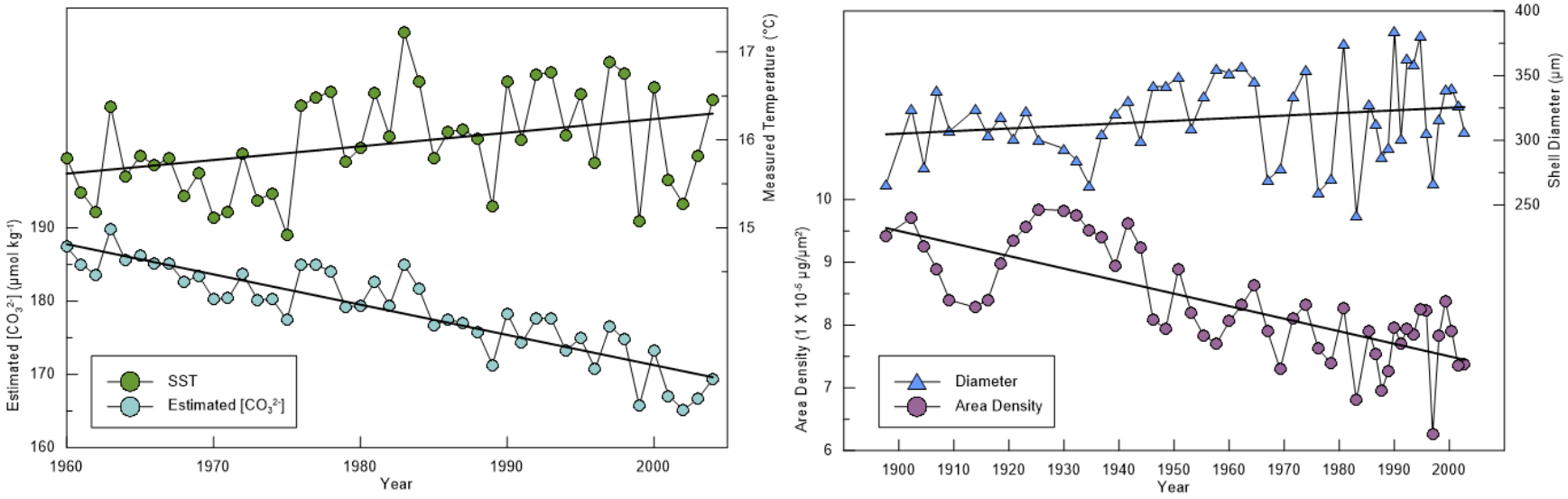


Figure 1.7 Left: Measured *in situ* sea surface temperature and estimates of surface [$CO_3^{2-}$] from the SBB (1955-2005). Right: Down core shell diameter and area density over the last century.

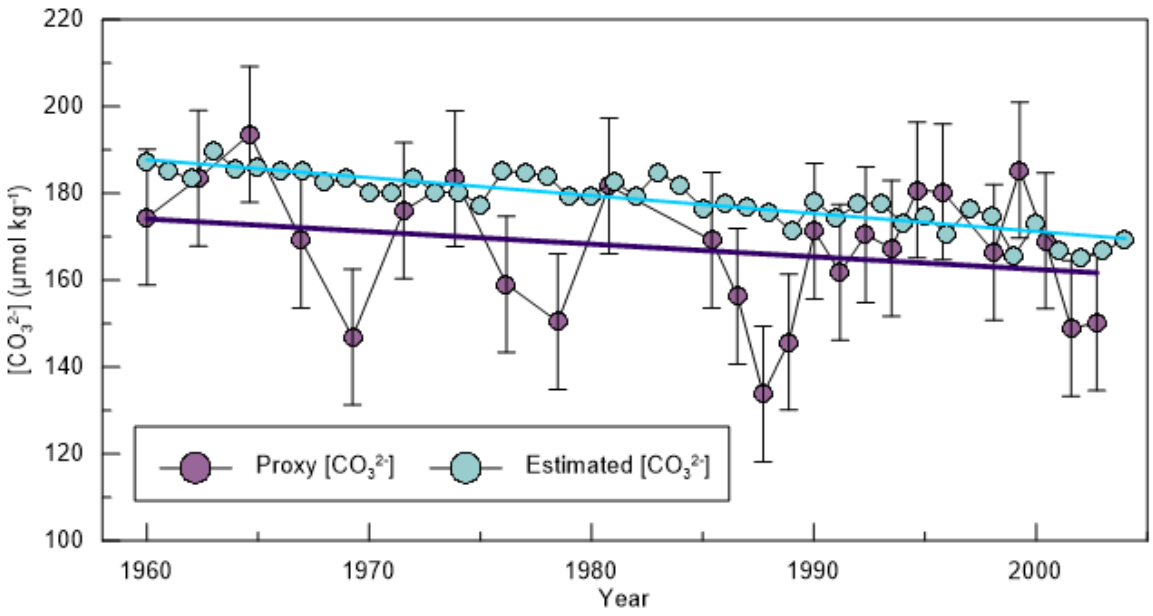


Figure 1.8 Comparison of calculated- and area density estimated-[$CO_3^{2-}$]. Error bars on area density-[$CO_3^{2-}$] represent the standard error of the estimate from our sediment trap regression.

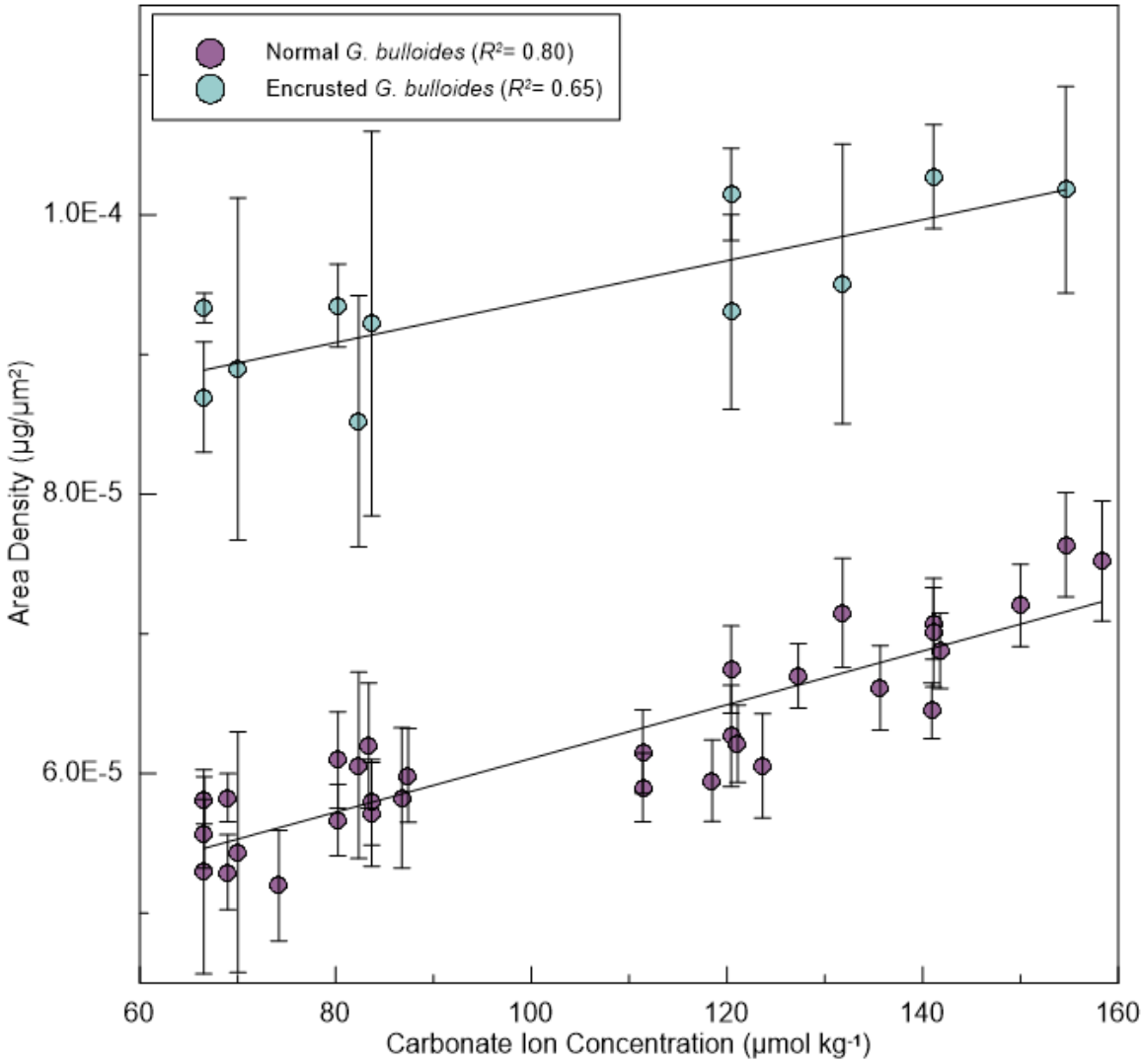


Figure 1.9 The linear relationship observed between normal and encrusted *G. bulloides* area density and [$CO_3^{2-}$] from our sediment trap analyses. Error bars represent 2 standard errors ($SE = 2\sigma/\sqrt{n}$).

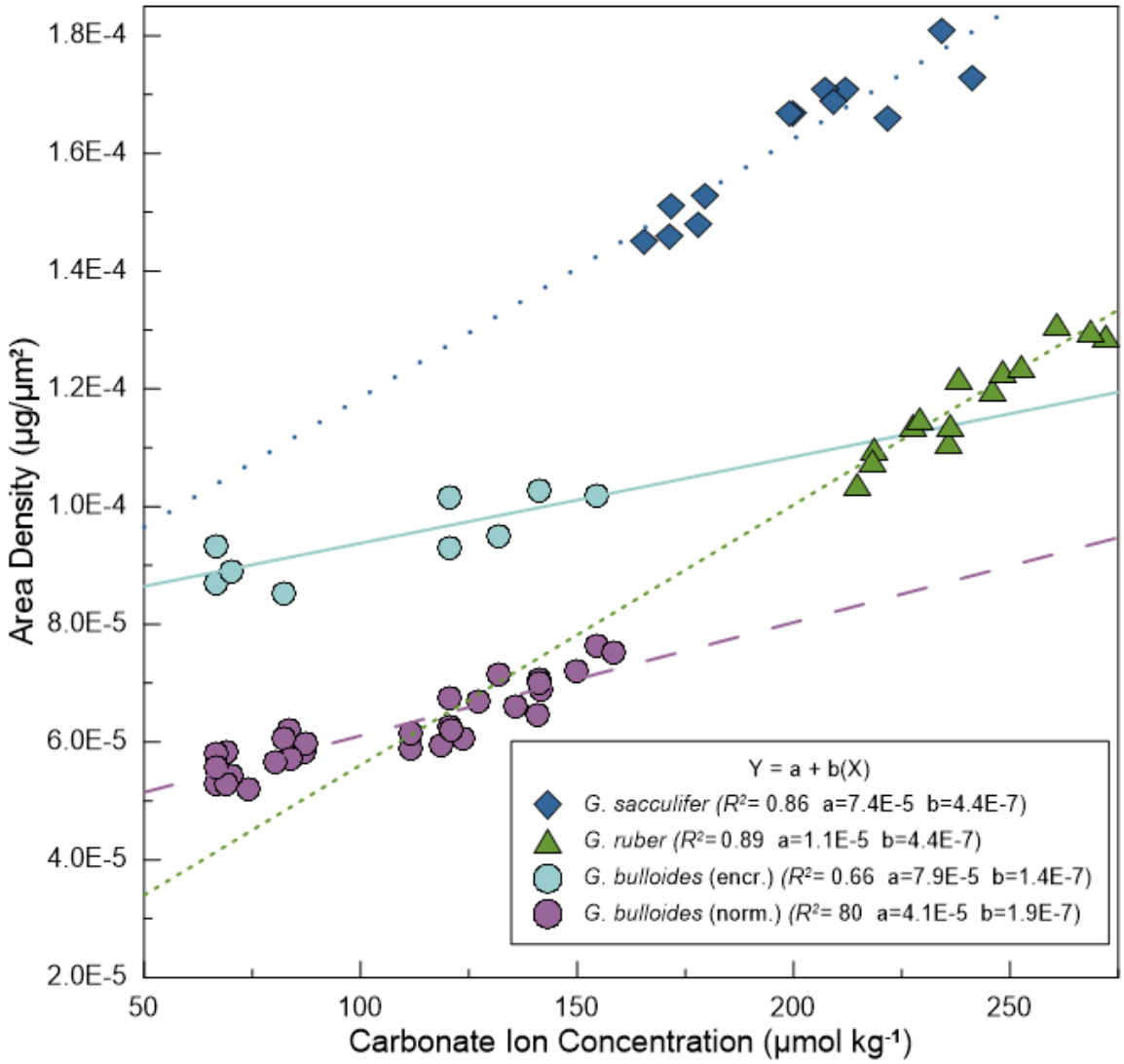


Figure 1.10 Comparison of area density calibrations for *G. bulloides* (normal and encrusted) (this study) and *G. ruber* and *G. sacculifer* [*Marshall et al.*, 2013]

# CHAPTER 2

## NATURAL AND ANTHROPOGENIC OCEAN ACIDIFICATION IN THE CALIFORNIA CURRENT AND CONSEQUENCES FOR MARINE CALCIFIERS

## 2.1 Abstract

The oceanic uptake of anthropogenic carbon mitigates climate change, but also results in global ocean acidification, i.e., an increase in ocean acidity and a corresponding reduction in the carbonate ion concentration ($[CO_3^{2-}]$). While the global-mean changes are well constrained by the changes in atmospheric $CO_2$, much less is known about the regional evolution of ocean acidification. Here, we use the calcification history recorded by fossil shells of calcifying zooplankton to reconstruct the progression of surface ocean acidification over the last century in the central California Current Ecosystem. Our records indicate a 20% reduction in calcification since ~1900, translating to a 35% decline in $[CO_3^{2-}]$ over this period. This larger than expected decrease is the result of a substantial regional modification of the global mean trends, driven primarily by stronger upwelling. This is supported by distinct signals in the concurrently recorded $^{13}C/^{12}C$ and $^{18}O/^{16}O$ isotopic composition of the carbonates. Our record also reveals a substantial interannual to decadal modulation of ocean acidification in the California Current Ecosystem by the Pacific Decadal Oscillation and the El Niño Southern Oscillation, modulations that are expected to continue influencing the future evolution. Based on the historic record, we predict that an unabated increase in atmospheric $CO_2$ will lead to a strong reduction in calcification of planktonic foraminifera.

## 2.2 Introduction

Over the last 150 years fossil fuel consumption, land use change and cement production have caused annual mean atmospheric $CO_2$ to increase from preindustrial levels of ~280 ppm to more than 400 ppm (Figure 2.1). At the same time an estimated

equivalent of 73 ppm of atmospheric $CO_2$ has been sequestered by the ocean (Khatiwala et al., 2013; Le Quéré et al., 2015) resulting in a 0.1 reduction in global mean surface pH (Sabine et al., 2004; Brewer, 1997; Le Quéré et al., 2014). The rate of $CO_2$ release has increased exponentially over this time period with the vast majority (>80%) of anthropogenic $CO_2$ emissions having occured over the last century, particularly since the year 1960. As the marine carbonate system has shifted to accommodate more carbon, the concentration of the dissolved carbonate ion ($CO_3^{2-}$) has decreased significantly as it is consumed via buffering reactions to maintain seawater pH (Figure 2.1). Many marine calcifiers that depend on the availability of $CO_3^{2-}$ to precipitate their calcium carbonate ($CaCO_3$) shells and skeletons respond adversely to the wide-scale changes occurring in the surface ocean (Feely et al., 2004; Sabine et al., 2004; Orr et al., 2005; Ries et al., 2009). Field studies of corals, coccolithophores, pteropods, and foraminifera, the ocean's major pelagic calcium carbonate producing organisms, have repeatedly indicated calcification stress in response to declining [$CO_3^{2-}$] (e.g. De'ath et al., 2009; Meier et al., 2014; Moy et al., 2009; de Moel et al., 2009; Bednarsek et al., 2014; 2016).

Marine calcifiers depend on the availability of dissolved ions in seawater, predominantly $Ca^{2+}$ and $CO_3^{2-}$, to form their shells and skeletons. Studies have shown that the reduced availability of $CO_3^{2-}$ results in inhibited calcification for a host of calcifying organisms, including but not limited to corals, mussels, oysters, pteropods and foraminifera, all of which are found in the CCS (Fabry et al., 2008; Hauri et al., 2009; Ries et al., 2009; Kroeker et al., 2013). While the reduction in the availability of $CO_3^{2-}$ hinders the ability of many organisms to form $CaCO_3$, the associated decline in pH as a

result of increasing [$H^+$] (Eq. 1) corresponds with a reduction in carbonate saturation state of seawater and dissolution of $CaCO_3$ (Eq. 2).

$$CO_2 + H_2O \rightleftharpoons H_2CO_3 \rightleftharpoons HCO_3^- + H^+ \rightleftharpoons CO_3^{2-} + 2H^+ \quad (1)$$

$$CO_2 + CaCO_3(s) + H_2O \rightleftharpoons 2HCO_3^- + Ca^{2+} \quad (2)$$

Planktonic foraminifera are ubiquitous calcite-secreting zooplankton that live for approximately 1 month and form their calcite shells in the upper several hundred meters of the water column. A recent plankton survey indicated that Rhizaria, a protist super-group of which foraminifera are a predominant constituent, comprise on average 30% of the total zooplankton population in the upper 500 meters of the water column in the global ocean, with estimates as high as 80% for the coastal upwelling zone off of California (Baird et al., 2016). Zooplankton represent the trophic level between primary producers and upper-trophic levels and therefore play a key role in marine food webs (Doney et al., 2012). Foraminifera are a particularly important group of calcifying zooplankton in that they that are responsible for a significant portion of the pelagic calcium carbonate flux (Schiebel, 2002; Kucera, 2007; Lebrato et al., 2010). Calcium carbonate and opal biominerals and dust particles act as mineral ballasts that facilitate the flux of organic carbon to the deep ocean that provides a net sink for atmospheric $CO_2$ on centennial time-scales (Armstrong et al., 2002). A global compilation of sediment trap data indicate that calcium carbonate biominerals account for an estimated 80% of particulate organic carbon flux below 1000 m due to the abundance and high density of $CaCO_3$ (Klaas & Archer, 2002)

Both modeling studies and observations suggest that ocean acidification (OA) will be particularly acute in coastal upwelling systems due to the low buffer capacity of these waters and natural upwelling processes that bring $CO_2$-rich intermediate waters to the ocean surface (Orr et al., 2005; Feely et al., 2008, 2010, 2016; Fabry et al., 2009; Hauri et al., 2009; Gruber et al., 2012). The California Current Ecosystem (CCE), a highly productive coastal upwelling system, has been identified as one of these vulnerable regions based on both observational and modeling studies (Feely et al., 2008; Gruber et al., 2012; Hauri et al., 2013; Turi et al., 2016). *In situ* measurements over the last decade indicate a considerable decline in $[CO_3^{2-}]$ in the CCE and shoaling of the saturation horizons for each of the $CaCO_3$ mineral polymorphs (calcite $\Omega_{cal}$ and aragonite $\Omega_{arg}$), reducing the volume of the surface ocean suitable for calcification. Model simulations suggest the aragonite saturation horizon in the CCE has already shoaled an estimated 150 meters since around 1850 (Gruber et al., 2012; Hauri et al., 2013; Turi et al., 2016). Model results are supported by observations of malformed and dissolved shells of aragonite-forming zooplankton (pteropods), particularly during periods of strong upwelling when the saturation horizon at times intersects with the sea surface (Bednarsek et al., 2014, 2016).

Direct observations of the marine carbonate system in the CCE are limited to the last decade (CalCOFI; 2009-Present) and initial surveys of the global ocean took place in the late 1970's as a part of the Geochemical Ocean Sections Study (GEOSECS), well after anthropogenic carbon began altering the marine carbonate system (GEOSECS; Takahashi et al., 1982). GEOSECS has been followed up by a number of globally distributed long-term monitoring programs, which have invariably indicated that the mean surface water pH

and [$CO_3^{2-}$] have declined over the last several decades as a result of increasing $pCO_2$ (Bates et al., 2014). While these observational records are critically important to our understanding of ocean chemistry, they do not provide a sufficiently long historical insight to this problem. Model simulations can close this gap but without constraints from *in situ* and/or proxy measurements, their validity remains unknown, especially with regard to their ability to capture variability. With atmospheric $CO_2$ concentrations projected to reach anywhere from less than 500 to more than 900 ppm by the close of the 21$^{st}$ century, understanding how pH and [$CO_3^{2-}$] have declined over the last century is central to projecting how the marine carbonate system will respond in the future (IPCC AR5 Report). The lack of long-term OA records currently limits our ability to put recent observations into the context of past changes and hinders assessing how natural decadal climate variability affects the marine carbonate system. Here, we provide the first century-long OA record for the CCE, which has been shown to be particularly susceptible when it comes to OA. This century-long record of [$CO_3^{2-}$] is in agreement with *in situ* measurements collected during the last decade and confirms the progression of OA suggested by models. In addition, our results show large variations in [$CO_3^{2-}$] associated with Pacific Decadal Oscillation (PDO) climatic forcing. If the relationship between PDO and OA is a widespread phenomenon, then we can expect OA will be modulated by this climatic state, thereby shifting the time of emergence of the anthropogenic signal into the future. Despite this modulation, the anthropogenic signal is large, with the past history implying very low $CO_3^{2-}$ levels in the near future.

## 2.3 METHODS

### 2.3.1 CALCIFICATION INTENSITY

A recent sediment trap study conducted in the Santa Barbara Basin, California found that calcification of the surface-mixed layer planktonic foraminifera species, *Globigerina bulloides*, is strongly controlled by ambient [$CO_3^{2-}$] (Osborne et al., 2016). This study as well as others demonstrate that shell wall thickness varies as a function of [$CO_3^{2-}$] and therefore this shell characteristic can be used as a proxy for [$CO_3^{2-}$] (Spero et al., 1997; Bijma et al., 1999; Barker & Elderfield, 2002; Marshall et al., 2013; Osborne et al., 2016). Foraminiferal calcification intensity, represented by both rate and efficiency of calcification, is defined as the amount of calcite deposited relative to the size of the individual and thereby generally reflects shell thickness (Weinkauf et al., 2013). In order to properly estimate foraminiferal calcification intensity, size-normalization is of vital importance because shell size, which inherently effects overall shell weight, is not controlled by ambient [$CO_3^{2-}$] but rather seawater temperature.

While several shell weight size-normalization techniques used to estimate calcification intensity exist, we chose to use the area density method, which is an area-normalizing shell weight method that uses individual rather than bulk population measurements (Marshall et al., 2013). This method is currently the most effective size-normalization technique (compared to measure-based weights and sieve-based weights) that best constrains shell thickness. Approximately 40 individual *G. bulloides* shells were picked from the >150 µm size-fraction of each sediment sample for area density analyses. Individual *G. bulloides* shells with abnormally formed shells or that had visible clay and/or organic material were excluded from our analyses as these characteristics could

effect weight and area measurements. While there can still be a considerable amount of variability within a single sediment sample, statistical analyses by Osborne et al. (2016) indicate that taking the average of at least 40 individuals significantly decreases the standard error of the mean. Each shell is individually weighed in a copper weigh boat using a high precision microbalance (Mettler Toledo XP2U; ±0.43 µg) in an environmentally controlled weigh room. Next, each individual is photographed positioned umbilical side up using a binocular microscope (Zeiss Stemi 2000-C) fitted with a camera (Point Grey Research Flea3 1394b). The microscopic imaging program (Orbicule Macnification 2.0) was used to analyze shells photos for length (Feret diameter) and the 2-D surface area or silhouette. The Macnification 2.0 program uses the RGB images to calculate a region of interest and generates an outline of the shell image, which is then used to estimate a pixel 2-D area. Pixel measurements are converted to lengths (µm) and areas ($\mu m^2$) by calibrating an image of a 1 mm microscale taken at the same magnification and working distance as shell photos. Individual shell weights were then divided by their corresponding areas and a mean area density value was calculated for each sample population.

The presence of an encrusted cryptic morphospecies of *G. bulloides* has been documented in the Santa Barbara Channel (Sautter and Thunell, 1991; Darling et al., 2003; Bemis et al., 2002). Further investigation indicated that the less abundant and cool water loving "encrusted" morphospecies calcifies and fractionates stable carbon and oxygen isotopes differently than the more abundant "normal" morphospecies (Bemis et al., 2002; Osborne et al., 2016). Due to the offset in calcification intensity and the intention to use these *G. bulloides* shells for later stable isotope analyses, morphometric

measurements collected during area density processing are also used to identify and remove encrusted individuals from our sample populations (Osborne et al., 2016; Marshall et al., 2015). The species-specific area density response of the normal *Globigerina bulloides* morphospecies to ambient [$CO_3^{2-}$] has been constrained using individuals collected in the Santa Barbara Basin (SBB) by a sediment trap time-series (Equation 2). Stable isotope results from this 3.5-year sediment-trap analysis indicate that on average *G. bulloides* calcify in the 40 m depth range, although seasonal variability in depth habit does occur in association with upwelling.

$$\text{Calcification Intensity } (\mu g/\mu m^2) = 1.92^{-7} ([CO_3^{2-}]) + 4.19^{-5} \quad (1)$$

### 2.3.2 Stable Isotope Measurements

At least 100µg (30-40 individuals) of *G. bulloides* used for area density analyses were pooled to measure the stable oxygen ($\delta^{18}O$) and carbon ($\delta^{13}C$) isotopic composition. Foraminifera were cleaned for 30 minutes in 3% $H_2O_2$ followed by a brief sonication and acetone rinse prior to analyses. Stable isotope measurements were carried out on an Isoprime isotope ratio mass spectrometer equipped with a carbonate preparation system. The long-term standard reproducibility is 0.07‰ for $\delta^{18}O$ and 0.06‰ for $\delta^{13}C$. Results are reported relative to Vienna Pee Dee Belemnite (V-PDB).

### 2.3.3 Box Core Sediments

A 0.5-meter long box-core collected in the Santa Barbara Basin was used for the down core analyses included in this study (SBB; 34˚14'N, 120˚02'W; 580 m water depth). An age model for this core was developed using $^{210}Pb$ geochronology with an error of less than 1 year (Osborne et al., 2016). The lowermost sediments date back to the year 1895 and the uppermost sediments represent the year 2005 (average sedimentation rate 0.34

cm $yr^{-1}$). The upper 10 centimeters of the core was sampled at half-centimeter resolution and the lower 40 centimeters were sampled at centimeter resolution. High-resolution sampling allows for nearly annual resolution for the upper 20 years of the core and roughly ~2 year resolution for the lower 80 years of the core.

### 2.3.4 Marine carbonate System Calculations

The marine carbonate system for the historic record was calculated using the proxy [$CO_3^{2-}$] estimates and a salinity-based estimate of total alkalinity (Fassbender et al., 2016). We estimate the seawater boron concentration using a chlorinity relationship derived for North Pacific (Lee et al., 2010) and then determine the concentration of [$HCO_3^-$] using the formulation for total alkalinity (Equation 2). In order to estimate DIC we sum the estimated [$CO_3^{2-}$] with the derived [$HCO_3^-$] and assume that any concentration of [$CO_2$] is less than 1% of DIC (Zeebe and Wolf-Gladrow, 2001; Equation 3). We assume a constant seawater temperature and salinity based on the mean surface temperature from the Santa Barbara Basin and salinity from Scripps Pier (salinity) Shore Stations 50 year time-series and assume surface pressure of 1 for these calculations (T=16 ˚C, S=33.5 ppt, P=1 atm).

$$\text{Total Alkalinity} = [HCO_3^-]+2[CO_3^{2-}]+[B(OH)_4^-] \quad (2)$$

$$\text{Dissolved Inorganic Carbon} = [HCO_3^-]+[CO_3^{2-}] \quad (3)$$

For the projection of the carbonate system in to the future we use projected atmospheric $CO_2$ to estimate $pCO_2$ following Henry's Law and again assume a constant total alkalinity. Henry's Law constants ($K_0$) were determined using the R package by Jean-Marie Epitalon, Aurelien Proye, and Jean-Pierre Gattuso. The $K_0$ determined as a

part of this package follow the formulation of Weiss (1974) and account for changes in temperature, salinity and pressure. We assume a constant seawater temperature, salinity and pressure for these calculations (T=16 ˚C, S=33.5 ppt, P=1 atm).

$$pCO2(\mu atm)=XCO_2(ppm)(p\text{Atm}-pH_2O)$$

$XCO_2$= Projected $[CO_2]$

$p$Atm= 1

$pH_2O$= determined in R according to *Weiss*, (1974)

The saturation state of seawater was calculated using the proxy $[CO_3^{2-}]$ values for the historic record or the predicted $[CO_3^{2-}]$ values for the forward projection. Calculations were made using the CO2Sys program assuming that the concentration of calcium in seawater has remained constant (10.28 mmol $kg^{-1}$; Broecker and Peng, 1982). Stoichiometric solubility constants determined by Mucci (1983) for each mineral were used in these calculations. We again assume a constant seawater temperature, salinity and pressure for these calculations (T=16 ˚C, S=33.5 ppt, P=1 atm).

## 2.4 Results and Discussion

### 2.4.1 Calcification and Thinning Shells Over the Last Century

The calcification intensity of nearly 2,000 individual *G. bulloides* shells was measured using 52 sediment samples from a 0.5-meter long box-core collected in the Santa Barbara Basin (SBB; 34˚14'N, 120˚02'W; 580 m water depth; Table 2.1). The *G. bulloides* used for our calcification intensity measurements were also used for oxygen and carbon stable isotopic composition analyses. Down core calcification intensity and

shell size measurements indicate that *G. bulloides* produced 20% thinner and 7% larger shells, respectively, by the close of the 20$^{th}$ century relative to those from 1900. The relationship between increasing shell size and warming sea surface temperatures is evident in the comparison of shell diameter and the oxygen isotopic composition of the same *G. bulloides* shells (Figure 2.2) *Globigerina bulloides* calcification intensity was converted to [$CO_3^{2-}$] using the relationship derived for this species from the SBB (Osborne et al., 2016).

Estimates of [$CO_3^{2-}$] from calcification intensity indicate an ~35% decline in surface ocean [$CO_3^{2-}$] over the 20$^{th}$ century (271 to 173 ±16 µmol kg$^{-1}$) or nearly a 100 µmol kg$^{-1}$ change (Figure 2.3). The decline in calcification is apparent in scanning electron micrographs of shell wall cross sections of similarly sized *G. bulloides* from the top and bottom of the sediment core (Figure 2.3). Our proxy-based [$CO_3^{2-}$] estimates are compared to results from a hindcast model simulation determined for various depths within the SBB water column from 1979 to 2012. These simulations of the carbonate system are based on an eddy-resolving ocean biogeochemical model forced with observation-based variations of wind stress and fluxes of heat and freshwater (Turi et al., 2016). The modeled long-term trend is in agreement with our proxy record. However, the model simulations indicate overall lower [$CO_3^{2-}$] values relative to our estimates based on calcification intensity, in part due an overall negative bias in the model (Hauri et al., 2013). Recent *in situ* surface ocean [$CO_3^{2-}$] measurements from the Santa Barbara Basin by the California Cooperative Oceanic Fisheries Investigation (CalCOFI; 2009-2015) and NOAA's Ocean Acidification Program (2011-2013) are in excellent agreement with the trend of our estimated [$CO_3^{2-}$] values although these datasets do not overlap with our

sediment record. An additional comparison to the oligotrophic North Pacific (Hawaii Ocean Time-series) also shows a similar long-term decline albeit with significantly higher [$CO_3^{2-}$] values, reflecting the subtropical location of this time-series. This regional difference illustrates the inherently low [$CO_3^{2-}$] conditions in the CCE.

Because the relative concentrations of the dissolved inorganic carbon species (DIC; $CO_2$, $HCO_3^-$, $CO_3^{2-}$) co-vary in a predictable nature so do the variables of the marine carbonate system (DIC, Total Alkalinity, pH, $pCO_2$). Six equations with 4 unknowns represent the variables of the marine carbonate system, and therefore knowledge of two variables can be used to determine the remainder of the system. Using our down core [$CO_3^{2-}$] values and salinity-based estimate of total alkalinity (Fassbender et al., 2016) we estimated how pH has evolved over the last century (Table 2.2). We estimate that the [$H^+$] of seawater has increased by 90%, translating to a 0.25 unit decline in pH in this region (8.17-7.92), thereby exceeding the global average of 0.1 units by more than a factor of two. Our estimated decadal rate of pH decline for this region over the last century (-0.025 $dec^{-1}$) is slightly higher than the rate of pH decline modeled recently for the entire California Current System (-0.020 $dec^{-1}$; 1979-2012; Turi et al., 2016), and more broadly with observations for the North Pacific (-0.017 $dec^{-1}$; 1991-2006; Byrne et al., 2010) and the HOT time-series (-0.019 $dec^{-1}$). Regional model simulations for the CCE emphasize that the central portion of the system, where our study region is located, has experienced a large decline in pH as a result of focused strong upwelling (Gruber et al., 2012; Turi et al., 2016).

The saturation state of seawater with respect to calcium carbonate ($\Omega$) was also quantified using our [$CO_3^{2-}$] estimates. Because the concentration of calcium in seawater

([$Ca^{2+}$]; 10.28 mmol $kg^{-1}$) is conservative, [$CO_3^{2-}$] can be considered the dominant control on Ω. An Ω value of 1 indicates that the water mass is saturated with respect to $CaCO_3$, while values above 1 represent supersaturated conditions where calcification is favored and values below 1 indicate an undersaturated environment where $CaCO_3$ preferentially dissolves. The long-term trend in our reconstruction indicates that Ω of the mineral form calcite (Ωcal) decreased by 1.5 units (4.6-3.1), while the Ω of the mineral aragonite (Ωarg) decreased by 1 unit (3.0-2.0) representing a 50% decline in saturation states since 1900. Episodic acidification events result in saturation states that can be as low as 2.43 Ωcal and 1.56 Ωarg. The decadal rate of decline in Ωarg recorded in our proxy reconstruction (-0.10 $dec^{-1}$) is comparable to model estimates for the upper 60 m of the water column spanning the last ~35 years for the entire CCS (-0.12 $dec^{-1}$; 1979-2012; Turi et al., 2016).

### 2.4.1 Climatic Modulation of Ocean Acidification

While we attribute the long-term decline in [$CO_3^{2-}$] to anthropogenic $CO_2$-driven ocean acidification, there is also considerable decadal and sub-decadal scale variability around the long-term trend. In order to best visualize this variability, we have removed the long-term anthropogenic trend in [$CO_3^{2-}$] and compare the detrended [$CO_3^{2-}$] record to a Pacific Decadal Oscillation index (Hare et al., 1996). This comparison reveals that decadal fluctuations in [$CO_3^{2-}$] co-vary with shifts between positive and negative phases of PDO (Figure 2.4). During positive (warm) phases of PDO the carbonate system shifts to a higher [$CO_3^{2-}$] state, while negative (cool) phases of PDO coincide with overall lower [$CO_3^{2-}$] values (Figure 2.4a). PDO is associated with changes in the strength of the Aleutian Low, resulting in basin-wide temperature, pressure and wind stress anomalies in

the Pacific (Mantua and Hare, 2002). Within the CCE, the positive (warm) phase of PDO coincides with weaker Aleutian Low winds, resulting in decreased coastal upwelling, warmer sea surface temperatures and reduced productivity. Conversely, the negative (cold) phase of PDO produces the opposite set of conditions.

Since coastal upwelling controls the amount of acidic subsurface waters that reach the surface and PDO regulates the strength of upwelling, we hypothesize that this mechanism alters the surface carbonate system on decadal time-scales. We use a two-pronged approach to test if decadal shifts in upwelling strength are recorded in our study region and if they are found in association with PDO shifts. First we use the stable oxygen isotopic composition ($\delta^{18}O$) as a temperature proxy to compare values recorded by a surface (*G. bulloides*) and a deep (*Neogloboquadrina incompta*) dwelling foraminifera species. An increased offset ($\Delta\delta^{18}O$) in the temperatures recorded by the surface and deep dwelling species represents an increase in stratification or a decline in upwelling strength (Pak and Kennett, 2002). The $\Delta\delta^{18}O$ is positively correlated with the PDO index; positive phases are marked by a higher $\Delta\delta^{18}O$, which represent decreased upwelling/increased stratification (Figure 2.4b). A reduction in upwelling of low pH waters would alleviate the bottom-up stress on the surface carbonate system, giving rise to higher surface [$CO_3^{2-}$]. We also use the stable carbon isotopic composition ($\delta^{13}C$) of *G. bulloides* shells, which records the isotopic composition of DIC (Ferguson et al., 2013). The seasonal signal in $\delta^{13}C$ recorded by *G. bulloides* in our study region varies inversely with upwelling strength (Figure 2.5); lower $\delta^{13}C$ coincides with peak upwelling when the subsurface DIC that is $^{12}C$-enriched due to remineralization is introduced to the surface. After removing the long-term decline in $\delta^{13}C$ due to the $^{13}C$ Suess Effect (Keeling et al.,

1979; Figure 2.6), we find that the residual changes in $\delta^{13}C$ positively correlate with PDO and our $\Delta\delta^{18}O$ record (Figure 2.4b). This confirms that upwelling weakens in the CCE during positive PDO resulting in higher than expected [$CO_3^{2-}$] during these periods and strengthens during negative phases of PDO resulting in lower than expected [$CO_3^{2-}$]. These upwelling records also indicate a long-term increase in stratification (Figure 2.7), which is supported by CalCOFI (1950-present) observations of warming sea surface temperatures, deepening of the thermocline depth and declining zooplankton biomass (Roemmich and McGowan, 1995; McGowan et al., 2003; Di Lorenzo et al., 2003).

The El Niño Southern Oscillation (ENSO) also correlates with sub-decadal shifts in the [$CO_3^{2-}$] record. El Niño events, typically lasting 6-18 months, produce similar anomalies as positive PDO phases and are marked by decreased windstress, reduced upwelling, and elevated [$CO_3^{2-}$], while La Niña events are similar to negative PDO phases and coincide with lower [$CO_3^{2-}$]. Five years of continuous observations from a mooring in the SBB observed the progression of the 2010 La Niña confirming the relationship between La Niña, increased coastal upwelling and increased acidity of surface waters off the continental shelf of California (Nam et al., 2011). We observe several rapid, extreme acidification events that unexpectedly coincide with the three largest El Niño events of the last century (1997/1998, 1982/1983 and 1986/1987) (Figure 2.8). The anomalous declines in [$CO_3^{2-}$] associated with these specific El Niño events are also captured in the hindcast model simulations for the SBB (Turi et al., 2015; Figure 2.9). This deviation from the typical trend of elevated [$CO_3^{2-}$] in association with El Niño events is likely owing to the substantial shift in surface current dynamics that occur during exceptionally strong El Niño conditions that result in the advection of low pH

waters from the Equatorial Pacific to the coastal California region (Bograd and Lynn, 2001; Di Lorenzo et al., 2005; Nam et al., 2015). This phenomenon suggests that not only chemical but also physical processes play an important role in marine carbonate system dynamics in this region.

### 2.4.1 Future Implication of Ocean Acidification on Plankton Calcification

Our record of foraminiferal calcification intensity and [$CO_3^{2-}$] during the last century provides insight as to how the carbonate system in the CCE may vary in the future. Projections of [$CO_3^{2-}$] through the end of the 21$^{st}$ century are generated based on the four atmospheric $CO_2$ Representative Concentration Pathways (RCP) scenarios (Table 2.3; Figure 2.10) described by the IPCC AR5 report (Chapter 12). RCPs represent a range of scenarios including a significant decline in $CO_2$ emissions (RCP 2.6, 421 ppm) to "business as usual" emissions (RCP 8.5, 936 ppm). The projections made here represent a baseline change that can be expected for this region and are in excellent agreement with global modeled carbonate system projections (Bopp et al., 2013; Table 2.4). However, a hindcast estimation of [$CO_3^{2-}$] using this technique indicates the net change in the marine carbonate system is underrepresented compared to our proxy reconstruction for this region. This is likely due to the fact that projections based only on atmospheric $CO_2$ concentrations and seawater alkalinity cannot represent the regional influence of upwelling. Therefore these projections represent a conservative estimate for the progression of ocean acidification in the CCE and large variations around the projected long-term trend should be expected based on the response of this system to climatic forcing observed in the historic record.

We highlight the results for the 538 ppm scenario (RCP 4.5) as it is an optimistic projection that meets the carbon emission and mean temperature goals (2˚ C temperature cap) set forth during the 2015 Paris climate agreements. Despite efforts to abate carbon emissions, under this scenario, $[CO_3^{2-}]$ decreases by an additional 25% by the close of the 21st century, representing a 54% decline in $[CO_3^{2-}]$ relative to the year 1900. Surface waters will likely remain supersaturated with respect to both aragonite and calcite on average, although modulation by PDO may result in undersaturation during negative PDO phases with episodic undersaturation in concert with strong El Niños and other extreme events (Hauri et al., 2013). Likewise, pH decreases by an additional 0.14 units over the course of the 21st century, resulting in a net 0.39 unit decline in pH since the beginning of the 20th century. Marine calcifiers that depend on the availability of $[CO_3^{2-}]$ will likely respond adversely to such conditions, with estimates for *G. bulloides* indicating at least a 30% reduction in calcification from 1900 to 2100. Under the business as usual scenario (RCP 8.5) scenario where $CO_2$ more than triples preindustrial values to 936 ppm, $[CO_3^{2-}]$ will likely decrease by 70% resulting in a 40% reduction in calcification. Episodic undersaturation as a result of climatic modulation becomes increasingly more likely as $[CO_3^{2-}]$ nears undersaturation thresholds under this scenario and permanent aragonite undersaturation in the surface ocean is likely by the close of the 21st century.

## 2.5 Conclusions

Our 20th century reconstruction of $[CO_3^{2-}]$ for the central CCE region underlines the significant shifts that have already occurred in the marine carbonate system over the last century in response to anthropogenic $CO_2$. This record also indicates that the marine

carbonate system experiences considerable variability, which we associate with shifts in costal upwelling strength related to PDO and ENSO. Over decadal time-scales positive/negative phases of PDO correlate with an overall elevated/reduced [$CO_3^{2-}$] state, indicating that anthropogenic acidification will be both amplified and dampened in association with decadal shifts in this climatic mode. Over shorter time-scales, ENSO correlates with [$CO_3^{2-}$] in the same fashion (El Niño/La Niña, elevated/reduced [$CO_3^{2-}$]). However very strong El Niño events produce anomalous conditions that deviate from the typical trend and are instead associated with dramatic and rapid acidification events. Various emission scenarios for the coming century indicate that [$CO_3^{2-}$] will continue to decline in response to anthropogenic $CO_2$ nearing permanent surface ocean undersaturation. The projected decline in calcification of planktonic foraminifera and other calcifiers will likely result in a reduction of the fraction of organic carbon reaching the seafloor via these ballasting minerals, consequently producing a positive feedback for $CO_2$ accumulation in the atmosphere and ocean. The response of the marine carbonate system is considerably different between each scenario indicating that reducing emissions is key to maintaining a surface ocean that is a suitable habitat for marine calcifiers. While projections of [$CO_3^{2-}$] are important for understanding how the system may progress in the future, our past record indicates [$CO_3^{2-}$] will not decline linearly and that modulation by climatic forcing will be important in the coming century.

Table 2.1 Down core ages and morphometric measurements

| Sample Number | Core Depth (cm) | Age | *n* | Area Density | Weight (ug) | Area ($um^2$) | Diameter (um) |
|---|---|---|---|---|---|---|---|
| 5 | 2.5 | 2002 | 39 | 7.38E-05 | 4.46 | 58373 | 307 |
| 6 | 3.0 | 2001 | 39 | 7.35E-05 | 4.79 | 64730 | 327 |
| 7 | 3.5 | 1999 | 38 | 7.90E-05 | 5.70 | 71948 | 340 |
| 8 | 4.0 | 1998 | 38 | 8.19621E-05 | 5.99 | 70435 | 339 |
| 9 | 4.5 | 1997 | 38 | 7.65E-05 | 4.81 | 62072 | 316 |
| 10 | 5.0 | 1996 | 29 | 6.56E-05 | 3.18 | 47321 | 267 |
| 11 | 5.5 | 1995 | 40 | 8.23E-05 | 4.72 | 57106 | 306 |
| 12 | 6.0 | 1994 | 40 | 8.24E-05 | 7.13 | 85885 | 381 |
| 13 | 6.5 | 1992 | 40 | 7.85E-05 | 6.20 | 77636 | 359 |
| 14 | 7.0 | 1991 | 39 | 7.94E-05 | 6.25 | 79605 | 364 |
| 15 | 7.5 | 1990 | 40 | 7.70E-05 | 4.53 | 56804 | 301 |
| 16 | 8.0 | 1989 | 37 | 8.01E-05 | 7.11 | 88434 | 385 |
| 17 | 8.5 | 1988 | 37 | 6.72E-05 | 3.93 | 53465 | 294 |
| 18 | 9.0 | 1987 | 17 |  | 3.57 | 52906 | 287 |
| 19 | 9.5 | 1986 | 40 | 7.55E-05 | 4.51 | 59296 | 313 |
| 20 | 10.0 | 1984 | 40 | 7.91E-05 | 5.13 | 64606 | 328 |
| 21 | 11.0 | 1982 | 28 | 6.80E-05 | 2.54 | 36812 | 242 |
| 22 | 12.0 | 1980 | 38 | 8.27E-05 | 6.87 | 83249 | 374 |
| 23 | 13.0 | 1977 | 40 | 7.39E-05 | 3.44 | 45509 | 270 |
| 24 | 14.0 | 1975 | 29 | 7.62E-05 | 3.32 | 43502 | 260 |
| 25 | 15.0 | 1973 | 38 | 8.32E-05 | 6.39 | 76960 | 355 |
| 26 | 16.0 | 1971 | 39 | 8.10E-05 | 5.47 | 68269 | 334 |
| 27 | 17.0 | 1968 | 18 | 7.30E-05 | 3.62 | 50341 | 278 |
| 28 | 18.0 | 1966 | 23 | 7.91E-05 | 3.67 | 45552 | 269 |
| 29 | 19.0 | 1964 | 34 | 8.63E-05 | 6.13 | 73619 | 346 |
| 30 | 20.0 | 1961 | 37 | 8.32E-05 | 6.29 | 79173 | 357 |
| 31 | 21.0 | 1959 | 40 | 8.06E-05 | 6.00 | 74304 | 352 |
| 32 | 22.0 | 1957 | 37 | 7.71E-05 | 5.52 | 78096 | 355 |
| 33 | 23.0 | 1954 | 40 | 7.83E-05 | 5.29 | 67781 | 334 |
| 34 | 24.0 | 1952 | 38 | 8.20E-05 | 4.26 | 59167 | 310 |
| 35 | 25.0 | 1950 | 32 | 8.90E-05 | 6.53 | 72870 | 349 |
| 36 | 26.0 | 1947 | 40 | 7.94E-05 | 5.73 | 72136 | 342 |
| 37 | 27.0 | 1945 | 36 | 8.08E-05 | 5.73 | 70943 | 342 |
| 38 | 28.0 | 1943 | 39 | 9.24E-05 | 5.04 | 54511 | 299 |
| 39 | 29.0 | 1941 | 38 | 9.63E-05 | 6.00 | 67339 | 331 |
| 40 | 30.0 | 1938 | 39 | 8.94E-05 | 4.87 | 62358 | 321 |

| | | | | | | | |
|---|---|---|---|---|---|---|---|
| 41 | 31.0 | 1936 | 40 | 9.39E-05 | 4.57 | 56911 | 305 |
| 42 | 32.0 | 1934 | 34 | 9.51E-05 | 3.73 | 45452 | 265 |
| 43 | 33.0 | 1931 | 27 | 9.75E-05 | 4.45 | 51212 | 285 |
| 44 | 34.0 | 1929 | 33 | 9.83E-05 | 4.15 | 54732 | 294 |
| 45 | 35.0 | 1927 | 37 | 8.49E-05 | 3.11 | 36889 | 242 |
| 46 | 36.0 | 1924 | 39 | 9.84E-05 | 4.84 | 57141 | 300 |
| 47 | 37.0 | 1922 | 40 | 9.56E-05 | 5.34 | 63047 | 323 |
| 48 | 38.0 | 1920 | 25 | 9.35E-05 | 4.48 | 55287 | 302 |
| 49 | 39.0 | 1917 | 38 | 8.99E-05 | 5.44 | 61554 | 318 |
| 50 | 40.0 | 1915 | 36 | 8.40E-05 | 4.64 | 57970 | 304 |
| 51 | 41.0 | 1913 | 38 | 8.28E-05 | 5.07 | 61423 | 324 |
| 52 | 42.0 | 1911 | 39 | 8.14E-05 | 5.77 | 65143 | 329 |
| 53 | 43.0 | 1908 | 39 | 8.40E-05 | 4.38 | 56820 | 307 |
| 54 | 44.0 | 1906 | 38 | 8.88E-05 | 5.83 | 70591 | 339 |
| 55 | 45.0 | 1904 | 23 | 9.25065E-05 | 4.33 | 47869 | 279 |
| 56 | 46.0 | 1901 | 27 | 9.71E-05 | 6.01 | 66762 | 324 |

Table 2.2 Down core estimates of the marine carbonate system

| Year | Salinity | Temp (˚C) | TA (mmol/kgSW) | TCO2 (mmol/kgSW) | pH | $CO_3^{2-}$ (mmol/kgSW) | ΩCa | ΩAr |
|---|---|---|---|---|---|---|---|---|
| 2003 | 33.5 | 16 | 2250.0 | 2083.6 | 7.93 | 126.1 | 3.04 | 1.95 |
| 2002 | 33.5 | 16 | 2250.0 | 2085.4 | 7.93 | 125.0 | 3.01 | 1.93 |
| 2000 | 33.5 | 16 | 2250.0 | 2056.6 | 7.99 | 142.5 | 3.43 | 2.20 |
| 1999 | 33.5 | 16 | 2250.0 | 2031.7 | 8.05 | 157.9 | 3.80 | 2.44 |
| 1998 | 33.5 | 16 | 2250.0 | 2060.5 | 7.98 | 140.1 | 3.38 | 2.17 |
| 1997 | 33.5 | 16 | 2250.0 | 2141.5 | 7.78 | 93.0 | 2.24 | 1.44 |
| 1996 | 33.5 | 16 | 2250.0 | 2039.5 | 8.03 | 153.0 | 3.69 | 2.37 |
| 1995 | 33.5 | 16 | 2250.0 | 2039.0 | 8.03 | 153.4 | 3.70 | 2.37 |
| 1993 | 33.5 | 16 | 2250.0 | 2059.1 | 7.99 | 140.9 | 3.39 | 2.18 |
| 1992 | 33.5 | 16 | 2250.0 | 2054.5 | 8.00 | 143.8 | 3.46 | 2.22 |
| 1991 | 33.5 | 16 | 2250.0 | 2067.2 | 7.97 | 136.0 | 3.28 | 2.10 |
| 1990 | 33.5 | 16 | 2250.0 | 2053.4 | 8.00 | 144.5 | 3.48 | 2.23 |
| 1989 | 33.5 | 16 | 2250.0 | 2089.7 | 7.92 | 122.5 | 2.95 | 1.89 |
| 1988 | 33.5 | 16 | 2250.0 | 2105.7 | 7.88 | 113.1 | 2.73 | 1.75 |
| 1987 | 33.5 | 16 | 2250.0 | 2075.1 | 7.95 | 131.2 | 3.16 | 2.03 |
| 1985 | 33.5 | 16 | 2250.0 | 2056.4 | 7.99 | 142.6 | 3.44 | 2.21 |
| 1983 | 33.5 | 16 | 2250.0 | 2113.9 | 7.85 | 108.4 | 2.61 | 1.68 |
| 1981 | 33.5 | 16 | 2250.0 | 2037.4 | 8.03 | 154.4 | 3.72 | 2.39 |
| 1978 | 33.5 | 16 | 2250.0 | 2083.3 | 7.93 | 126.3 | 3.04 | 1.95 |
| 1976 | 33.5 | 16 | 2250.0 | 2071.2 | 7.96 | 133.6 | 3.22 | 2.07 |
| 1974 | 33.5 | 16 | 2250.0 | 2034.9 | 8.04 | 155.9 | 3.76 | 2.41 |
| 1972 | 33.5 | 16 | 2250.0 | 2046.1 | 8.01 | 148.9 | 3.59 | 2.30 |
| 1969 | 33.5 | 16 | 2250.0 | 2088.1 | 7.92 | 123.4 | 2.97 | 1.91 |
| 1967 | 33.5 | 16 | 2250.0 | 2056.4 | 7.99 | 142.6 | 3.44 | 2.21 |
| 1965 | 33.5 | 16 | 2250.0 | 2018.6 | 8.07 | 166.1 | 4.00 | 2.57 |
| 1962 | 33.5 | 16 | 2250.0 | 2034.7 | 8.04 | 156.0 | 3.76 | 2.41 |
| 1960 | 33.5 | 16 | 2250.0 | 2048.4 | 8.01 | 147.5 | 3.55 | 2.28 |
| 1958 | 33.5 | 16 | 2250.0 | 2066.9 | 7.97 | 136.2 | 3.28 | 2.11 |
| 1955 | 33.5 | 16 | 2250.0 | 2060.6 | 7.98 | 140.1 | 3.37 | 2.17 |
| 1953 | 33.5 | 16 | 2250.0 | 2041.1 | 8.03 | 152.1 | 3.66 | 2.35 |
| 1951 | 33.5 | 16 | 2250.0 | 2004.9 | 8.10 | 174.8 | 4.21 | 2.70 |
| 1948 | 33.5 | 16 | 2250.0 | 2054.5 | 8.00 | 143.8 | 3.46 | 2.22 |
| 1946 | 33.5 | 16 | 2250.0 | 2047.4 | 8.01 | 148.1 | 3.57 | 2.29 |
| 1944 | 33.5 | 16 | 2250.0 | 1987.1 | 8.13 | 186.2 | 4.48 | 2.88 |
| 1942 | 33.5 | 16 | 2250.0 | 1966.9 | 8.17 | 199.1 | 4.80 | 3.08 |
| 1939 | 33.5 | 16 | 2250.0 | 2002.9 | 8.10 | 176.1 | 4.24 | 2.72 |
| 1937 | 33.5 | 16 | 2250.0 | 1978.9 | 8.15 | 191.4 | 4.61 | 2.96 |
| 1935 | 33.5 | 16 | 2250.0 | 1972.9 | 8.16 | 195.2 | 4.70 | 3.02 |
| 1932 | 33.5 | 16 | 2250.0 | 1960.5 | 8.18 | 203.3 | 4.90 | 3.14 |
| 1930 | 33.5 | 16 | 2250.0 | 1956.5 | 8.19 | 205.8 | 4.96 | 3.18 |
| 1925 | 33.5 | 16 | 2250.0 | 1955.5 | 8.19 | 206.5 | 4.97 | 3.19 |
| 1923 | 33.5 | 16 | 2250.0 | 1970.1 | 8.16 | 197.0 | 4.75 | 3.05 |
| 1921 | 33.5 | 16 | 2250.0 | 1981.0 | 8.14 | 190.0 | 4.58 | 2.94 |
| 1918 | 33.5 | 16 | 2250.0 | 2000.1 | 8.11 | 177.9 | 4.29 | 2.75 |

| | | | | | | | | |
|---|---|---|---|---|---|---|---|---|
| 1916 | 33.5 | 16 | 2250.0 | 2030.7 | 8.05 | 158.5 | 3.82 | 2.45 |
| 1914 | 33.5 | 16 | 2250.0 | 2036.8 | 8.03 | 154.7 | 3.73 | 2.39 |
| 1912 | 33.5 | 16 | 2250.0 | 2000.4 | 8.11 | 177.6 | 4.28 | 2.75 |
| 1909 | 33.5 | 16 | 2250.0 | 2030.9 | 8.05 | 158.4 | 3.82 | 2.45 |
| 1907 | 33.5 | 16 | 2250.0 | 2005.5 | 8.10 | 174.4 | 4.20 | 2.70 |
| 1905 | 33.5 | 16 | 2250.0 | 1986.4 | 8.13 | 186.6 | 4.49 | 2.89 |
| 1902 | 33.5 | 16 | 2250.0 | 1962.6 | 8.18 | 201.9 | 4.86 | 3.12 |
| 1898 | 33.5 | 16 | 2250.0 | 1977.3 | 8.15 | 192.5 | 4.64 | 2.98 |

Table 2.3 Projected changes in the marine carbonate system based on AR5 RCP scenarios

| | $CO_2$ | | | |
|---|---|---|---|---|
| Year | RCP 2.6 | RCP 4.5 | RCP 6.0 | RCP 8.5 |
| 2000 | 368.87 | 368.87 | 368.87 | 368.87 |
| 2005 | 378.81 | 378.81 | 378.81 | 378.81 |
| 2010 | 389.29 | 389.13 | 389.07 | 389.32 |
| 2020 | 412.07 | 411.13 | 409.36 | 415.78 |
| 2030 | 430.78 | 435.05 | 428.88 | 448.83 |
| 2040 | 440.22 | 460.85 | 450.70 | 489.44 |
| 2050 | 442.70 | 486.54 | 477.67 | 540.54 |
| 2060 | 441.67 | 508.87 | 510.63 | 603.52 |
| 2070 | 437.48 | 524.30 | 549.82 | 677.08 |
| 2080 | 431.62 | 531.14 | 594.26 | 758.18 |
| 2090 | 426.00 | 533.74 | 635.65 | 844.80 |
| 2100 | 420.90 | 538.36 | 669.72 | 935.87 |

| | $pCO_2$ | | | |
|---|---|---|---|---|
| Year | RCP 2.6 | RCP 4.5 | RCP 6.0 | RCP 8.5 |
| 2000 | 355.37 | 355.37 | 355.37 | 355.37 |
| 2005 | 364.95 | 364.95 | 364.95 | 364.95 |
| 2010 | 375.04 | 374.89 | 374.84 | 375.08 |
| 2020 | 396.99 | 396.09 | 394.38 | 400.57 |
| 2030 | 415.02 | 419.13 | 413.19 | 432.41 |
| 2040 | 424.12 | 443.98 | 434.21 | 471.53 |
| 2050 | 426.50 | 468.74 | 460.19 | 520.77 |
| 2060 | 425.51 | 490.25 | 491.95 | 581.44 |
| 2070 | 421.48 | 505.12 | 529.70 | 652.31 |
| 2080 | 415.83 | 511.71 | 572.52 | 730.44 |
| 2090 | 410.42 | 514.21 | 612.39 | 813.90 |
| 2100 | 405.50 | 518.66 | 645.22 | 901.64 |

| | $CO_3^{2-}$ | | | |
|---|---|---|---|---|
| Year | RCP 2.6 | RCP 4.5 | RCP 6.0 | RCP 8.5 |
| 2000 | 167.52 | 167.52 | 167.52 | 167.52 |
| 2005 | 164.48 | 164.48 | 164.48 | 164.48 |
| 2010 | 161.39 | 161.44 | 161.46 | 161.38 |
| 2020 | 155.08 | 155.33 | 155.80 | 154.10 |
| 2030 | 150.26 | 149.21 | 150.74 | 145.90 |
| 2040 | 147.95 | 143.13 | 145.46 | 136.97 |

| | | | | |
|---|---|---|---|---|
| 2050 | 147.35 | 137.57 | 139.44 | 127.20 |
| 2060 | 147.60 | 133.08 | 132.74 | 116.96 |
| 2070 | 148.61 | 130.15 | 125.58 | 106.93 |
| 2080 | 150.05 | 128.89 | 118.36 | 97.71 |
| 2090 | 151.46 | 128.42 | 112.35 | 89.49 |
| 2100 | 152.77 | 127.59 | 107.85 | 82.23 |

| | pH | | | |
|---|---|---|---|---|
| Year | RCP 2.6 | RCP 4.5 | RCP 6.0 | RCP 8.5 |
| 2000 | 8.08 | 8.08 | 8.08 | 8.08 |
| 2005 | 8.07 | 8.07 | 8.07 | 8.07 |
| 2010 | 8.06 | 8.06 | 8.06 | 8.06 |
| 2020 | 8.04 | 8.04 | 8.04 | 8.03 |
| 2030 | 8.02 | 8.01 | 8.02 | 8.00 |
| 2040 | 8.01 | 7.99 | 8.00 | 7.97 |
| 2050 | 8.01 | 7.97 | 7.98 | 7.93 |
| 2060 | 8.01 | 7.96 | 7.95 | 7.89 |
| 2070 | 8.01 | 7.94 | 7.93 | 7.85 |
| 2080 | 8.02 | 7.94 | 7.90 | 7.80 |
| 2090 | 8.02 | 7.94 | 7.87 | 7.76 |
| 2100 | 8.03 | 7.93 | 7.85 | 7.72 |

Table 2.4 Absolute values and relative changes of carbonate system parameters reconstructed for the 20th century from *G. bulloides* calcification intensity and projected parameters based on atmospheric $CO_2$ predictions. Only relative changes in projected pH are reported here due to high error propagation of calculating pH.

| | Year 1900 | Year 2000 | $\Delta_{2000-1900}$ | RCP 2.6 | $\Delta_{2100-2000}$ | RCP 4.5 | $\Delta_{2100-2000}$ | RCP 6.0 | $\Delta_{2100-2000}$ | RCP 8.5 | $\Delta_{2100-2000}$ |
|---|---|---|---|---|---|---|---|---|---|---|---|
| $CO_2$ (ppm) | 296 | 370 | 73 | 421 | 51 | 538 | 169 | 670 | 300 | 936 | 566 |
| $[CO_3^{2-}]$ (µmol/kgsw) | 271 | 173 | -98 | 153 | -20 | 128 | -45 | 108 | -65 | 82 | -91 |
| Ωarg | 3.0 | 2.0 | -1.0 | 1.8 | -0.2 | 1.4 | -0.6 | 1.1 | -0.9 | 0.7 | -1.3 |
| Ωcal | 4.6 | 3.1 | -1.5 | 2.8 | -0.4 | 2.2 | -1.0 | 1.7 | -1.4 | 1.1 | -2.1 |
| pH | 8.19 | 7.92 | -0.25 | | -0.05 | | -0.14 | | -0.23 | | -0.36 |
| pH (Bopp et al., 2013) | | | | | -0.07 | | -0.15 | | -0.22 | | -0.33 |

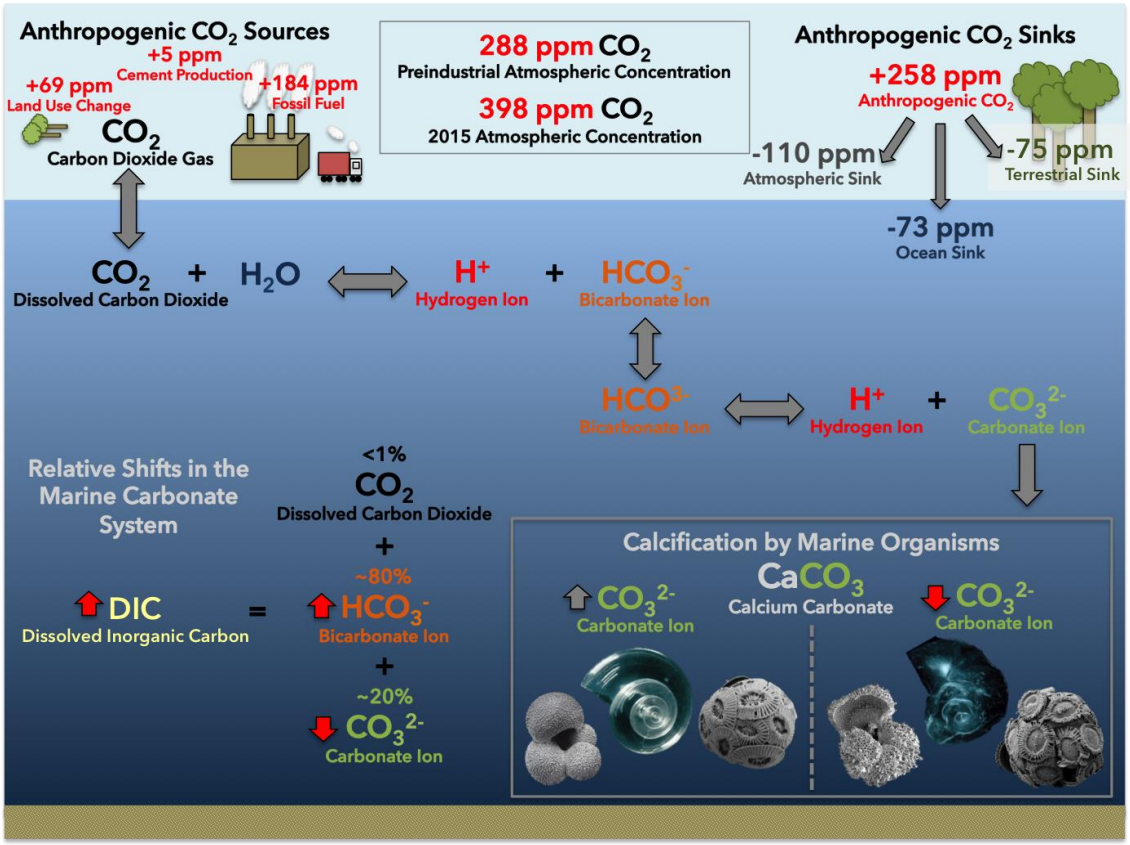


Figure 2.1 The increase in atmospheric $CO_2$ due to fossil fuel burning, land use change and cement production increases surface ocean $CO_2$ and causes a redistribution of dissolved inorganic carbon species (Le Quéré et al., 2015). $CO_2$ quickly reacts with water to form carbonic acid ($H_2CO_3$; not shown above), which almost instantaneously dissociates into a bicarbonate ion ($HCO_3^-$) and releases a hydrogen ion ($H^+$). The increase in $H^+$ as a result of this reaction lowers seawater pH ($pH=-\log(H^+)$), causing ocean acidification. Carbonate ion ($CO_3^{2-}$) reacts with increasingly concentrated $H^+$ to alleviate seawater acidity thereby forming more $HCO_3^-$. The decreased availability of $CO_3^{2-}$ adversely affects marine organisms that use this ion to build their $CaCO_3$ shells and skeletons. Images of planktonic foraminifera, pteropod and coccolithophore shells illustrate the effect of $CO_3^{2-}$ on shell formation (Images National Geographic Society, Müller et al., 2015).

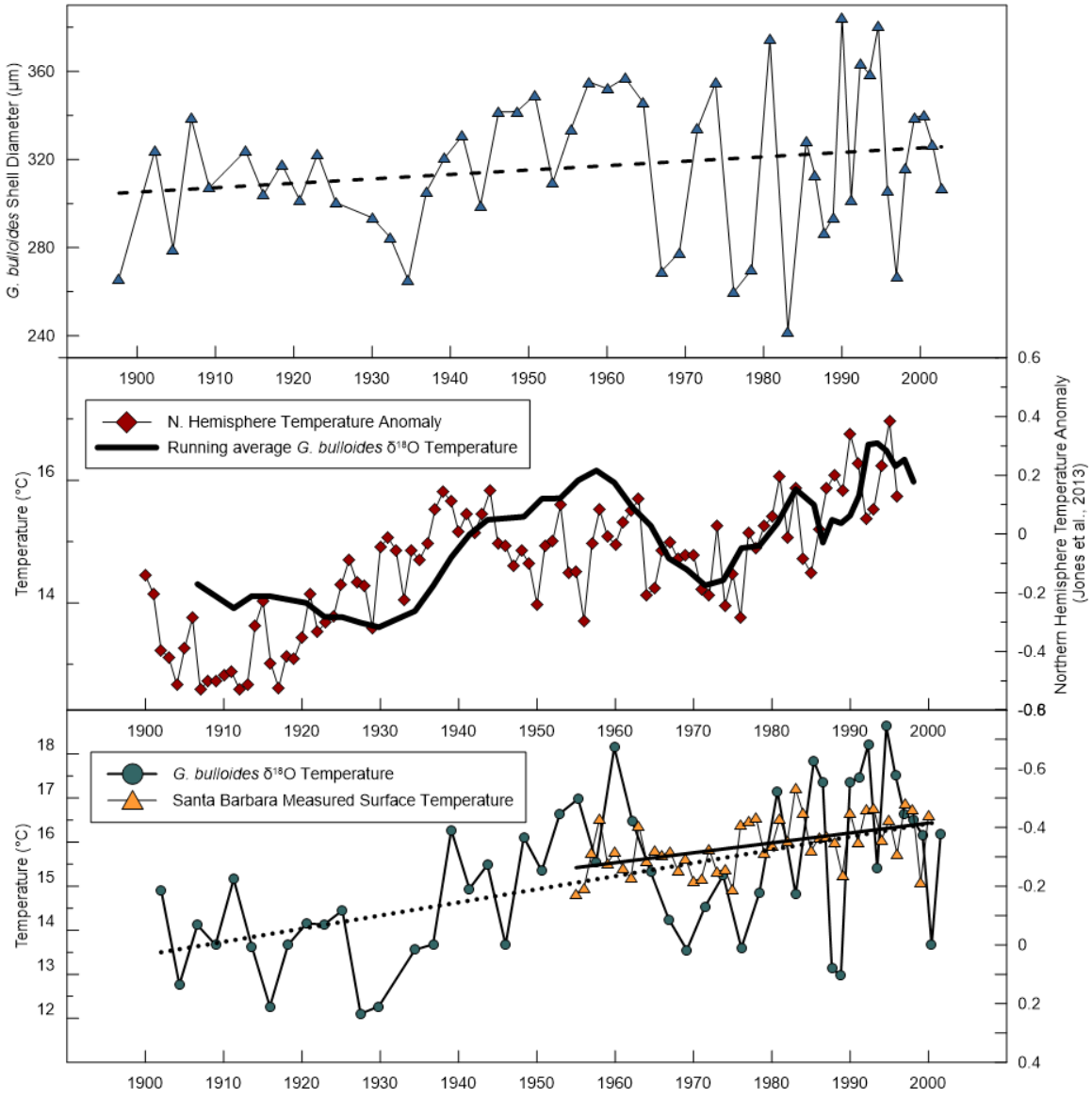


Figure 2.2 The long-term shift in *G. bulloides* shell diameter increases in concert with warming sea surface temperatures. We compare the relative changes that are recorded *G. bulloides* $\delta^{18}O$ to a Northern Hemisphere Temperature anomaly for the 1900-2000 period and see a good agreement between temperature trends recorded in these records (Jones et al., 2013). We also compared *G. bulloides* $\delta^{18}O$ to *in situ* sea surface temperature measurements made in the SBB (1955-Present; Shore Stations Program) and see an excellent agreements between sea surface temperature and the $\delta^{18}O$ recorded in our *G. bulloides* shells.

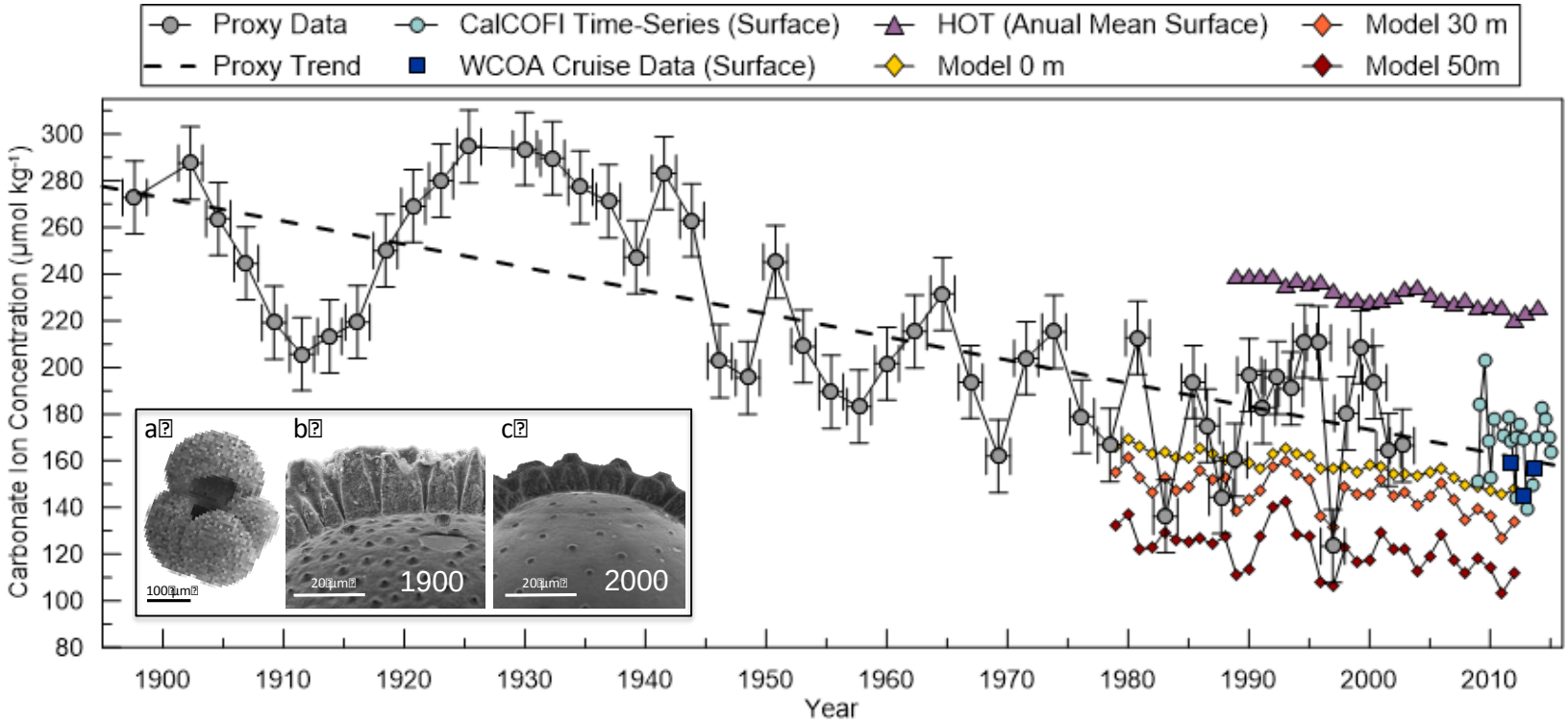


Figure 2.3 Estimated [$CO_3^{2-}$] derived from *G. bulloides* area density (1895-2000) compared to model simulations at 0, 30 and 50 meters (1979-2012) and *in situ* measurements from the Santa Barbara Basin made by CalCOFI and NOAA's West Coast OA Cruises and Hawaii Ocean Time-series (HOT) data from the oligotrophic North Pacific. (a) SEM images show a typical *G. bulloides* specimen from the SBB and shell wall cross-sections of similarly sized shells from the (b) upper- and (c) lower-most samples of the box-core clearly illustrating the difference in shell wall thickness over the past century.

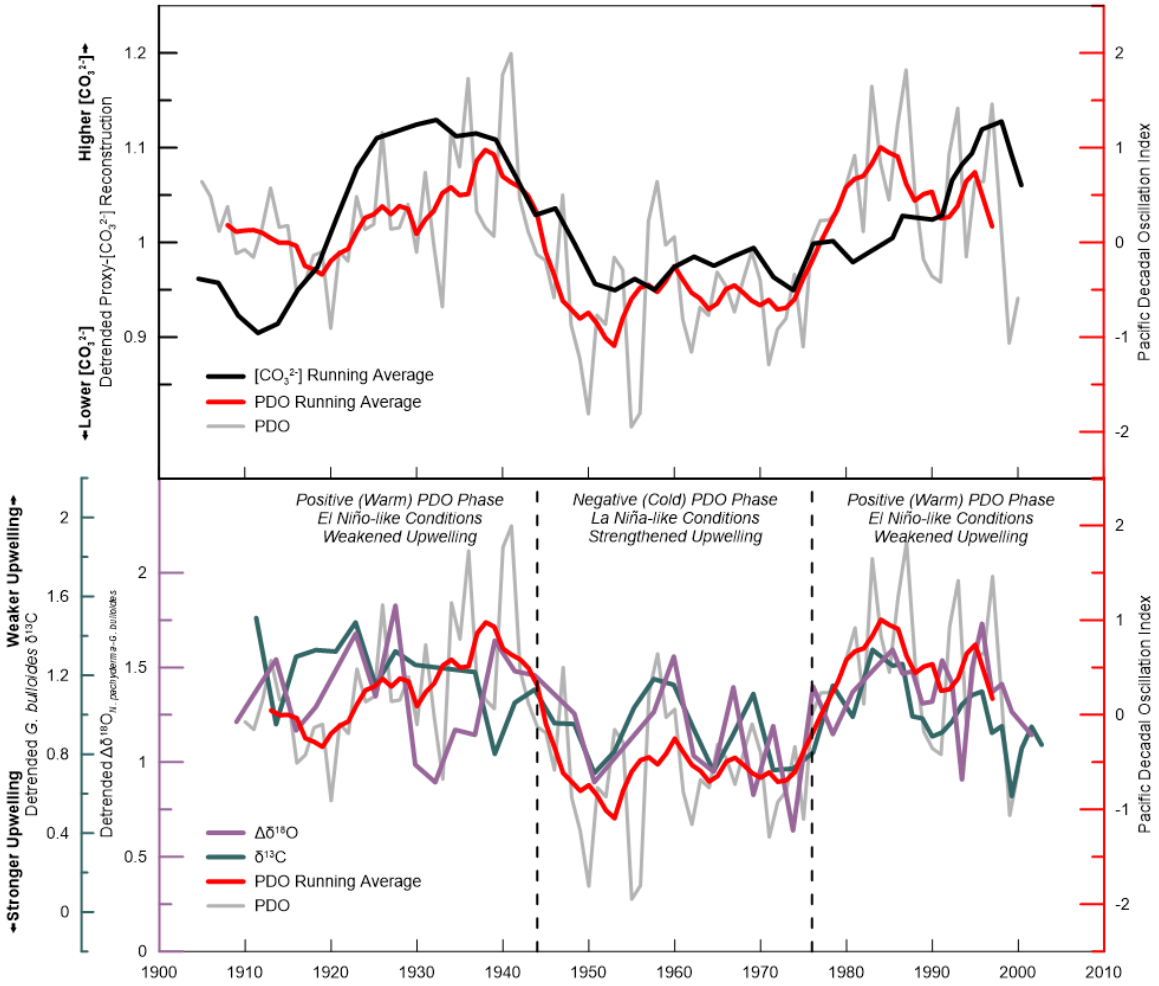


Figure 2.4 Upper panel shows the $[CO_3^{2-}]$ record with the long-term anthropogenically-driven decline removed. The detrended dataset is shown with the Pacific Decadal Oscillation (PDO) index indicating a correlation between high/low $[CO_3^{2-}]$ and positive/negative PDO phases. Both data sets are shown as 5-period running means. The lower panel shows detrended $\Delta\delta^{18}O_{\textit{N. incompta-G. bulloides}}$ and *G. bulloides* $\delta^{13}C$ again to highlight the natural variability not associated with anthropogenic ocean acidification. These datasets are plotted again with the PDO index indicating a relationship between weakened/strengthened upwelling and positive/negative PDO phase.

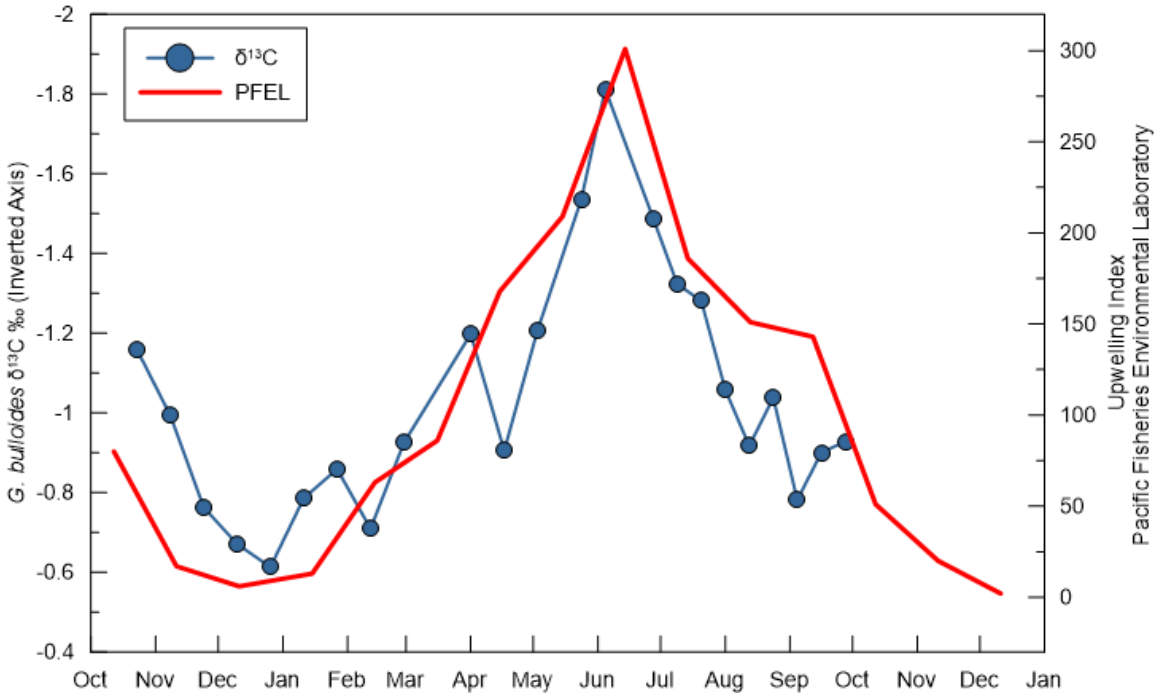


Figure 2.5 $\delta^{13}C$ of *G. bulloides* recorded in a year long (October 2013-October 2014) set of sediment trap samples from the Santa Barbara Basin. These data are plotted with an upwelling index from the Pacific Fisheries Environmental Laboratory (PFEL) with higher values indicating increased upwelling strength. Note that the $\delta^{13}C$ data are plotted on an inverted axis, therefore $\delta^{13}C$ and upwelling strength are inversely related. The more negative $\delta^{13}C$ values are associated with stronger upwelling of subsurface waters that are relatively $^{12}C$-enriched due to remineralization of organic matter.

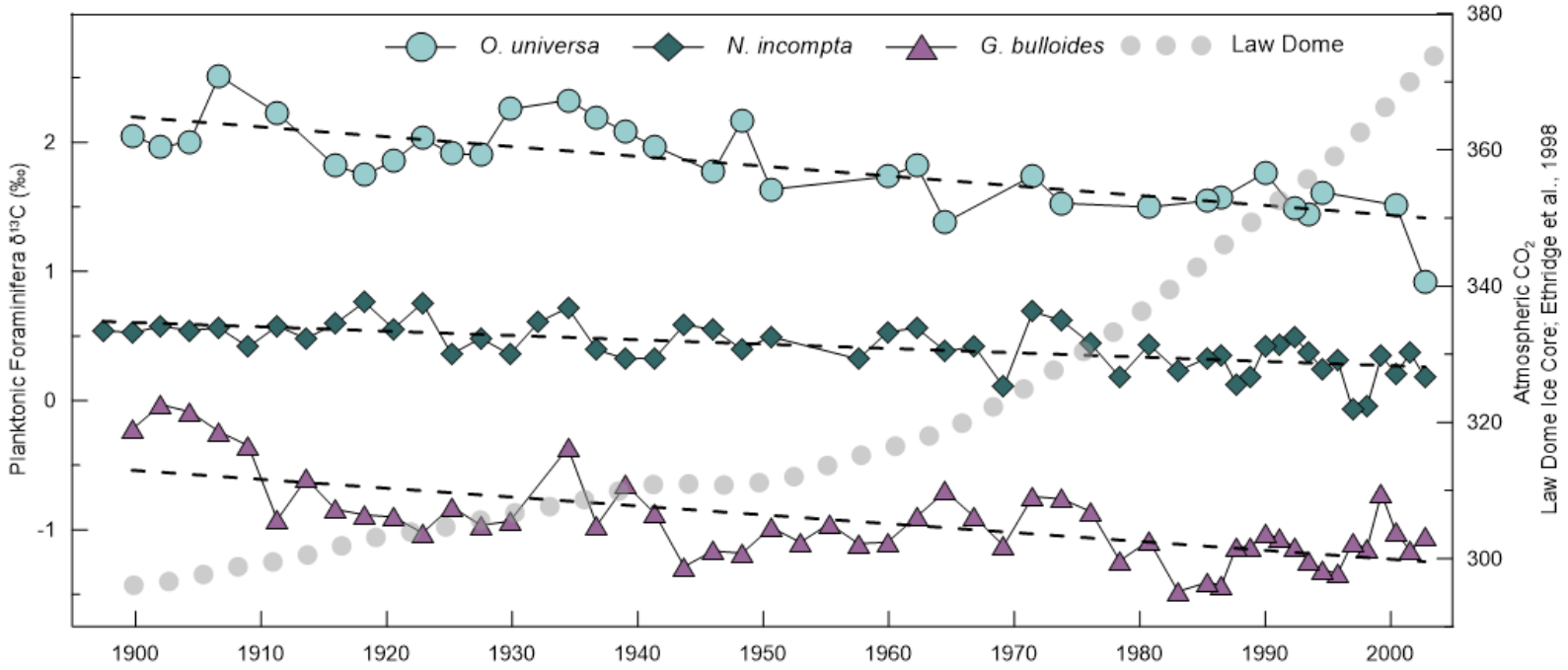


Figure 2.6 The negative trend in $\delta^{13}C$ recorded by several species of planktonic foraminifera (*Orbulina universa*, *G. bulloides* and *N. incompta*) over the down core record indicate the influence of fossil fuel carbon in the surface ocean referred to as the $^{13}C$ Suess Effect. These data are plotted with atmospheric $CO_2$ concentrations recorded from the Law Dome ice core record (Etheridge et al., 1998

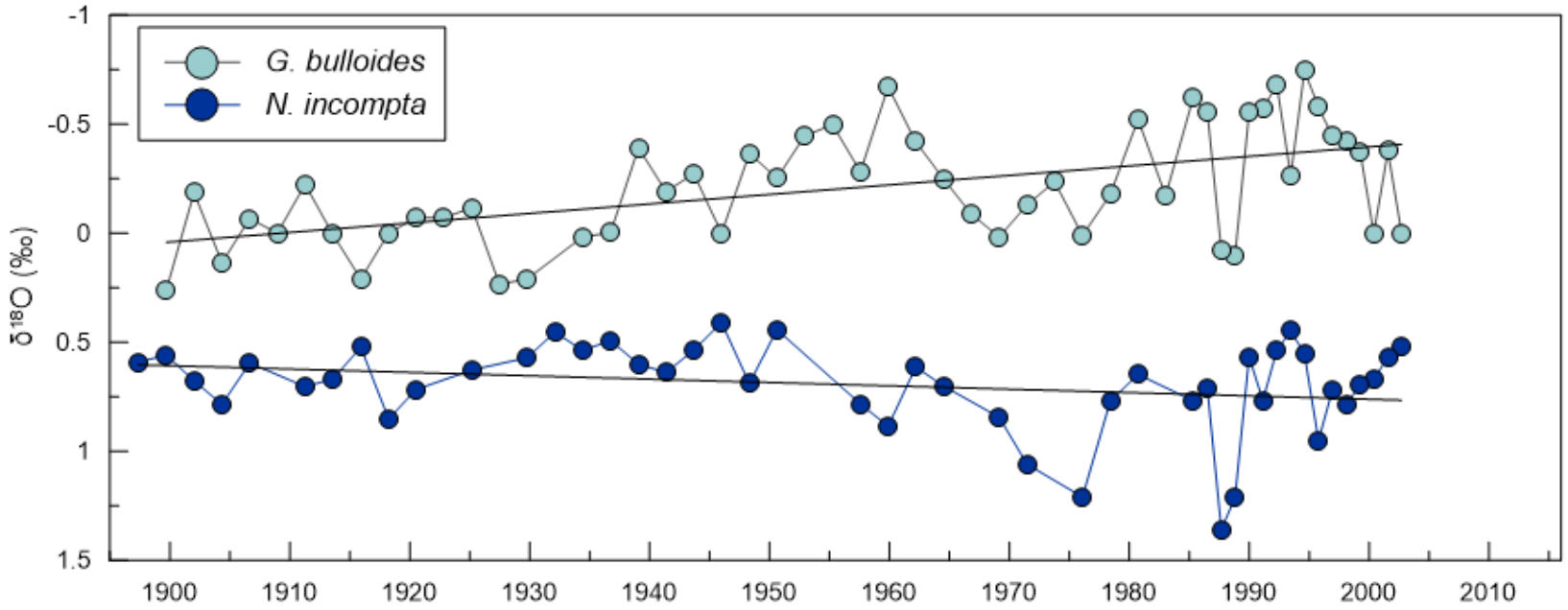


Figure 2.7 $\delta^{18}O$ of *G. bulloides* (surface-mixed layer) and *N. incompta* (sub-thermocline) measured over the last century. Because $\delta^{18}O$ and temperature are negatively correlated, these data are plotted on an inverted y-axis. $\delta^{18}O$ values for *G. bulloides* at present are more negative relative to values from 1900 indicating surface ocean warming. *N. incompta* $\delta^{18}O$ indicates the opposite trend suggesting that the calcification temperature for each of these species has diverged over the last century which we interpret here as an increase in stratification.

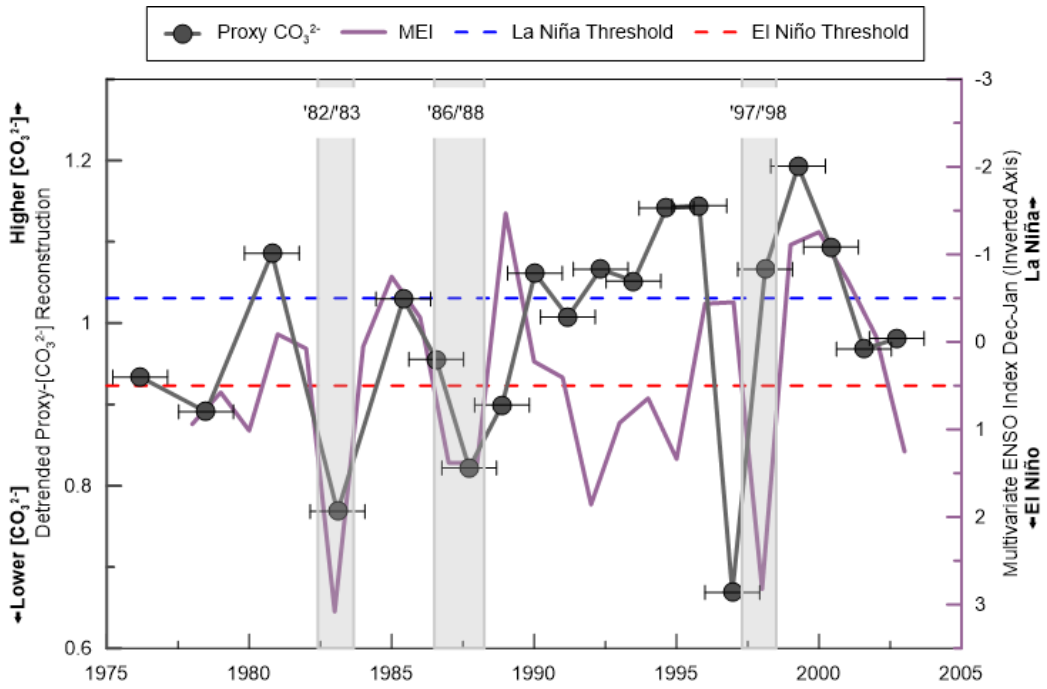


Figure 2.8 Three rapid acidification events recorded in the [$CO_3^{2-}$] reconstruction occur anomalously in association with strong El Niño events (1982/1983, 1986/1987 and 1997/1998). These data are shown with the Multivariate ENSO index (inverted axis). These events deviate from the typical relationship between positive MEI (El Niño) and elevated [$CO_3^{2-}$] which, for example, can be seen here from 1990-1995 when elevated [$CO_3^{2-}$] coincides with El Niño conditions.

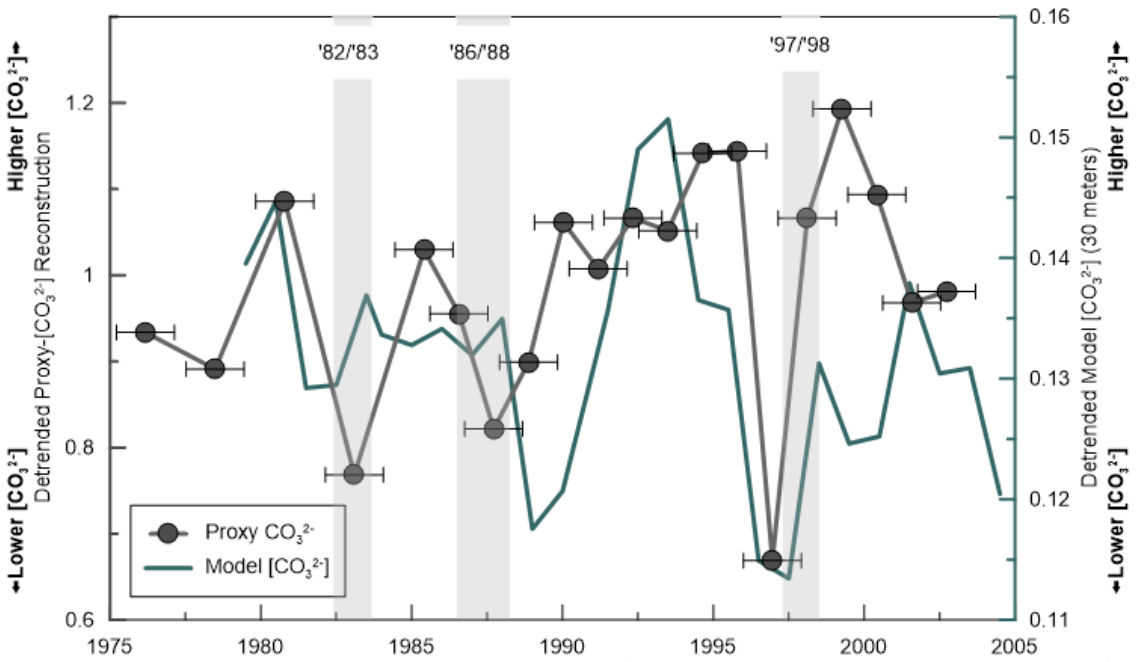


Figure 2.9 Comparison of detrended proxy [$CO_3^{2-}$] values to detrended modeled [$CO_3^{2-}$] values for the 1975-2005 interval when the three large El Nino events occur. While the exact timing of the 1982/3 and 1986/7 do not align as well as the 1997/8 event, errors in the age of the sediment samples suggest that the negative carbonate excisions could well overlap.

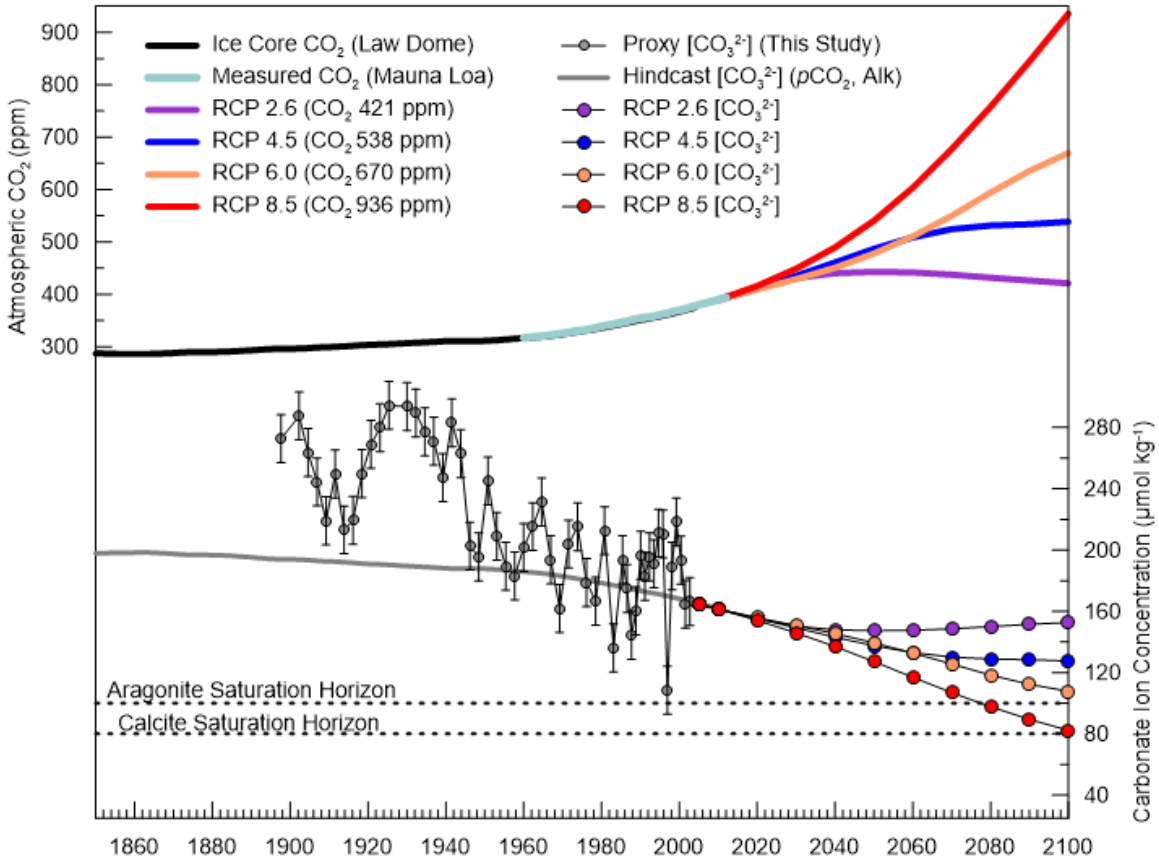


Figure 2.10 Projections of [$CO_3^{2-}$] in association with the four RCP $CO_2$ pathways outlined in the IPCC AR5 Report. Historic atmospheric $CO_2$ concentrations from the Mauna Loa Time-Series and the Law Dome Ice Core as well as our proxy [$CO_3^{2-}$] reconstruction are shown as a historical reference to the $CO_2$ model projections. The [$CO_3^{2-}$] at which aragonite and calcite become undersaturated are highlighted as dashed lines (Broecker and Peng, 1982).

# CHAPTER 3

## BORON CONCENTRATION OF NON-DINOFLAGELLATE HOSTING PLANKTONIC FORAMINIFERA CALCITE AND SEAWATER CARBONATE CHEMISTRY

## 3.1 ABSTRACT

The concentration of boron in marine carbonates (B/Ca ratio) has been proposed to covary with seawater carbonate chemistry. However, a number of studies have evaluated the B/Ca proxy in planktonic foraminifera and found that boron incorporation may not be a straightforward process. The majority of previous research has focused on tropical species that host large photosynthetic symbionts, which interfere with ambient carbonate chemistry and the incorporation of boron into the calcite lattice. This study focuses on evaluating the boron concentration of subtropical and subpolar species that are asymbiontic or host small intra-shell non-dinoflagellate symbionts. (*Globigerina bulloides*, *Neogloboquadrina incompta* and *Neogloboquadrina dutertrei*) collected as part of a time series sediment trap study in the Santa Barbara Basin (SBB). Replicate measurements of B/Ca ratios across size-fractions generally indicate no size-dependent uptake of boron that has previously been recorded for dinoflagellate symbiont bearing species. Both *Neogloboquadrina* species indicate strong correlation with the calcite saturation of seawater, carbonate ion concentration and pH. However the relationship between *G. bulloides* and these variables is more complex. The presence of two morphospecies of *G. bulloides* (encrusted and normal) in our sampling population may account for high B/Ca ratios and poor duplicates that occur in samples collected during winter and peak upwelling months when the encrusted morphospecies is present in the SBB. A further analysis of individual *G. bulloides* of each morphospecies from this study region is essential to determining if trace element offsets exist and to assess the influence that cryptic morphospecies have on bulk B/Ca ratios. Down core measurements of *N. incompta* B/Ca indicate a steady decline over the last century as a result of ocean

acidification that is in good agreement with carbonate system records developed for the region. We conclude that B/Ca ratios of non-dinoflagellate/symbiont-barren foraminifera faithfully record seawater carbonate chemistry. However inter-species and morphospecies differences may be significant and careful application of the B/Ca proxy to a single morphospecies is essential to creating meaningful data.

## 3.2 INTRODUCTION

Understanding past carbon cycling in the oceans is important to identifying processes that have influenced climate in the past and understanding how climate may progress in the future. To address this problem, considerable effort has gone into developing and applying proxies for the marine carbonate system, especially by using the fossil shells of calcifying zooplankton known as planktonic foraminifera that are widely preserved in marine sediments. The concentration of boron in the calcium carbonate produced by marine calcifiers, or the boron to calcium ratio (B/Ca), is one such proxy that has been proposed to covary with marine carbonate system variables.

The relative concentrations of the two aqueous species of dissolved B in seawater vary as a function of seawater pH. Low pH conditions coincide with higher concentrations of the trigonal species, boric acid ($B(OH)_3$) whereas high pH conditions coincide with the tetrahedral species, borate ion ($B(OH)_4^-$). Studies of the B isotopic composition of marine carbonates is similar to that of the isotopic composition of $B(OH)_4^-$ in seawater, suggesting that $B(OH)_4^-$ is preferentially incorporated into marine carbonates (Equation 1; Hemming and Hanson, 1992). To corroborate these results, a culture study using the planktic foraminifer *Orbulina universa* used an isotope mass

balance approach to estimate the fraction of boric acid incorporated for a low pH culture when boric acid incorporation would hypothetically be highest and found that only 3-8% of the total B was from boric acid (Allen et al., 2011). Therefore the concentration of B in planktic foraminifera should be positively correlated with seawater pH; higher pH, higher proportion of $B(OH)_4^-$, higher B/Ca. A theoretical framework for how B incorporates in to foraminiferal shells poses that the charged $B(OH)_4^-$ is attracted to the growth surface where it is de-hydroxylated to a trigonal form ($BO_3^{3-}$) during incorporation into the calcite structure (Equation 1; Hemming et al., 1995, 1998). This mechanism explains how a tetrahedral ion replaces a trigonal ion space in the calcite lattice and why the $\delta^{11}B$ of foraminifera shells reflect the $\delta^{11}B$ of the tetrahedral rather than the trigonal form of B. Further, synchotron x-ray spectromicroscopy of foraminiferal shells indicate B hosted in shell calcite is solely trigonal $BO_3$ (Branson et al., 2015).

$$CaCO_3 + B(OH)_4^- \Leftrightarrow CaHBO_3 + HCO_3^- + H_2O \quad (1)$$

Developing the B/Ca carbonate chemistry proxy, particularly for foraminifera, has been the focus of many core-top, culture and sediment trap studies. Culture experiments using three tropical spinose species of planktic foraminifera that harbor dinoflagellate symbionts (*Orbulina universa*, *Globigerinoides sacculifer* and *Globigerinoides ruber* (pink)) found that B/Ca ratios respond positively to increases in pH (Allen et al., 2011, 2012). These studies also showed that foraminiferal B/Ca had no significant response to large changes in temperature (Δ˚C 6-8) and a minor positive response to large increases in salinity (Δ 33-40). Shell wall profiles of cultured *Orbulina universa* and benthic *Amphistegina lessonii* documented high and low B banding within the shell wall that are anti-correlated with Mg/Ca banding (Allen et al., 2011; Branson et al., 2015). Banding

even occurred in *O. universa* shells when all seawater chemistry variables were held constant and only light was varied (12-hours dark, 12-hours light; Allen et al., 2011). The authors suggest that the banding could be an artifact of vital effects in relation to diurnal changes in symbiont photosynthetic activity (Allen et al., 2011). Dissolution-induced changes in B/Ca in two symbiont-bearing species (*G. sacculifer* and *G. ruber*) observed in core-top sediments further supports the observation that B incorporation into dinoflagellate symbiont-bearing species is heterogeneous (Dai et al., 2016). Furthermore the lack of dissolution effect on B/Ca ratios observed in these same core-top samples for two species that harbor small intra-shell algal symbionts (*N. dutertrei* and *P. obliquiloculata*), suggest that there is a homogeneous distribution of B in non-dinoflagellate bearing foraminiferal shells (Dai et al., 2016; Gastrich, 1987).

Despite positive culture results for *G. ruber*, a compilation of globally distributed plankton tow, sediment trap, and core top B/Ca data for *G. ruber* (white) shells indicates no significant relationship with carbonate chemistry and moderately strong correlations with nutrient concentration ($[PO_4^{3-}]$ $R^2$=0.33) and salinity ($R^2$=0.40) (Henehan et al., 2015). However, it is important to note that the individuals included in this compilation were a combination of the *G. ruber* white chromotype, which is compositely represented by four distinct geonotypes (Darling et al., 2008). A sediment trap evaluation of *G. ruber* B/Ca ratios from the Bermuda Atlantic Time Series (BATS) where there is little to no change in carbonate chemistry found a considerable seasonal signal of 20-30 µmol/mol B/Ca that could not be attributed to changing seawater pH (Babila et al., 2014). Additionally size-fraction replicates (200-300 µm and 300-400 µm) indicate an average 10-20% offset with higher B/Ca consistently observed in the larger sized foraminifera

samples (Babila et al., 2014). The authors conclude that increasing photosynthetic activity of dinoflagellate symbionts hosted on *G. ruber* spines elevate the ambient pH in the microevnrionment around the foraminifera so that larger individuals that host a greater number of symbionts have higher B/Ca ratios (Babila et al., 2014).

An additional sediment trap study (*G. ruber* (pink), *O. universa* and *G. truncatulinoides*) indicated a positive relationship between shell thickness (measured by area density) and B/Ca ratios, and concluded that carbonate chemistry did not exert control on B/Ca ratios but rather calcification rate (Salmon et al., 2016). Foraminiferal area density (measure of how much calcite is deposited relative to shell size) has been linked to calcification intensity, which reflects both calcification rate and efficiency (Osborne et al., 2016; Weinkauf et al., 2016; Marshall et al., 2013). Correlations between calcification rate and B/Ca ratios have also previously been reported in both foraminiferal core-top assessments and synthetic inorganic calcite precipitation studies (Ni et al., 2007; Uchikawa et al., 2015; Kaczmarek et al., 2015). Interestingly, studies that have applied the area density proxy thus far have shown that carbonate ion concentration is the main control on calcification intensity (area density), and therefore a correlation with B/Ca would inherently suggest a correlation with carbonate chemistry (Marshall et al., 2013; Weinkauf et al., 2016; Osborne et al., 2016).

A recent study of symbiont-barren foraminifera *(Neogloboquadrina incompta* and *Globigerina bulloides*) from North Pacific core-top samples found a strong positive correlation between B/Ca ratios and pH, carbonate ion concentration and the calcite saturation of seawater (Quintana Krupinaski et al., submitted). The positive result with asymbiontic foraminifera substantiates that B/Ca ratios of species that harbor

dinoflagellate symbionts should not be used as seawater carbonate chemistry proxies. In this study, we further evaluate B/Ca ratios of the asymbiotic species *N. incompta* and *G. bulloides* and also study *N. dutertrei* using sediment trap material from the Santa Barbara Basin (SBB), California. While *N. incompta* (non-spinose) and *G. bulloides* (spinose) are classified as symbiont-barren foraminifera, *N. dutertrei* (non-spinose) harbors small intracellular symbionts that could affect B incorporation (Hemleben et al., 1989).

## 3.3 Materials and Methods

### 3.3.1 Sediment Trap and Down Core Material

Planktonic foraminifera (*N. dutertrei*, *N. incompta* and *G. bulloides*) used in this study were collected as part of an ongoing sediment trap time series in the center of the SBB (34˚14'N, 120˚02'W, ~580 m water depth; Thunell; et al., 1995, 2007; Thunell, 1998; Figure 1.1). McLean Mark VII-W automated sediment traps equipped with 0.5 $m^2$ funnel openings are deployed for 6-month periods and samples are collected continuously on a bi-weekly basis. Of the two sediment traps on the mooring (~150 and ~480 m water depth), we primarily use samples collected by the upper trap. Sediment trap sample bottles are buffered and poisoned with a sodium azide solution prior to deployment. Recovered sediments have historically been split and archived using a sodium borate buffered solution. However, the main sample suite used in this study was collected in 2013-2015 and was split using unbuffered deionized water in order to prevent B contamination. These samples were immediately washed over a 125 µm sieve and dried in a 40˚C oven. Cleaning tests conducted on samples that were archived in sodium borate

buffer for varying amounts of time (6 months to 7 years) were used to determine if contamination as a result of the sodium borate archival process could be resolved.

Water column hydrographic and chemical data conducted on a monthly basis at the site of the sediment trap mooring by the Plumes and Blooms Program (http://www.oceancolor.ucsb.edu/plumes_and_blooms) were used in this study. However, because the Plumes and Blooms Program does not routinely measure carbonate chemistry variables, we use model simulations of the marine carbonate system for comparison with our foraminiferal geochemical data. Model simulations were developed for various depths using an eddy-resolving ocean biogeochemical model forced with observation-based variations of wind stress and fluxes of heat and freshwater (Turi et al., 2016). While the trends in modeled carbonate variables are in good agreement with *in situ* measurements, the overall values are not (Osborne et al., unpublished; Figure 3.1). A negative bias in the model has already been identified and has been attributed to the over emphasis of wind observations, which drive a stronger upwelling signal and result in lower pH carbonate system (Hauri et al., 2013). A comparison of surface calcite saturation values measured by the CalCOFI time-series in SBB indicates a relatively consistent offset of higher measured Ω calcite values compared to mean annual model data (Figure 3.2). A complication of *in situ* sea surface [$CO_3^{2-}$] measurements from 2007-2010 to coeval daily values estimated by the model also indicates an average offset in [$CO_3^{2-}$] that equate to a nearly identical Ω calcite offset observed in the annual time-series comparison. For the period when there are available *in situ* measurements of carbonate system variables and model datasets overlap (2007-2015), the mean offset between measured and model data are used to correct model values.

A down core record was also generated of B/Ca ratios of *N. incompta* that spans the last century. The 0.5 m box-core used in this study was collected in 2012 near the SBB sediment trap mooring and has been used for shell weight and stable isotope analyses of *G. bulloides* and stable isotope analyses of *N. dutertrei*. Due to this previous work, sediment material containing only *N. incompta* remained for down core trace element analyses. An age model was developed for this core using radiogenic activities of $^{210}$Pb and$^{137}$Cs and indicates that the lowermost sediments in the core date back to the year ~1900 (Osborne et al., 2016).

### 3.2.2 Trace Element Analyses

Typically 150-200 µg of foraminiferal calcite was pooled for each trace element analysis. Samples smaller than 100 µg often times did not provide sufficient material after the sample loss that occurs during the cleaning procedure. Foraminifera were picked from discrete size-fractions (150-250 µm, 250-355 µm, 355-425 µm and >425 µm) so that duplicate measurements for each species and sample could be measured when material was available. For *G. bulloides* and *N. incompta*, individuals from the smallest two size-fractions were only available and for some sampling periods only a single size-fraction was available due to low foraminiferal flux. Although it has been noted that two distinct genotypes of *G. bulloides* are present within the SBB (Darling et al., 2003), these cryptic morphospecies were not identified and separated for our trace element analyses.

Each sample was weighed and loaded in to 1.5 ml polypropylene centrifuge tube for sample cleaning. Samples were cleaned following the method of Boyle and Kegwin (1985). For the borate-buffered sediment trap samples used for the cleaning test portion

of the study, additional reductive and acid leach treatments were conducted. Prior to the final acid leach, cleaned samples were transferred to new 1.5 ml polypropylene vials that had been cleaned in a quartz-distilled 10% hydrochloric acid (HCl) reflux bath and rinsed with B-free MQ water. Sample cleaning and preparation took place in an over-pressured flow hood equipped with B-free HEPA filters to minimize atmospheric B contamination. All acids and 18.3 Mega-Ohm MQ water were mannitol-distilled using a Teflon distillation setup and stored in Teflon containers. Distillation of a 500 ml volume using 2 grams of mannitol would typically take place over the course of a week due to the low sub-boiling distillation temperature (80-90˚C).

Five gravimetrically prepared multi-element standard solutions were prepared for foraminiferal trace element analyses. Standard solutions were prepared using a fixed calcium concentration with varying concentrations of trace elements (Li, B, Mg, Al, Mn, Fe, Zn, Sr, Cd, U). Standard 0 was mixed with only calcium and is used analytically as the blank for Standards 1-4. Concentrations of the trace elements mixed in Standards 1-4 were chosen based on the previously measured ranges in planktonic foraminifera. Stock standard solutions were prepared at 1000 ppm calcium and stored in Teflon containers in a clean laboratory with controlled environmental conditions. Working standards were diluted to the desired calcium concentration to match sample calcium concentrations (typically 20 or 30 ppm) on the day of sample analysis using the same batch of acid used for sample preparation.

Trace element analyses were conducted using a Thermo Element II HR-ICP-MS. Instrumental settings and our analytical methods were adapted from Misra et al. (2014) In order to minimize the difficulty of measuring B in marine carbonates., specialized

equipment and analytical techniques were used in this study. The overall low concentration of B in foraminiferal calcite and high instrumental blank are addressed by using hydrofluoric acid (HF) in our mixed acid matrix. The use of HF limits the adsorption of B onto instrumental surfaces. Therefore the use of HF significantly reduces instrumental B blanks. A specialized Teflon spray chamber, platinum injector and platinum sample (normal) and skimmer (H) cones were used for B analyses due to their resistance to degradation as a result of prolonged contact with HF. A sample and standard mixed acid matrix of 0.1 N $HNO_3$ + 0.06 N HF were used in our analyses. A lower concentration of HF is used in our study relative to Misra et al. (2014; 0.1N $HNO_3$ + 0.3N HF) due to the instability of the high calcium concentration samples analyzed in our study. When the 0.3N HF mixed acid matrix was used in standard dilutions, back-to-back calibrations resulted in shifting Ca concentrations due to the reaction of HF with calcite and the formation of calcium fluoride precipitates in solution. When we attempted to use the 0.3N HF mixed acid matrix with our foraminiferal samples, calcium fluoride precipitates formed and would not redissolve. Results from Misra et al. (2014) indicate that a 0.06N HF concentration in the acid matrix still effectively washes out residual B in the system resolving the issue of carry over between sample analyses while maintaining a low B blank.

Dip checks, which are used to determine the calcium concentration of each sample, are essential to matrix-matching foraminiferal trace element samples to standards (Yu et al., 2005). Because calcium dominates foraminifera-based sample solutions, significant variations in calcium concentrations result in significant matrix effects. The low ionization potential of B has been illustrated by measuring a standard solution at

varying calcium concentrations, which results in lower B/Ca ratios being measured at higher calcium concentrations due to matrix induced mass-related discrimination (Yu et al., 2005; Misra et al., 2014). For this reason, using a sufficient sample size is also important to minimizing matrix effects. Small sample size results in a low calcium concentration of the stock sample dilution that is dissolved in 2% $HNO_3$. Therefore the sample dilution used for analysis has a relatively higher $HNO_3$ normality and lower HF normality due to the smaller volume of the mixed acid matrix used for dilution, resulting in matrix effects for these samples.

Just prior to analysis, samples are dissolved in 100 µl of mannitol-distilled 2% $HNO_3$ to create a concentrated stock of each sample. Acidified samples then are placed in a sonication bath for 30 minutes and individually vortexed to ensure full dissolution of sample material. Dip checks are conducted using a 10 µl aliquot of each concentrated sample stock and diluted up to a 200 µl volume using the 0.1N $HNO_3$ + 0.06N HF (20x dilution factor). The calcium concentration of each sample is determined relative to a 10 ppm calcium dilution of Standard 0. Calcium concentrations of the concentrated sample stocks are then used to create a sample dilution to the target calcium concentration for that analytical run. Typically the target calcium concentration for our foraminiferal analyses is 20 ppm however for *N. dutertrei* analytical runs, a 30 ppm calcium concentration is used due to the lower B concentration in this species. Sample dilutions are made in quartz-distilled HCL refluxed 1.5 ml polypropylene vials that are sonicated with mannitol-distilled B-free MQ immediately prior to use. The total volume of sample dilution ranged from 250-500 µl depending on the concentration and volume of solution needed of the concentrated stock sample. Down core dilutions were always measured in

400-500 µl dilutions due to unusual matrix effects that occurred in smaller sample dilutions of core samples.

Each analytical run began with a 5-minute acid matrix washout to minimize instrumental B blank. Following the washout a total of 4 acid matrix blanks and typically 4 procedural blanks in 1.5 ml polypropylene sample vials were measured. Standard solutions were then measured back-to-back in order of increasing multi-element concentration. Each foraminiferal sample was bracketed with a "dip" where the sample probe is immersed in a 15 ml vial of the acid matrix and then a sample-specific acid matrix blank after a take up time of 2.5 minutes. Sample specific blanks were prepared in quartz-distilled HCL refluxed 1.5 ml polypropylene vials that were sonicated with mannitol-distilled B-free MQ immediately prior to use. While the instrumental boron blank accounts on average for 20% of the B measured for a given sample, the standard deviation of blanks measured during a single analytical run are extremely consistent with standard deviations of repeat measurements representing only 5% of the blank value. Procedural blanks measured at the beginning of the first analytical run for that sample batch are almost always within error of instrumental blanks. Standard 2, which contains the multi-element concentrations most like the samples, was measured after every third sample as an internal consistency standard. A maximum of 15 samples were measured in a single analytical run so that drift would not affect the relationship between the standards measured at the beginning of the run and samples measured at the end of the run (approximately 2.5 hour sequence).

To assess the analytical precision of our B method for calcite matrix samples, we created a homogenized foraminifera standard. The foraminifera (*Globorotalia menardii*)

used to create our standard were taken from a single sediment trap sample representative of a 2-week sampling period from the Cariaco Basin Time-Series. A large foraminiferal bloom resulted in a huge accumulation of foraminifera, ideal for creating a large foraminifera-based standard. The approximately 10 mg of foraminifera were cleaned in 2 mg batches following the cleaning procedure described above for sample preparation. Approximately 200 µg subsamples of crushed and homogenized foraminifera were used for replicate measurements and resulted in excellent repeatability of both B/Ca and Mg/Ca measurements (Figure 3.3).

## 3.4 Results and Discussion

### 3.4.1 Trace Element Cleaning of Planktonic Foraminifera for Boron Analyses

In order to determine if sediment trap samples from the Santa Barbara Basin that were stored in sodium borate can be used for B analyses we conducted several cleaning tests. For the purpose of this study we examined samples collected from 2007-2010 when *in situ* carbonate system variables were measured and area density results were available (Osborne et al., 2016). Boron-free sediment trap treatments of the top trap began in mid-2013 while the bottom trap remained buffered with sodium borate. This allows us to make a direct comparison of the B/Ca in foraminifera from samples collected at the same time but treated differently (borate-treated vs. borate-free).

The first cleaning test determined the boron concentration of the leachates from each step conducted during the foraminifera trace element cleaning procedure of the borate treated samples (Boyle and Kegwin, 1985). First, samples underwent a clay removal process; a series of MQ and methanol sonication and rinses. Since the deep trap

sits in suboxic waters, treatments aimed at eliminating manganese-rich overgrowths that may form under low oxygen conditions (reductive step; sodium hydroxide buffered 4% hydrazine) and any organic matter retained on the surface or inside of foraminifera shells (oxidative step; sodium hydroxide buffered 1% hydrogen peroxide) were performed. The final step was a weak acid leach (0.001% nitric acid) in a 30 second to 1 minute sonication bath that is aimed at removing any chemical residues produced during the cleaning procedure. Due to the fact that high boron concentrations were anticipated for this test, we decided to repeat each of the cleaning steps. This would also help to devise a specialized cleaning procedure for borate treated samples by determining if doubling any of the cleaning steps would be more effective at removing the borate contamination. A 400 µl leachate aliquot from the final rinse after each cleaning step was acidified to a 0.1N HNO3 + 0.06 HF matrix and measured on the Element HR-ICP-MS.

The boron concentrations of the leachates decreased significantly (~50%) from the initial to final cleaning step (Figure 3.4). This suggests that borate contamination is not restricted to the surface of foraminiferal shells, as evidenced by initial rinses during the clay removal step accounting for approximately half of the boron removal. The next largest decrease in boron concentration occurs after the first reductive step accounting for approximately one-quarter of the boron removal. The aggressive nature of the chemical solution used in the reductive step typically results in the majority of calcite lost during the cleaning procedure and likely removes outer calcite layers that contain a considerable fraction of the boron contamination. An increase in boron concentration of the leachate from the first oxidative treatment is likely due to boron being mobilized from organic material that is oxidized during this step. The general consistency in boron concentration

between the two final acid leaches suggests that the boron in these leaches is the primary foraminiferal shell signal rather than contamination.

For the next cleaning test we compare the B/Ca ratios of *G. bulloides* and *N. dutertrei* calcite from a sample that had been stored in borate for six months. This sample was divided into four equal fractions for *G. bulloides* and five fractions of *N. dutertrei*. Due to the larger shell size and robustness during cleaning, there was more sample material available to conduct tests using *N. dutertrei*. Each fraction underwent different chemical cleaning steps (reductive, oxidative, acid leach). For both species, the first fraction underwent only clay and reductive treatments, the second underwent clay, reductive and oxidative treatments and the third fractions underwent clay, reductive, oxidative and varying levels of acid leach treatments. These results are compared to time-equivalent top trap samples that were not borate buffered and indicate that final B/Ca values for the buffered samples are within error of the non-buffered samples. For both species rigorous acid leach is essential for removing all of the B contamination. *Neogloboquardina dutertrei* required three 1 minute acid leaches and *G. bulloides* needed three 30-second acid leaches before the outer contaminated calcite layers were removed (Figure 3.5). Mg/Ca ratios were also measured for these samples and indicate that a more rigorous cleaning results in significantly lower Mg/Ca ratios, especially for *N. dutertrei* due to the fact that outer calcite layers are enriched in Mg and removal of this layer effects the whole shell Mg/Ca signal (Barker et al., 2003). However, boron is incorporated more homogenously through foraminiferal shells therefore preferential removal of the outer surface during more rigorous cleaning does not significantly affect the whole shell B/Ca ratios.

Based on the results of these cleaning tests, we applied a modified cleaning procedure to a series of borate-treated samples from the 2007-2010. In addition to the traditional cleaning protocol we added a second reductive treatment and a triple acid leach treatment. Despite this more aggressive cleaning, boron concentrations of *G. bulloides* from the borate buffered samples from 2007-2010 were often more than two times higher than expected B/Ca values (Figure 3.6). Based on these results we conclude that there is a time-dependent factor to how the borate buffer alters the original foraminiferal B/Ca. Therefore we suggest that samples archived in sodium borate buffer are not suitable for boron analyses even when additional cleaning steps are used.

### 3.4.2 Sediment Trap B/Ca Ratios in *Neogloboquadrina* Species

A total of 26 sediment trap samples from October 2013-October 2014 were used to generate a year-long time-series of B/Ca ratios for both *N. dutertrei* (Figure 3.7) and *N. incompta* (Figure 3.8). Ekman-induced upwelling that begins in February and persists through July results in an overall lower flux of both species during this period and produces some gaps in the B/Ca time-series. When sufficient sample material was available, replicate measurements of B/Ca ratios were made on different size-fractions (11 out of 19 *N. dutertrei* samples and 3 out of 17 *N. incompta* samples). The greater size range and larger individual mass of *N. dutertrei* easily allowed for replicate measurements, while the lower abundance and smaller individual size (generally restricted to the 150-255 µm size-fraction) of *N. incompta* hampered sample replication.

Replicate measurements indicate that both species generally yield B/Ca ratios within error regardless of shell size (Figure 3.7 and 3.8). This differs from previous

studies of dinoflagellate symbiont-bearing foraminifera that demonstrated that photosynthetic activity of symbionts result in poor replicate measurements across size-fractions (Babila et al., 2014). The result for *N. dutertrei* is particularly interesting due to the fact that this species does in fact harbor symbionts. However, the dinoflagellate symbionts hosted by some spinose foraminifera typically range from 8-12 µm in size, while many non-spinose species including *N. dutertrei* host coccoid alga that are 1.5-3.5 µm in size (Gastrich, 1987; Fehrenbacher et al., 2011). Our results reinforce that the relative activity of these small intracellular symbionts, which are limited by light, is much less than the large dinoflagellate symbionts that are found on extracellular spines of surface dwelling species (Gastrich, 1987).

The large errors associated with *N. dutertrei* B/Ca replicates in March and August 2014 are the result of small sample sizes ($n$ = 4, <100µg) for each measurement (Figure 3.7). As with other foraminiferal geochemical analyses ($\delta^{18}O$, Mg/Ca), ideally a large number of individuals are included in bulk measurements to reduce the noise of intersample variability (Killingley et al., 1981; Ganssen et al., 2011; Schiffelbein and Hills, 1984). In order to further demonstrate that size-fraction does not affect B/Ca ratios, replicate measurements using individuals spanning all size-fractions (150µm-425µm) were made on three samples from October-December 2013 when *N. dutertrei* were highly abundant,. These broad size-fraction replicates produced values within error of the other sample replicates. The excellent replication of B/Ca values for various sized *N. dutertrei* indicates that the presence of symbionts in this species does not influence the B signal.

We compare B/Ca ratios of each species to modeled water column data to assess the relationship between shell geochemistry and seawater carbonate chemistry. Previous studies have shown that it is important to use water column properties from the depth of calcification in order to establish the best relationship between shell geochemistry and seawater conditions. A study from the Southern California Bight indicate that the $\delta^{13}C$ of *N. incompta* (also referred to as *N. pachyderma* (right coiling)) and *N. dutertrei* from this region are in equilibrium with $\delta^{13}C$ at the thermocline or sub-thermocline depths, which range between 25-40 meters water depth during non-upwelling periods when these species are most abundant (Sautter and Thunell et al., 1991; Figure 3.9). MOCNESS tows conducted in the Equatorial Pacific collected *N. dutertrei* from the sea surface to over 1,000 meters water depth but oxygen and carbon isotopic results indicate that *N. dutertrei* calcite is in equilibrium with seawater at ~30 meters water depth (Fairbanks et al., 1982). This suggests that *N. dutertrei* produce the majority of their shell calcite at ~30 meters water depth and then descend through the water column during later life stages (Fairbanks et al., 1982). A $\delta^{18}O$ study of *N. incompta* from core-top samples from our study region suggest that the mean calcification depth of this species is also ~30 meters water depth (Quintana Krupinaski et al., submitted). Calcification depths for both species in the Santa Barbara Basin were estimated using Mg/Ca derived temperatures ](Figure 3.9). Using the Anand et al (2003) Mg/Ca:temperature equation for *N. dutertrei* and a mixed calibration for non-symbiont bearing species, we estimate average calcification depths for *N. dutertrei* and *N. incompta* of ~30 m and ~40 m respectively, over the course of the sediment trap sampling period.

A comparison B/Ca and Mg/Ca time-series for each species to the calcite saturation of seawater and temperature, respectively, modeled at 30 meters water depth for *N. dutertrei* and 40 meters water depth (Table 3.1) for *N. incompta* (Table 3.1), indicates an excellent agreement with seasonal trends (B/Ca compared to Ω calcite Figures 3.10 and 3.11). The close agreement between sediment trap B/Ca and modeled carbonate chemistry demonstrates that B incorporation is very sensitive to ambient changes in B concentrations. The consistently higher and wider range of B concentrations in *N. incompta* (50-80 µmol/mol) relative to *N. dutertrei* (40-55 µmol/mol) indicates that there are species-specific differences in the incorporation rate of B into biogenic calcite. Culture studies have also indicated large species-specific B/Ca offsets in three planktonic foraminifrtal species (*G. ruber, G. sacculifer* and *O. universa*) grown in identical seawater composition (Allen et al., 2012; Allen et al., 2011). Previous studies have also shown that there are $\delta^{11}$B differences between species, which are relatively consistent over large changes in pH (Sanyal et al., 2001, 1996; Honisch et al., 2003;2007). In contrast, results from our study and cultures indicate that B/Ca differences between species increase considerably at higher pH (Allen et al., 2012).

While seasonal upwelling in the SBB provides a wide range of hydrographic conditions that is ideal for proxy calibration, upwelling also results in covariation of certain hydrographic parameters. Linear regressions between the independent variables examined in this study (list the variables) indicate collinearity between all of them (Figure 3.12; Table 3.3). Upwelling introduces sub-surface waters that are cool, saline and nutrient-rich due to the remineralization of organic matter at depth. Subsurface water masses are also enriched in dissolved inorganic carbon due to remineralization, which

results in naturally lower in pH, $[CO_3^{2-}]$ and Ω calcite of upwelled waters. Positive correlation between temperature and B/Ca observed in both species suggests that temperature may exert some control B/Ca ratios. However, temperature and the carbonate system parameters (pH, $[CO_3^{2-}]$ and Ω calcite) also are tightly correlated; therefore correlations with temperature may be spurious. A strong correlation between Mg/Ca (temperature proxy) and B/Ca ratios for both species illustrates the covariation of the independent variables that control shell geochemistry (Figure 3.13). Culture experiments indicate that temperature has a negligible effect on B/Ca in planktonic foraminifera (Allen et al., 2011, 2012) and North Pacific core-top results for *G. bulloides* and *N. incompta* indicate that the relationship between temperature and B/Ca ratios is spurious (Quintana Krupinaski et al., submitted). Inorganic calcite precipitation studies have also indicated negative or insignificant influence of temperature on B/Ca ratios (Mavromatis et al., 2015; Kaczmarek et al., 2016). A negative correlation between B/Ca ratios and salinity differs from previous results that suggest that salinity strongly influences B/Ca in the planktic species *G. ruber* (Henehan et al., 2015). Culture results indicate that salinity has some positive influence on B incorporation, however the opposite sign of this relationship in our dataset indicates the influence of salinity is minor relative to carbonate system variables (Allen et al., 2012). Nutrient concentration is also negatively correlated with B/Ca ratios in our dataset unlike the positive correlation observed in globally distributed core-tops for the symbiont-bearing species *G. ruber* (Henehan et al., 2015). No significant correlation between *N. incompta* and nutrient concentration was observed in North Pacific core-tops, perhaps due to the lack of symbionts in this species (Quintana Krupinaski et al., submitted).

The highest correlation coefficients observed in our study are between B/Ca and each of the carbonate system parameters (pH, $[CO_3^{2-}]$ and Ω calcite) (Table X). The slightly higher correlation coefficient observed between Ω calcite and B/Ca observed in both species supports the core-top results from the North Pacific (Quintana Krupinaski et al., submitted). This core-top study covered a wide range of hydrographic regimes and clearly demonstrated that B/Ca is most significantly correlated with Ω calcite (Quintana Krupinaski et al., submitted). The authors suggest that the Ω calcite of seawater exerts the strongest control on B/Ca ratios because of the mechanistic relationship between calcification rate and B incorporation into foraminiferal calcite (Quintana Krupinaski et al., submitted). The surface entrapment model proposes that faster crystal growth (which occurs at higher Ω calcite) reduces the time available for boron to escape via diffusion therefore resulting in more B being retained in newly formed calcite (Watson, 2004). The relationships between B/Ca of *N. dutertrei* and *N. incompta* and modeled Ω calcite values are highly significant (Figure 3.14). A comparison of the *N. incompta* regression developed as a part of this study with the North Pacific core-top data indicates an excellent agreement between the two sample sets.

### 3.4.3 The Influence of Mixed Genotypes on *G. bulloides* B/Ca

A sediment trap time-series of B/Ca ratios for *G. bulloides* was developed using both the October 2013-October 2014 samples included in the study of *Neogloboquadrina* species and an additional samples collected during the first half of 2015. A total of 29 out of 39 sediment trap samples from this period had sufficient material to make B/Ca measurements. All but three samples from the October 2013-2014 period provided enough material for size fraction replicates (150-250 μm and 250-355 μm). El Niño

conditions that started in 2015 resulted in overall lower foraminifera fluxes. Therefore *G. bulloides* from the 150-355 μm size fraction were used for geochemical analyses. Although two morphotypes of *G. bulloides* have previously been identified in our study region (Sautter and Thunell, 1991; Bemis et al., 2002) we did not distinguish between morphotypes for the trace element analyses. The *G. bulloides* B/Ca ratios generally duplicate well across size-fractions with the exception of during winter months and peak upwelling periods in the spring (Figure 3.15). This is likely due to an increase in the abundance of the encrusted *G. bulloides* morphospecies during these periods (Darling et al., 2003; Osborne et al., 2016). Sediment trap studies from the Southern California Bight indicate that the normal *G. bulloides* is found in abundance throughout the year while the encrusted morphotype is seasonally associated with cool periods (Sautter and Thunell 1991; Darling et al., 2003; Osborne et al., 2016). Down core studies from the SBB also indicate an increased abundance in encrusted individuals associated with glacial periods (Hendy and Kennett, 2000; Bemis et al., 2002). Using a combination of shell weight, area and diameter, it is possible to distinguish the two morphotypes of *G. bulloides* (Osborne et al., 2016). We applied this technique to a winter trap sample that had poor duplicates and found that encrusted individuals dominate this sample (Figure 3.16).

The additional sediment trap samples from December 2014-April 2015 included in our *G. bulloides* analyses demonstrates a similar seasonal range and trend for the winter to early spring sampling months. A comparison of *G. bulloides* B/Ca ratios to modeled Ω calcite and Mg/Ca to modeled temperature illustrates that higher than expected B and Mg values occur during winter and peak upwelling when encrusted individuals are typically found in greater abundance (B/Ca ratios versus Ω calcite; Figure

3.17). Quintana Krupinaski et al. (submitted) observe encrusted *G. bulloides* in some core-top samples and determined that the encrusted individuals have a higher B concentrations than the normal morphospecies. A difference in trace element concentrations is not surprising since offsets in stable isotopes have already been observed for the two forms (Osborne et al., 2016; Bemis et al., 2002). Laser ablation results from an Arabian Sea plankton tow reveal that individual *G. bulloides* have Mg/Ca offsets differences of 3 mmol/mol within a single sampling population which the authors attribute to the presence of two morphotypes (Sadekov et al., 2016). Analysis of trace element concentrations in individual specimens of the two *G. bulloides* morphotypes in our study region would be helpful for quantifying the geochemical differences that exist between these forms and determining the effect of pooling these individuals for paleoclimatic reconstructions. If encrusted forms have higher Mg and B concentrations, the inclusion of these individuals in down core reconstructions has the potential to significantly mute estimated changes in paleo-temperatures and carbonate system variables as a result of higher abundances of encrusted individuals during cold periods.

### 3.4.4 Down Core *N. incompta* B/Ca in Relation to Carbonate Chemistry Records

In order to further examine the potential of symbiont-barren foraminifera B/Ca ratios as a paleo-carbonate system proxy, we developed a record of B/Ca spanning the last 100 years for a box core from the SBB. This sediment core was previously used for area density and stable isotope analyses of *G. bulloides* and stable isotope analyses of *N. dutertrei* and *N. incompta* (Osborne et al., 2016); therefore only limited sample material of *N. incompta* was available for trace element analyses. There is a steadily decline in B/Ca ratios from ~1900 through ~1980, at which time B/Ca ratios increase dramatically

(Figure 3.18). Coincident with the increase in B increases in Fe and Al. Clay particles trapped on the surfaces of foraminifera shells represents a significant contamination source of boron and increases in Al/Ca and Fe/Ca ratios indicate that clay contamination was not effectively removed for the upper core samples. Shell morphology measurements of *G. bulloides* indicate a significant increase in shell surface area in the upper part of the core and this could be responsible for the increased clay contamination over the last 30 years of the record. Regardless, samples that indicated elevated Al/Ca and Fe/Ca ratios were excluded from the down core B/Ca record. A comparison of *N. incompta* B/Ca-estimated Ω calcite to *G. bulloides* area density-estimated Ω calcite indicate excellent agreement between these two reconstructions (Figure 3.19).

## 3.5 Conclusions

Our work suggests that B/Ca ratios of non-dinoflagellate bearing foraminifera have the potential to serve as a carbonate system proxy, specifically for Ω calcite of seawater. However, careful selection of individuals included in trace element analyses and application of appropriate calibration relationships is important. The offset between normal and encrusted *G. bulloides* from our study region suggests that vital effects can be significant (even between morphospecies) and genotype-specific calibrations are likely important. A global compilation of planktonic foraminifera genotypes indicate that *G. bulloides* is a highly cryptic species with seven sequenced genotypes to date. The diversity identified within the *G. bulloides* species concept highlights the need for additional geotype-specific work to assess consistency geochemical tracers on this

species. However, genetic work on *Neogloboquadrina* indicate these species are far less cryptic, for instance only a single genotype of *N. incompta* has been found in the Pacific and a second genotype in the Atlantic (Darling et al., 2008). The present state of foraminiferal B research indicates that B/Ca is strongly affected by species-specific and maybe even geotype-specifc vital effects while $\delta^{11}$B seems to be less affected, explaining why B/Ca and $\delta^{11}$B results oftentimes conflict. Future work to assess the influence of species-specific vital effects and resulting offsets in trace element incorporation is essential to further developing the B/Ca proxy prior to application to the fossil record.

Table 3.1 *Neogloboquadrina dutertrei* size fraction replicates and mean B/Ca values and Mg/Ca data

| Trap ID | Cup | Date | Average B/Ca (umol/mol) | 250-355um | 355-425um | >425um | >150um | B/Ca Error | Mg/Ca (mmol/mol) |
|---|---|---|---|---|---|---|---|---|---|
| 39 | 1 | 10/23/13 | 55.59 | 53.87 | 57.31 | | 55.63 | 3.44 | 1.678 |
| 39 | 2 | 11/8/13 | 55.87 | 55.61 | 56.01 | 55.98 | 54.50 | 1.41 | 1.686 |
| 39 | 3 | 11/24/13 | 53.77 | 53.58 | 54.40 | 53.35 | 52.86 | 1.29 | 1.685 |
| 39 | 4 | 12/10/13 | 51.61 | 53.23 | 50.39 | 51.22 | | 2.93 | 1.667 |
| 39 | 5 | 12/26/13 | 49.87 | 49.87 | | | | 2.49 | 1.641 |
| 39 | 6 | 1/11/14 | 50.68 | 51.10 | 50.25 | | | 1.20 | 1.602 |
| 39 | 7 | 1/27/14 | 51.82 | 51.34 | 52.29 | | | 1.35 | |
| 39 | 8 | 2/12/14 | 49.23 | 49.99 | 48.47 | | | 2.15 | 1.567 |
| 39 | 9 | 2/28/14 | 46.68 | 42.72 | 50.63 | | | 11.18 | |
| 39 | 10 | 3/16/14 | 44.73 | 44.73 | | | | 2.24 | 1.553 |
| 39 | 11 | 4/1/14 | | | | | | | 1.523 |
| 39 | 12 | 4/17/14 | 41.15 | 41.15 | | | | 2.06 | |
| 39 | 13 | 5/3/14 | 43.34 | 43.34 | | | | 2.17 | |
| 40 | 1 | 5/24/14 | | | | | | | 1.517 |
| 40 | 2 | 6/4/14 | | | | | | | 1.506 |
| 40 | 3 | 6/16/14 | | | | | | | |
| 40 | 4 | 6/27/14 | 47.23 | | 47.23 | | | 2.36 | 1.588 |
| 40 | 5 | 7/9/14 | 45.19 | 43.57 | 46.80 | | | 4.57 | 1.671 |
| 40 | 6 | 7/20/14 | 51.56 | 51.61 | 51.51 | | | 0.14 | |
| 40 | 7 | 8/1/14 | 54.06 | 56.44 | 51.68 | | | 6.73 | 1.615 |
| 40 | 8 | 8/12/14 | | | | | | | 1.651 |
| 40 | 9 | 8/24/14 | 51.18 | 51.18 | | | | 2.56 | |
| 40 | 10 | 9/4/14 | | | | | | | |
| 40 | 11 | 9/16/14 | 53.93 | 52.70 | 55.16 | | | 3.47 | 1.672 |
| 40 | 12 | 9/27/14 | 57.07 | | 57.07 | | | 2.85 | 1.661 |
| 40 | 13 | 10/9/14 | | | | | | | |

Table 3.2 *Neogloboquadrina incompta* size fraction replicates and mean B/Ca values and Mg/Ca data.

| Trap ID | Cup | Date | Average B/Ca (umol/mol) | 150-250 um | 250-355um | B/Ca Error | Mg/Ca (mmol/mol) |
|---|---|---|---|---|---|---|---|
| 39 | 1 | 10/23/13 | 64.78 | 66.69 | 62.87 | 2.70 | 1.49 |
| 39 | 2 | 11/8/13 | 70.41 | 67.50 | 73.32 | 4.12 | 1.61 |
| 39 | 3 | 11/24/13 | 72.37 | 72.37 | | 3.62 | 1.64 |
| 39 | 4 | 12/10/13 | 75.21 | 75.21 | | 3.76 | 1.65 |
| 39 | 5 | 12/26/13 | 78.51 | 78.51 | | 3.93 | 1.78 |
| 39 | 6 | 1/11/14 | | | | | 1.57 |
| 39 | 7 | 1/27/14 | 69.24 | 69.24 | | 3.46 | |
| 39 | 8 | 2/12/14 | 64.05 | 64.05 | | 3.20 | 1.47 |
| 39 | 9 | 2/28/14 | | | | | 1.40 |
| 39 | 10 | 3/16/14 | 57.46 | 57.46 | | 2.87 | |
| 39 | 11 | 4/1/14 | 59.12 | 59.12 | | 2.96 | 1.46 |
| 39 | 12 | 4/17/14 | | | | | 1.28 |
| 39 | 13 | 5/3/14 | 51.50 | 51.50 | | 2.58 | |
| 40 | 1 | 5/24/14 | | | | | |
| 40 | 2 | 6/4/14 | | | | | |
| 40 | 3 | 6/16/14 | | | | | |
| 40 | 4 | 6/27/14 | 57.84 | 57.84 | | 2.89 | 1.50 |
| 40 | 5 | 7/9/14 | 69.11 | 69.11 | | 3.46 | |
| 40 | 6 | 7/20/14 | 73.93 | 73.93 | | 3.70 | 1.62 |
| 40 | 7 | 8/1/14 | | | | | 1.58 |
| 40 | 8 | 8/12/14 | | | | | |
| 40 | 9 | 8/24/14 | | | | | 1.56 |
| 40 | 10 | 9/4/14 | 59.52 | 59.52 | | 2.98 | 1.48 |
| 40 | 11 | 9/16/14 | 65.29 | 65.29 | | 3.26 | 1.49 |
| 40 | 12 | 9/27/14 | 70.60 | 70.60 | | 3.53 | 1.68 |
| 40 | 13 | 10/9/14 | 75.65 | 78.24 | 73.06 | 3.66 | |

Table 3.1 Simle linear regression data of monthly resolved hydrographic data indicating cross-correlations between independent variables

| Date | Salinity | Temp | NO3 | pHin | pCO2 (matm) | HCO3 (mmol/kg SW) | CO3 (mmol/kg SW) | CO2 (mmol/kg SW) | B Alk (mmol/kg SW) | W Ca |
|---|---|---|---|---|---|---|---|---|---|---|
| 6/15/13 | 33.39 | 11.21 | 16.44 | 7.83 | 672.37 | 2046.43 | 83.91 | 29.51 | 41.81 | 2.79 |
| 7/15/13 | 33.35 | 11.55 | 15.39 | 7.83 | 669.01 | 2041.32 | 84.97 | 29.08 | 42.24 | 2.82 |
| 8/15/13 | 33.18 | 12.88 | 10.25 | 7.89 | 569.92 | 1991.31 | 100.07 | 23.92 | 49.23 | 3.18 |
| 9/15/13 | 33.10 | 13.88 | 6.18 | 7.95 | 499.47 | 1950.62 | 113.82 | 20.40 | 55.56 | 3.51 |
| 10/15/13 | 33.05 | 14.41 | 4.46 | 7.97 | 471.88 | 1931.52 | 120.27 | 19.00 | 58.46 | 3.66 |
| 11/15/13 | 32.99 | 14.80 | 3.65 | 7.98 | 458.70 | 1920.56 | 123.84 | 18.37 | 60.02 | 3.75 |
| 12/15/13 | 33.06 | 14.10 | 3.42 | 7.99 | 443.75 | 1916.62 | 127.30 | 17.77 | 61.67 | 3.83 |
| 1/15/14 | 33.13 | 13.79 | 2.38 | 8.01 | 423.90 | 1905.60 | 133.08 | 16.84 | 64.42 | 3.97 |
| 2/15/14 | 33.10 | 13.47 | 6.74 | 7.94 | 504.22 | 1958.65 | 112.06 | 20.92 | 54.89 | 3.47 |
| 3/15/14 | 33.13 | 12.56 | 10.08 | 7.90 | 554.37 | 1990.61 | 100.41 | 23.58 | 49.63 | 3.19 |
| 4/15/14 | 33.21 | 11.43 | 13.86 | 7.86 | 624.17 | 2024.67 | 88.97 | 27.22 | 44.31 | 2.92 |
| 5/15/14 | 33.35 | 11.28 | 15.93 | 7.84 | 650.15 | 2037.47 | 86.92 | 28.32 | 43.27 | 2.87 |
| 6/15/14 | 33.22 | 12.22 | 12.35 | 7.86 | 617.48 | 2014.87 | 92.60 | 26.21 | 45.78 | 3.00 |
| 7/15/14 | 33.11 | 13.37 | 8.39 | 7.92 | 530.08 | 1969.74 | 107.45 | 22.04 | 52.73 | 3.36 |
| 8/15/14 | 33.07 | 14.18 | 5.49 | 7.96 | 480.05 | 1939.11 | 118.23 | 19.48 | 57.65 | 3.61 |
| 9/15/14 | 33.07 | 14.37 | 4.86 | 7.96 | 473.29 | 1934.59 | 119.95 | 19.08 | 58.40 | 3.66 |
| 10/15/14 | 33.06 | 14.87 | 3.59 | 7.98 | 458.36 | 1921.30 | 124.99 | 18.20 | 60.56 | 3.78 |
| 11/15/14 | 33.02 | 15.91 | 2.82 | 7.99 | 447.15 | 1910.39 | 128.79 | 17.54 | 62.15 | 3.87 |
| 12/15/14 | 33.13 | 16.67 | 1.06 | 8.01 | 423.14 | 1880.29 | 143.17 | 15.73 | 67.96 | 4.21 |

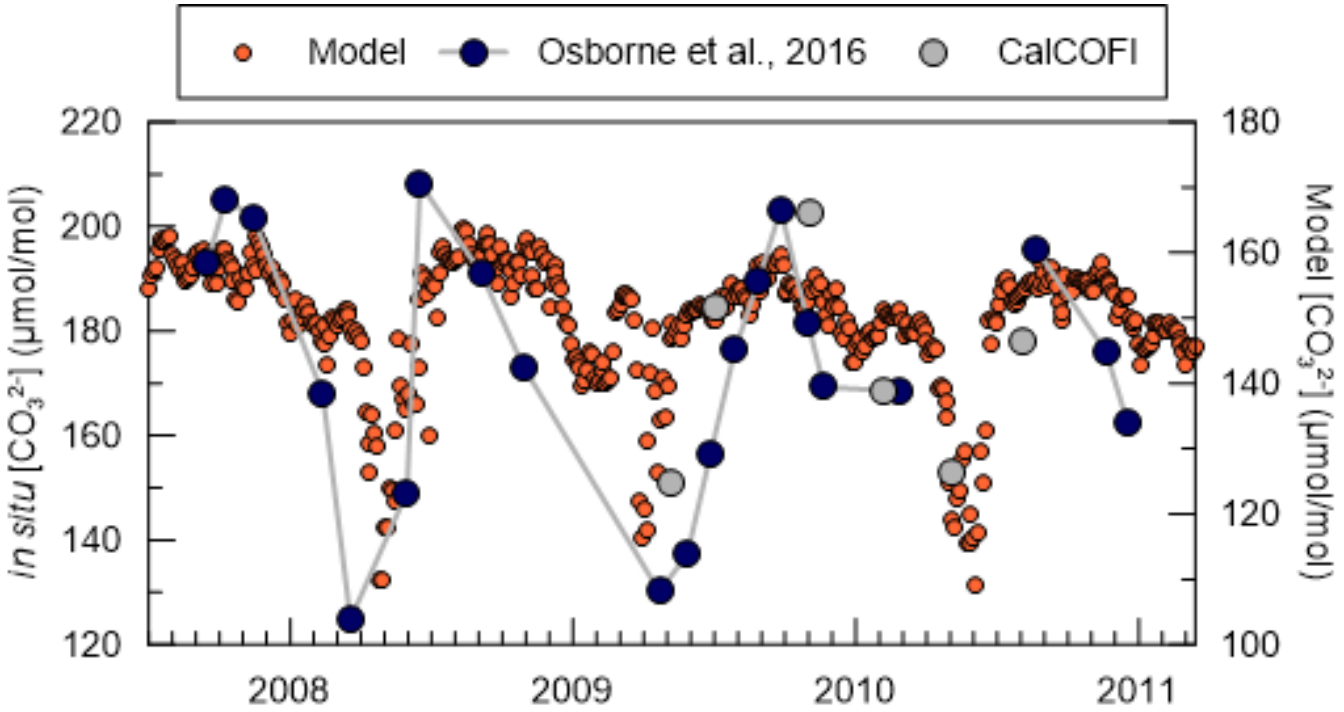


Figure 3.1 Comparison of *in situ* measurements of surface [$CO_3^{2-}$] (data from CalCOFI and Osborne et al., 2016) compared to modeled values. Note that the *in situ* data are plotted on the left y-axis and the model data are plotted on the right-hand y-axis due to the offset in the range of values. An offset in [$CO_3^{2-}$] was determined for each sample equaling an average of 33 µmol/mol. The conversion of this carbonate value to Ω calcite values yields the same average offset as the CalCOFI comparison shown in the below Figure #.

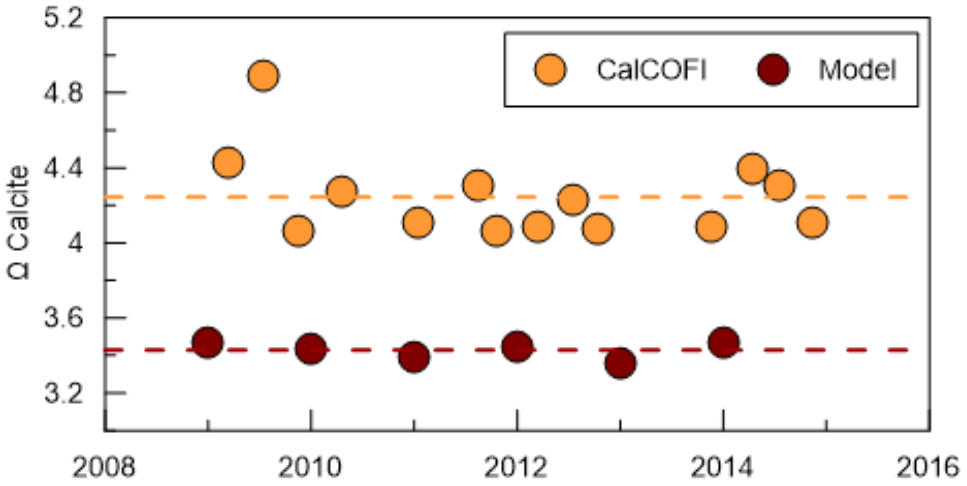


Figure 3.2 Comparison of *in situ* surface omega calcite values from the CalCOFI time-series compared to model estimates of surface omega calcite for the 2009-2015 period when these datasets over lap. The offset between these datasets is used to correct model values that are used in the B/Ca calibration portion of this study.

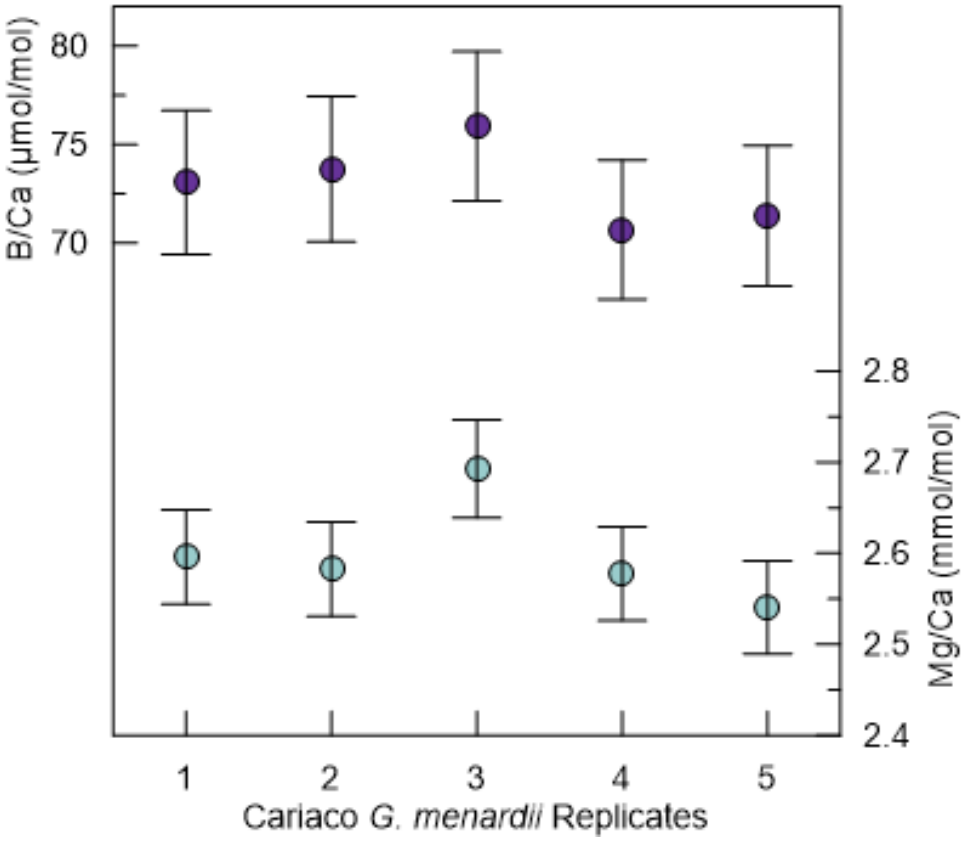


Figure 3.3 Replicate B/Ca and Mg/Ca measurements of a foraminifera matrix-specific standard. *Globorotalia menardii* shells from a 2-week-long sediment sample from the Cariaco Basin (150 meter depth) are used for our foraminiferal standard. Error bars represent fully propagated 2-sigma errors.

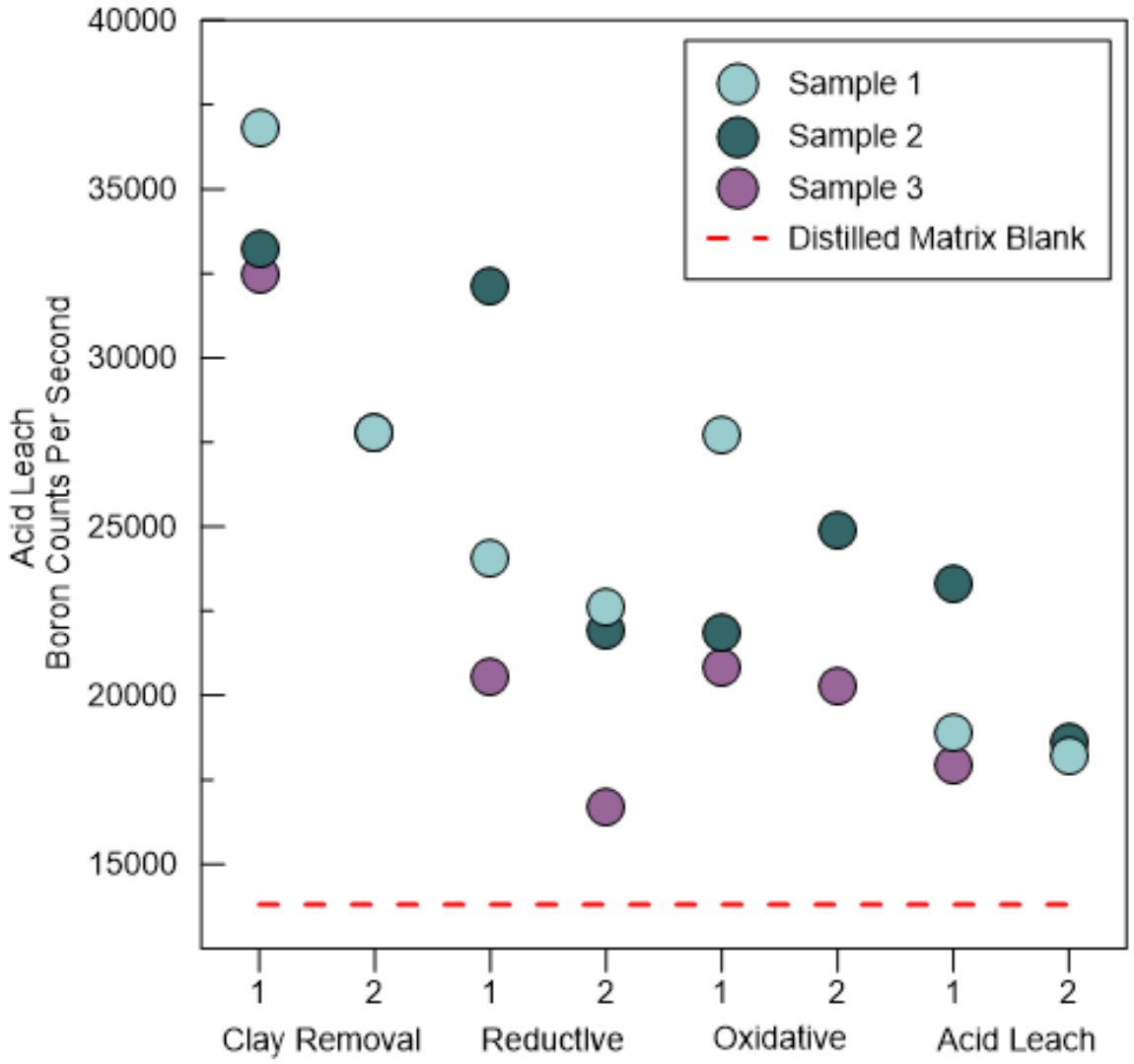


Figure 3.4 The leachates of each of the cleaning steps for 3 sediment trap samples that were archived in the sodium borate buffer are shown here in counts per second of boron.

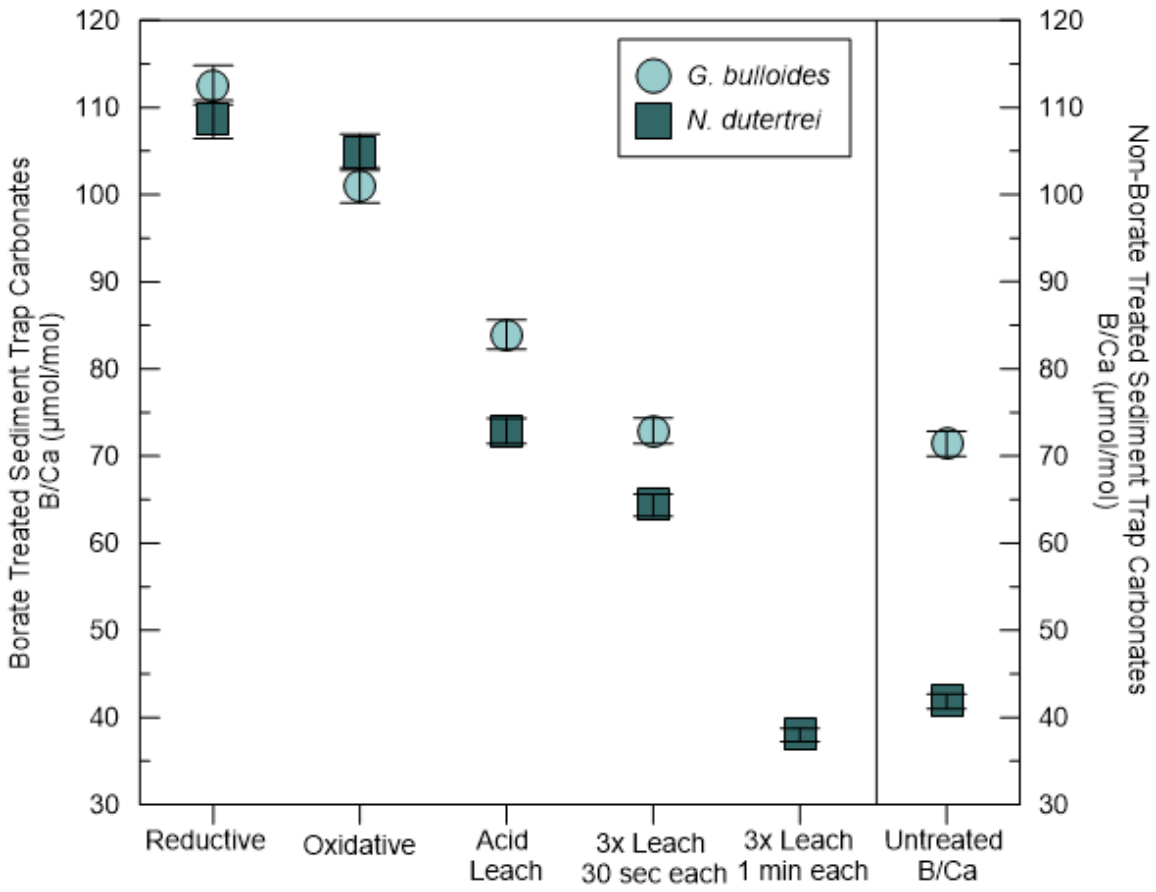


Figure 3.5 B/Ca ratios of *G. bulloides* and *N. dutertrei* from a single borate buffered (6-months) sediment trap sample. Foraminiferal populations were split into 4 to 5 fractions in order to evaluate how the borate buffer contamination is progressively removed from treated samples. The robust nature of *N. dutertrei* shells required an additional acid leach treatment of 3-times for 1 minute. The final acid leach treatments yield B/Ca ratios for both species that are comparable to those measured on populations from a time equivalent non-buffered sample.

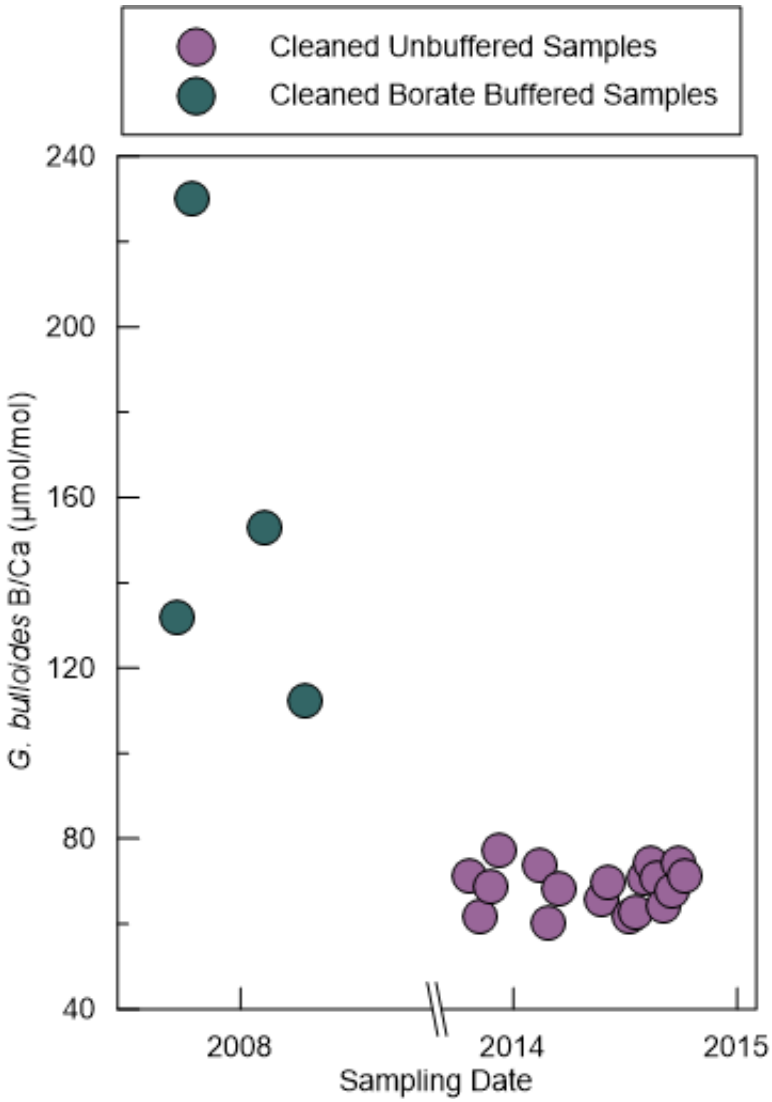


Figure 3.6 Comparison of B/Ca ratios of rigorously cleaned foraminifera that were preserved in a sodium borate buffer for 6-7 years with the B/Ca ratios of foraminifera that were not treated with sodium borate. This result indicates that prolonged storage of foraminifera in sodium borate inhibits the removal of the borate contamination.

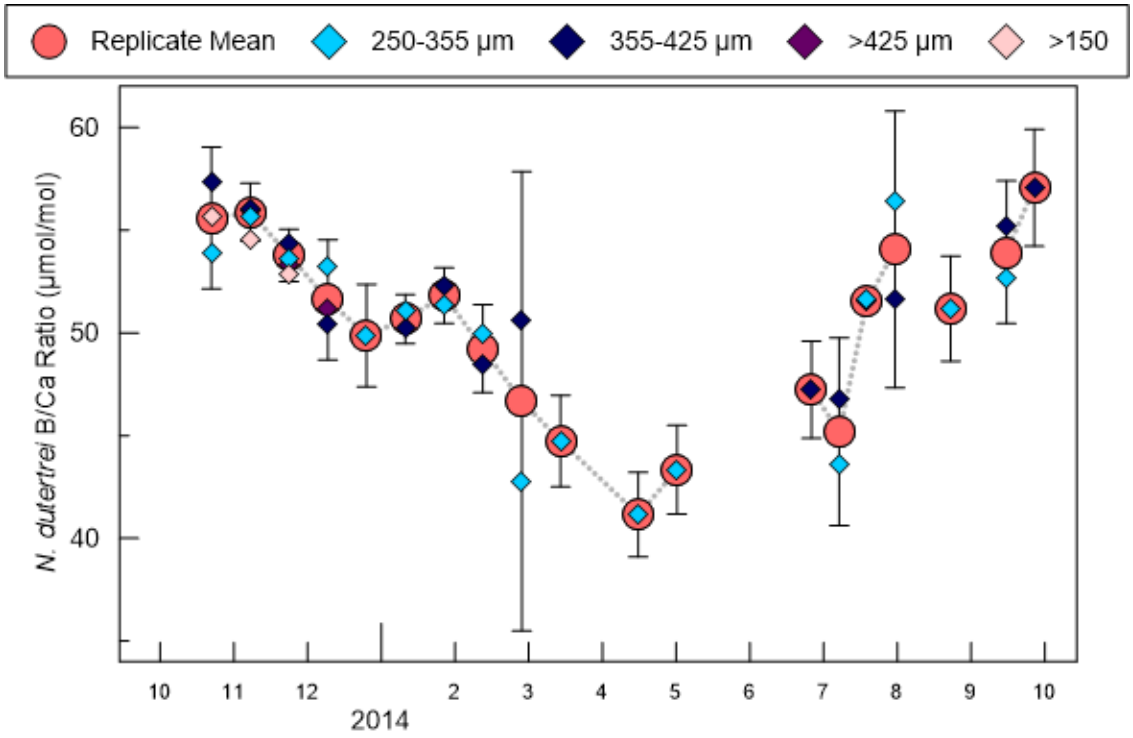


Figure 3.7 Time-series of *N. dutertrei* B/Ca measurements from sediment trap samples collected from October 2013-October 2014. Replicate measurements were made using three size-fractions and for several samples replicates were made without restricting size-fraction. Error bars on replicate means indicate 2-sigma errors of replicate measurements. When no replicates were made error bars represent the fully propagated analytical error associated with each measurement.

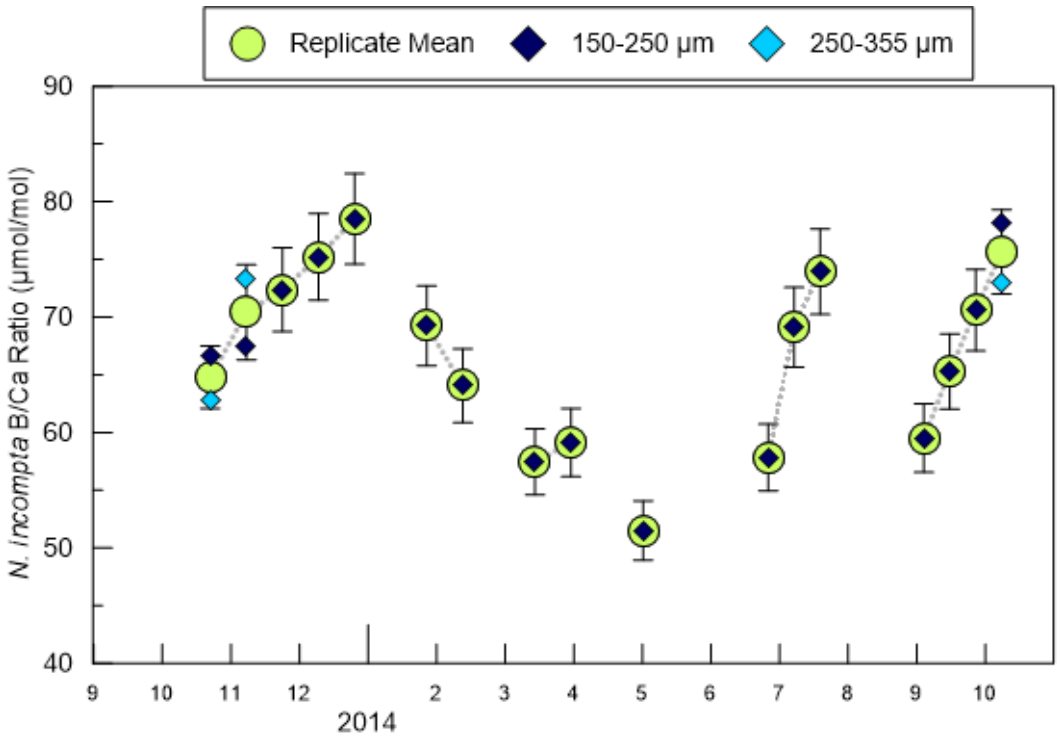


Figure 3.8 Time-series of *N. incompta* B/Ca measurements from sediment trap samples collected from October 2013-October 2014. Generally *N. incompta* was only found in abundance in the 150-250 µm size fraction. However, a limited number of replicate measurements were made using the 250-355 µm fraction. When no replicates were made error bars represent the fully propagated analytical error associated with each measurement. Error bars on replicate means indicate 2-sigma errors of replicate measurements.

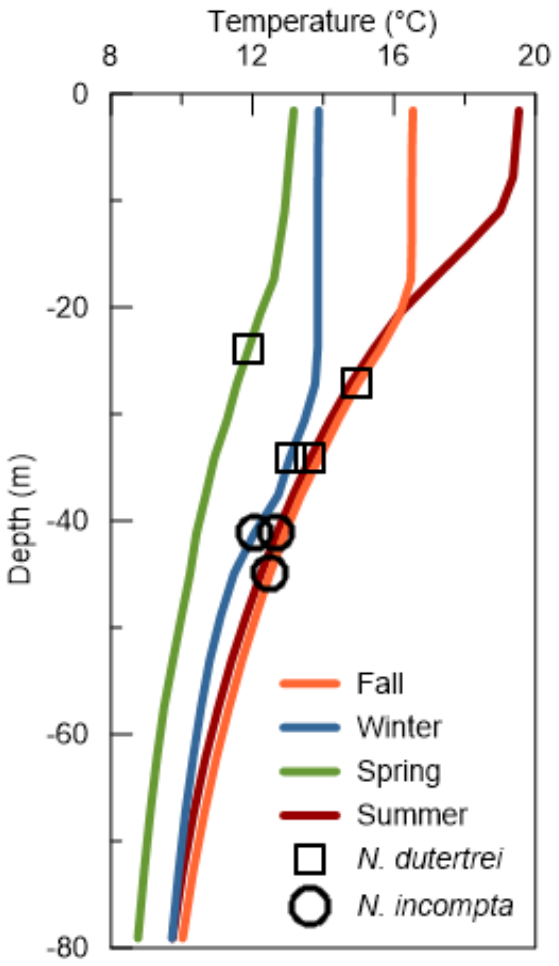


Figure 3.9 Temperature profiles 0-80 meters water depth from 2013-2014 modeled data throughout a seasonal cycle in the SBB. Open circles and squares indicate the Mg/Ca-derived calcification temperatures of *N. incompta* and *N. dutertrei* compared to the temperature profiles.

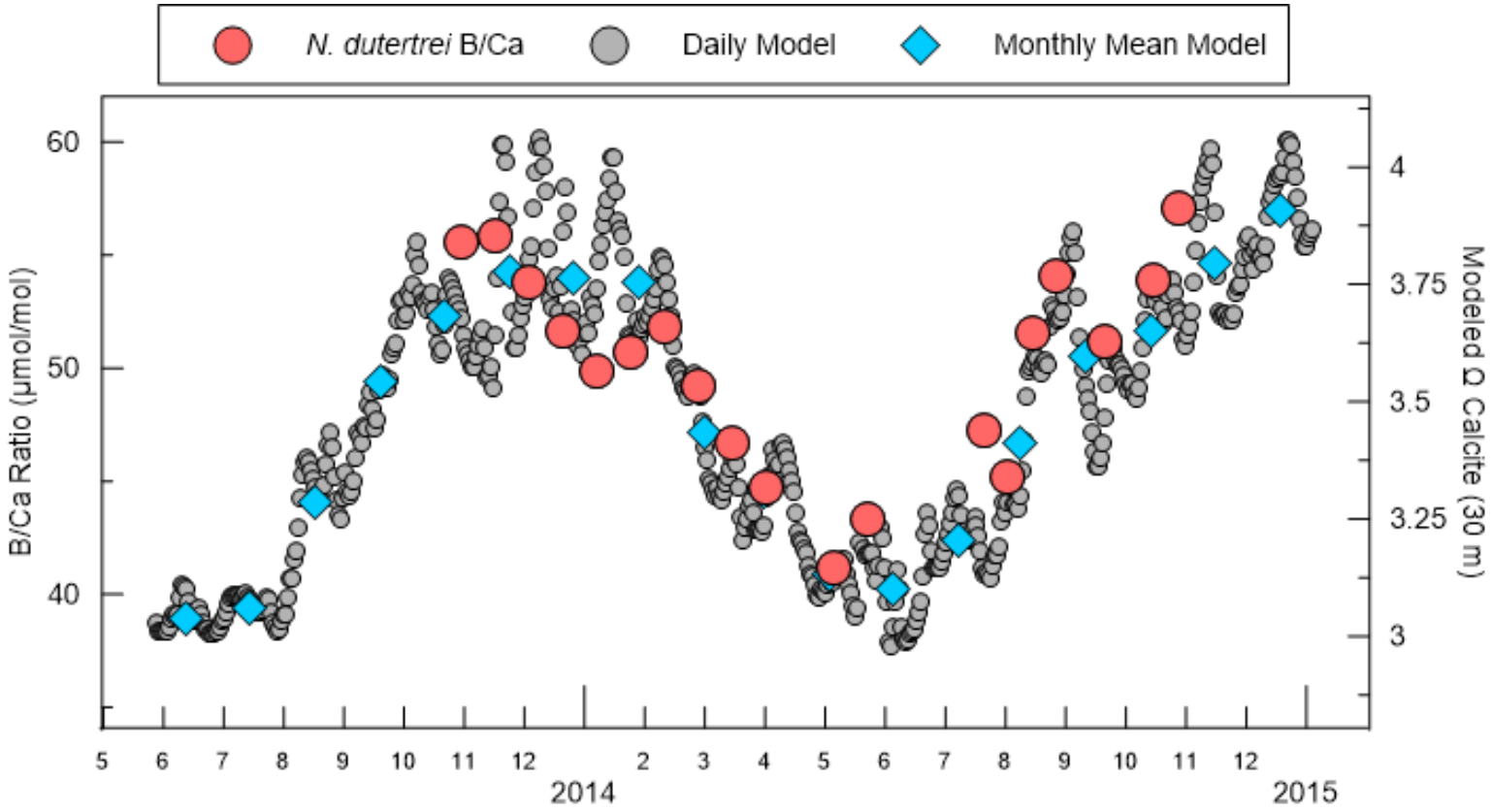


Figure 3.10 Mean replicate B/Ca ratios of *N. dutertrei* (pink circles) compared to modeled 30 meter Ω calcite. Model data is shown here as daily (gray circles) and monthly mean (blue diamonds) values.

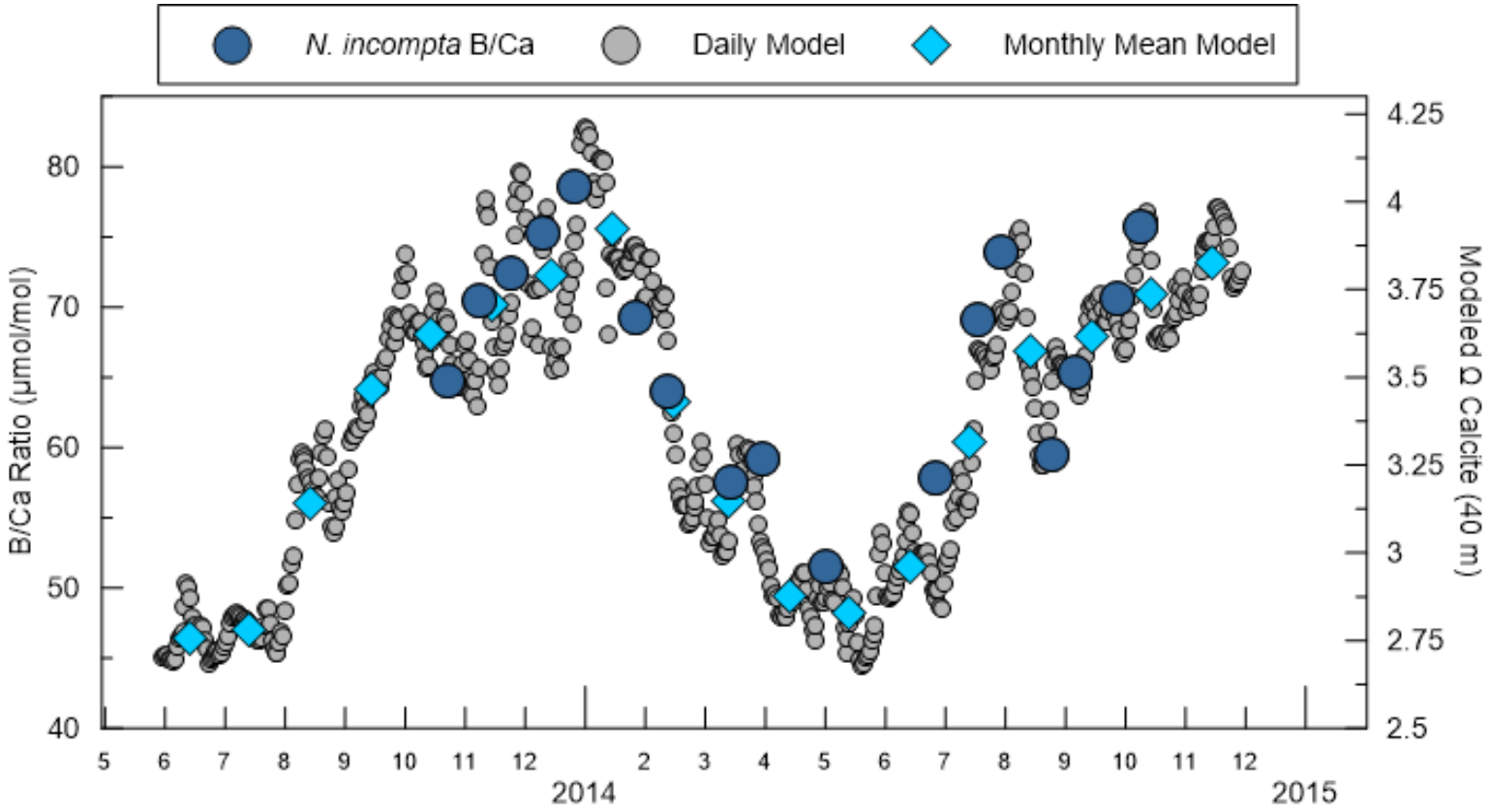


Figure 3.11 Mean replicate B/Ca ratios of *N. incompta* (navy circles) compared to modeled 30 meter Ω calcite. Model data is shown here as daily (gray circles) and monthly mean (light blue diamonds) values.

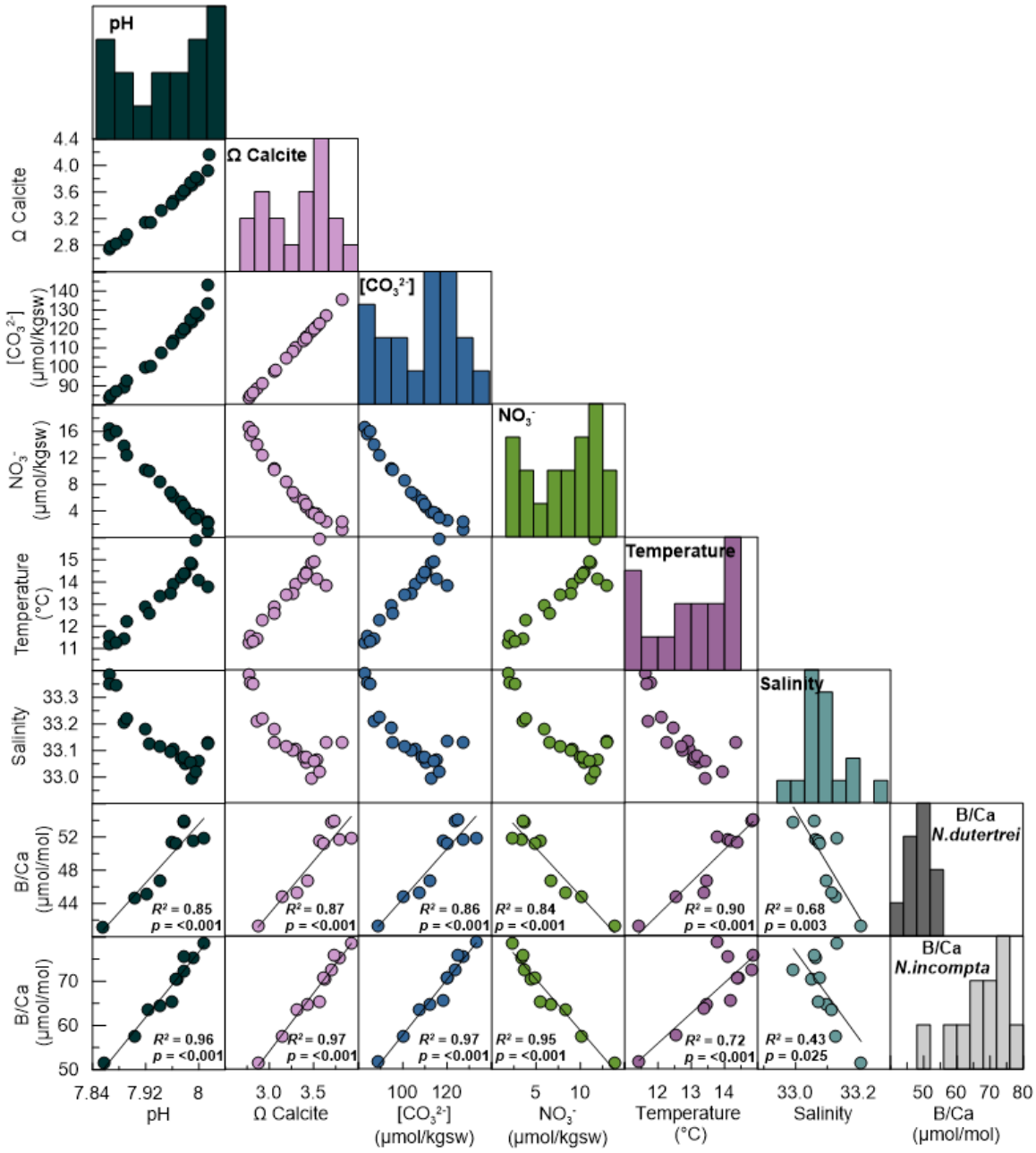


Figure 3.12 Matrix of linear regressions showing the relationship between the B/Ca ratios of *Neogloboquadrina* species and the monthly mean value determined for each independent variables. Histograms are included to show range and frequency for each variable.

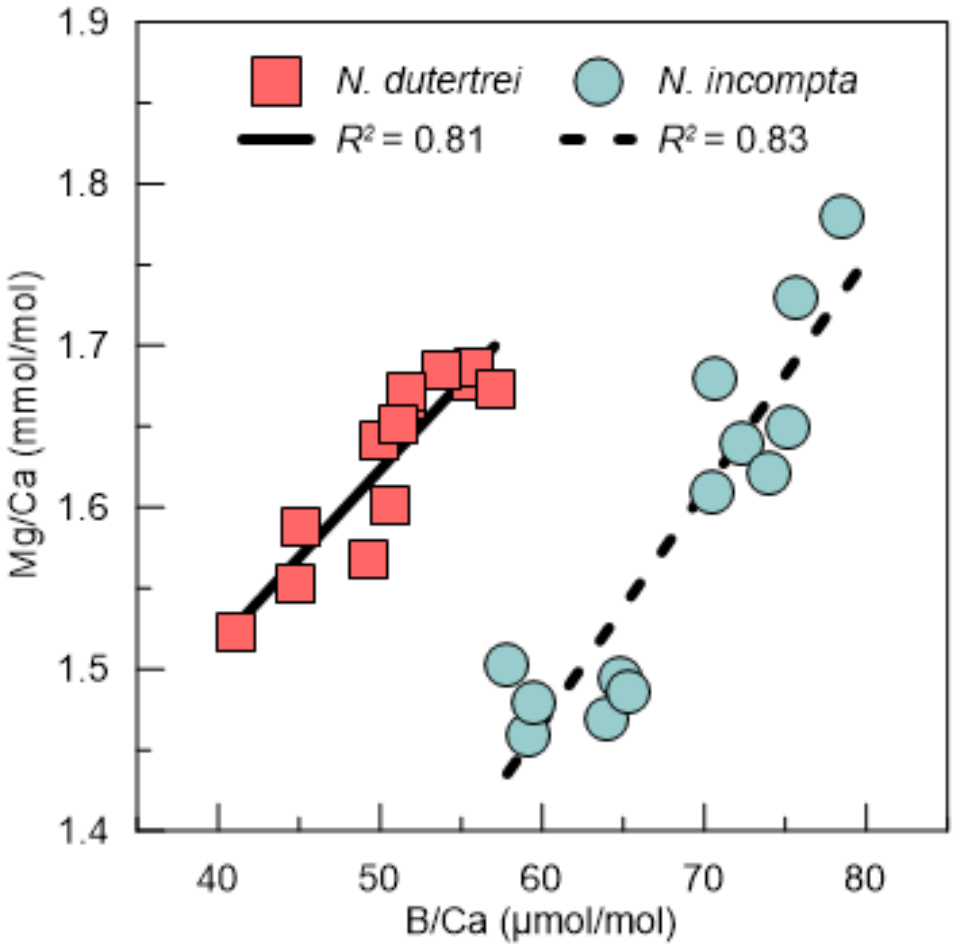


Figure 3.13 Correlations between Mg/Ca (a temperature proxy) and B/Ca ratios for both species support that temperature and carbonate system variables are collinear in our dataset.

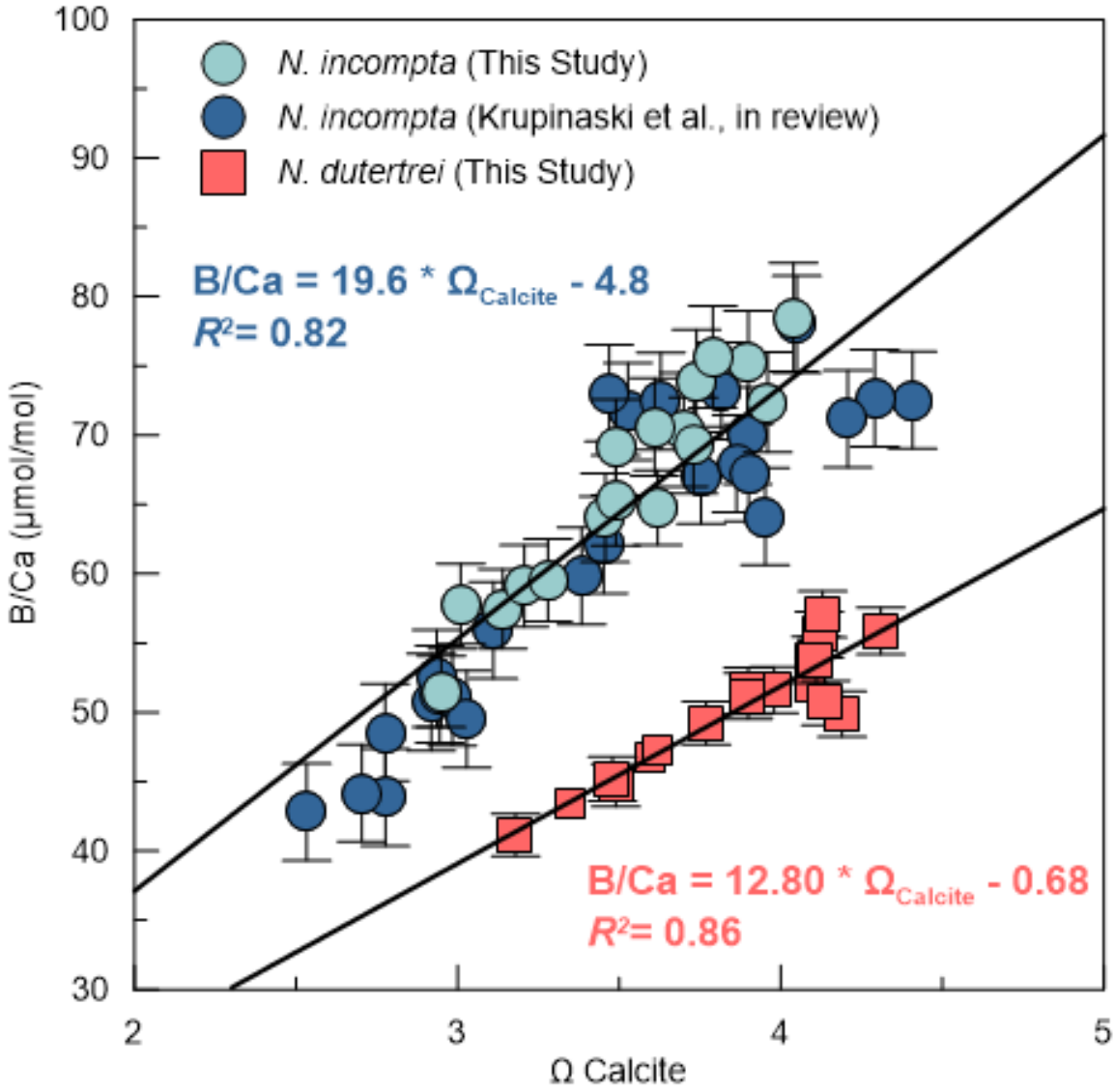


Figure 3.14 Calibration relationships for *N. incompta* and *N. dutertrei* from SBB sediment trap results. Final calibration equation presented here is pooled data from this study's sediment trap results and core-top results for the North Pacific (unpublished data, Quintana Krupinaski et al., in review).

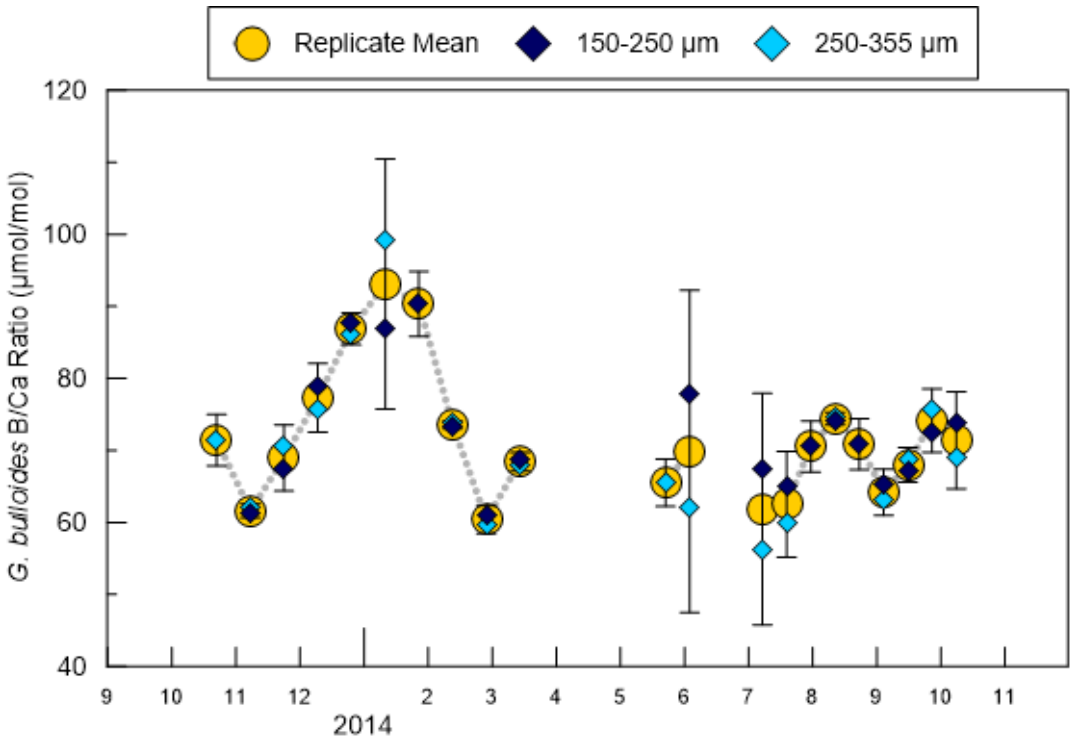


Figure 3.15 Time-series of *G. bulloides* B/Ca measurements from sediment trap samples collected from October 2013-October 2014. Replicates were made for the 150-250 µm and 250-355 µm size fractions when sufficient sample material as available. When no replicates were made error bars represent the fully propagated analytical error associated with each measurement. Error bars on replicate means indicate 2-sigma errors of replicate measurements.

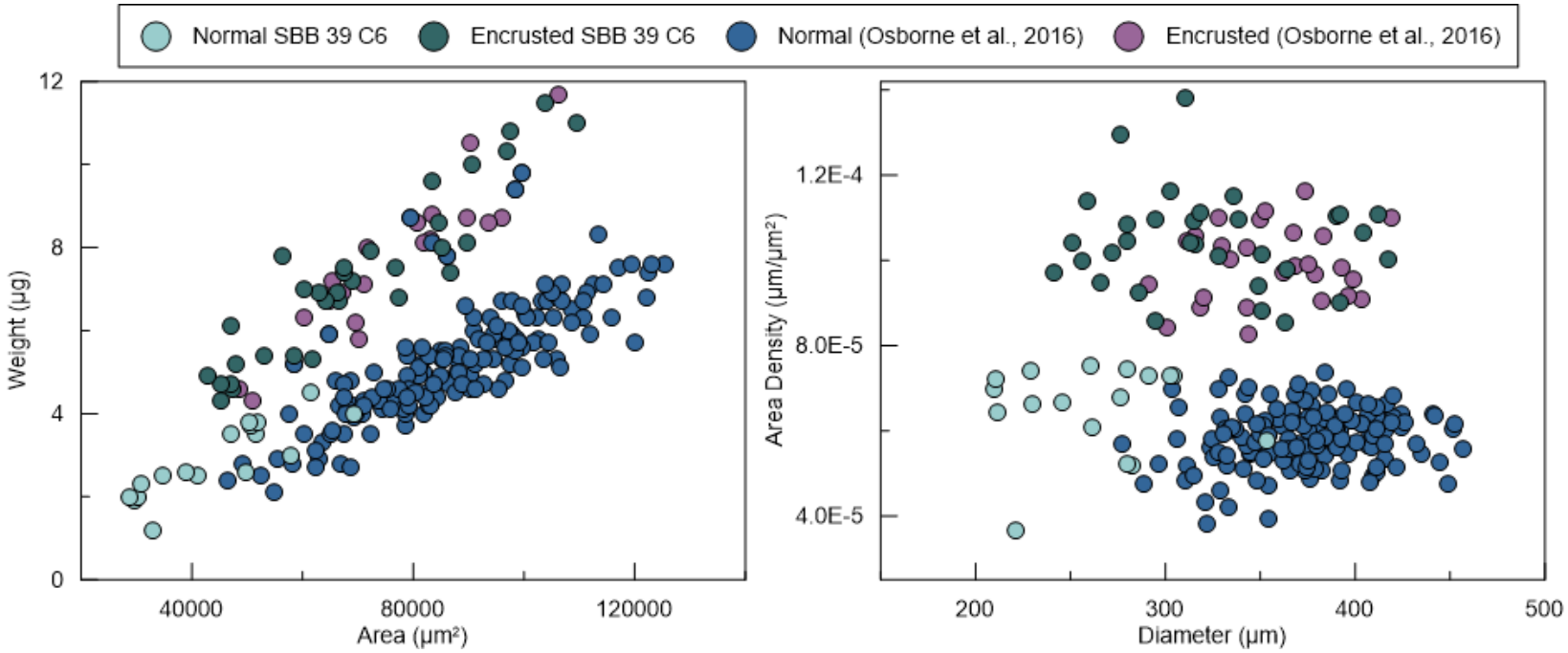


Figure 3.16 Morphometric analyses used to determine the presence of the normal and encrusted cryptic *G. bulloides* morphospecies during the January 2014 sampling period. The trend in weight-area and grouping of morphospecies in the area density-diameter analyses are shown here with previously identified morphospecies groups from the SBB (Osborne et al., 2016).

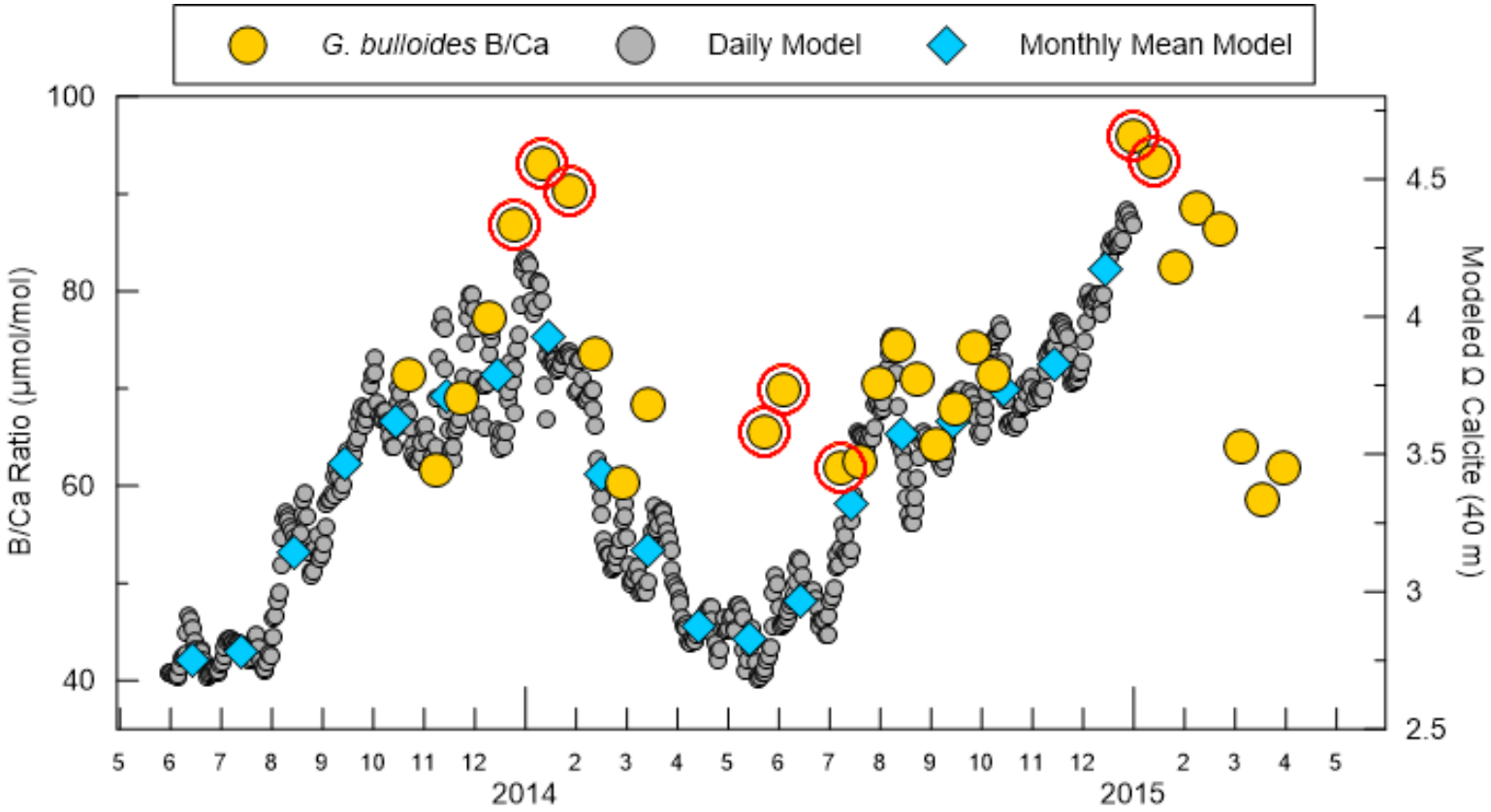


Figure 3.17.Mean B/Ca ratios of *G. bulloides* (yellow circles) compared to modeled 40-meter Ω calcite. A mean calcification depth of 40 meters was determined using *G. bulloides* $\delta^{18}O$ temperature estimates for a 3-year SBB sediment trap study (Osborne et al., 2016). Model data is shown here as daily (gray circles) and monthly mean (light blue diamonds) values. Red circles highlight samples that likely include encrusted individuals based on a comparison of B/Ca and Mg/Ca to Ω calcite and temperature, respectively.

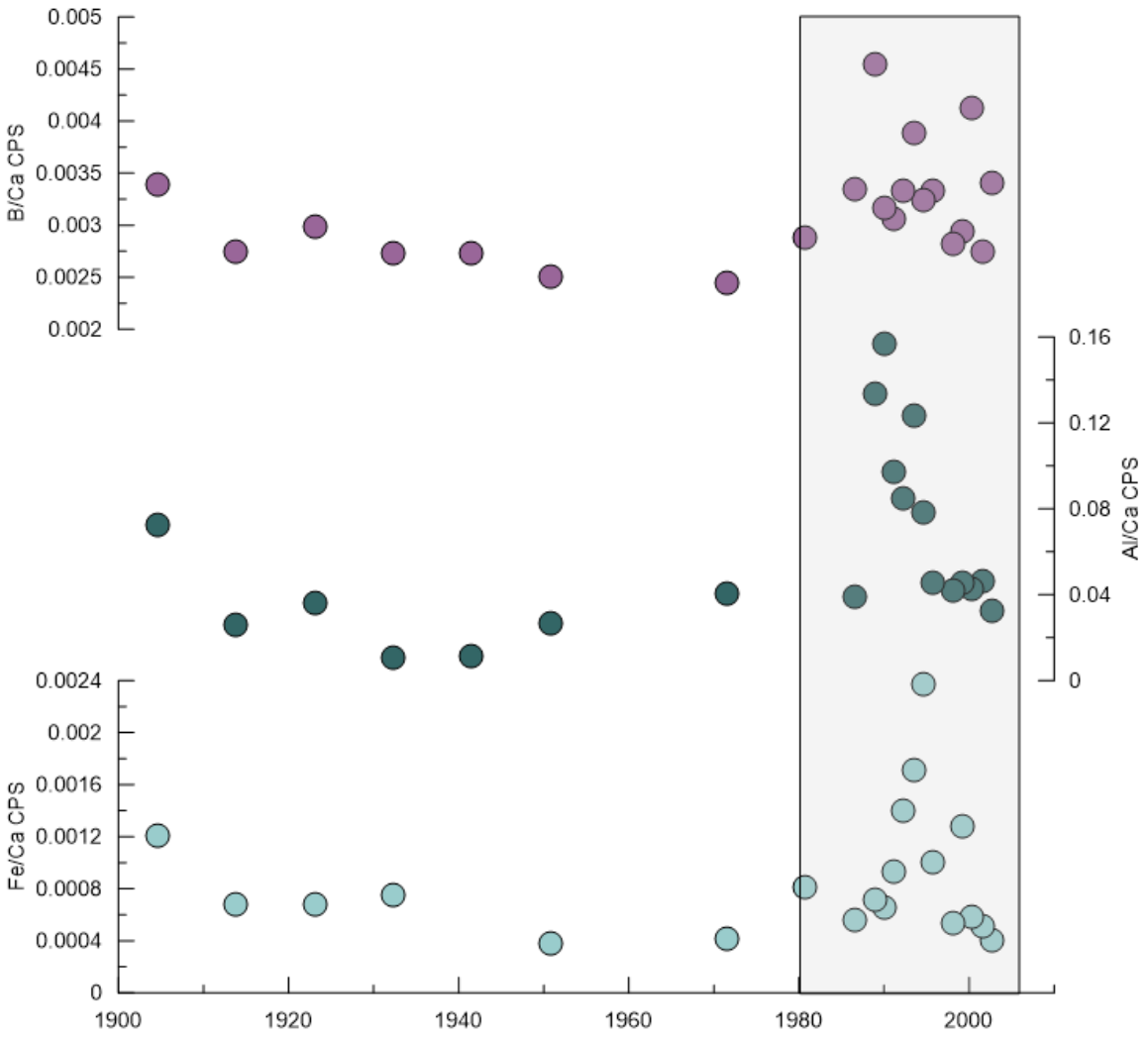


Figure 3.18 Down core measurements of boron, aluminum and iron to calcium ratios. Measurements are shown here as counts per second (CPS) indicating the intensity of the element concentration measured by the HR-ICP-MS. Grayed area indicates the sampling period when clay contamination is indicated by elevated Fe/Ca and Al/Ca.

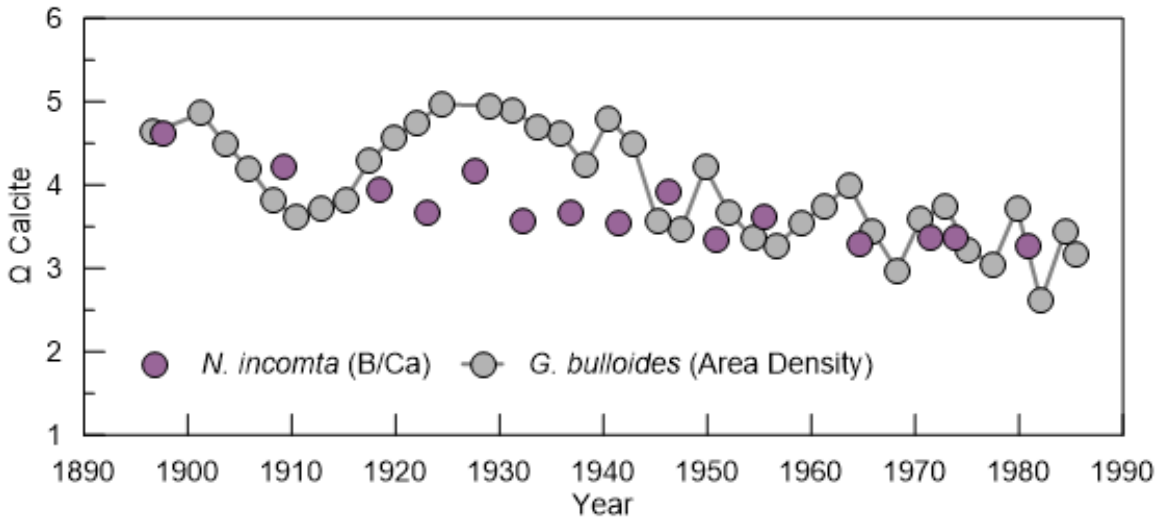


Figure 3.19 Down core estimates of Ω calcite from *N. incompta* B/Ca ratios and *G. bulloides* area density measurements.

# REFERENCES


Aldridge, D., C. J. Beer, and D. A. Purdie (2012), Calcification in the planktonic foraminifera *Globigerina bulloides* linked to phosphate concentrations in surface waters of the North Atlantic Ocean, *Biogeosciences*, 9(5), 1725–1739, doi:10.5194/bg-9-1725-2012.

Alin, S. R., R. A. Feely, A. G. Dickson, J. M. Hernandez-Ayon, L. W. Juranek, M. D. Ohman, and R. Goericke (2012), Robust empirical relationships for estimating the carbonate system in the southern California Current System and application to CalCOFI hydrographic cruise data (2005–2011), *Journal of Geophys. Research*, 117.

Allen, K., B. Hönisch, S. Eggins, J. Yu, H. Spero and H. Elderfield (2011), Controls on boron incorporation in cultured tests of planktic foraminifera Orbulina universa, *Earth Planet Sci. Lett*. 309, 291-301.

Allen, K., B. Hönisch, S. Eggins and Y. Rosenthal (2012), Environmental controls on B/Ca in calcite tests of the tropical planktic foraminifera species *Globigerinoides ruber* and *Globigerinoides sacculifer*, *Earth Planet Sci. Lett*. 351-352, 270-280.

Anand, P., H. Elderfield, and M. H. Conte (2003), Calibration of Mg/Ca thermometry in planktonic foraminifera from a sediment tap time series, *Paleoceanography*, 18(2), 1050, doi:10.1029/2002PA000846.

Armstrong, R. A., Lee, C., Hedges, J. I., Honjo, S. & Wakeham, S. G. (2002) A new, mechanistic model for organic carbon fluxes in the ocean based on the quantitative association of POC with ballast minerals. *Deep-Sea Res.* II 49, 219–236.

Babila, T., Rosenthal, Y., and Conte, M. H., (2014) Evaluation of the biogeochemical controls on B/Ca of *Globigerinoides ruber* white from the Ocean Flux Program, Bermuda, *Earth Planet Sci*. Lett. 404, 67-76.

Barker, S., and H. Elderfield (2002), Foraminiferal Calcification Response to Glacial-Interglacial Changes in Atmospheric $CO_2$, *Science* 297, 833-836.

Bates, N.R., Y. M. Astor, M.J. Church, K. Currie, J. E. Dore, M. González-Dávila, L. Lorenzoni, F. Muller-Karger, J. Olafsson, and J. M. Santana-Casiano (2014), A time-series view of changing ocean chemistry due to ocean uptake of anthropogenic CO2 and ocean acidification. *Oceanography* 27(1):126–141

Bé, A. W. H., S. M. Harrison, and L. Lott (1973), *Orbulina universa* d'Orbigny in the Indian Ocean, *Mar. Micropaleontol.*, 19(2), 150–192.

Bé, A. W. H. (1977), An ecological, zoogeographic and taxonomic review of recent planktonic Foraminifera, in *Oceanic Micropalaeontology*, edited by A. T. S. Ramsay, pp. 1–100, Academic Press, London, New York, San Francisco.

Bednaršek, N., Tarling, G. A., Bakker, D. C., Fielding, S., & Feely, R. A. 2014, Dissolution Dominating Calcification Process in Polar Pteropods Close to the Point of Aragonite Undersaturation, PloS One, 9(10), e109183.

Bednaršek, N., C. J. Harvey, I. C. Kaplan, R. A. Feely, J. Mozina (2016) Pteropods on the edge, Cumulative effects of ocean acidification, warming and deoxygenation, *Progress in Oceanography* 145, 1-24

Beer, C. J., R. Schiebel, and P. A. Wilson (2010a), Testing planktic foraminiferal shell weight as a surface water [$CO_3^{2-}$] proxy using plankton net samples, *Geology*, 38(2), 103–106.

Beer, C. J., R. Schiebel, and P. A. Wilson (2010b), Technical note: On methodologies for determining the size-normalised weight of planktic foraminifera, Biogeosciences, 7(7), 2193–2198, doi:10.5194/bg-7-2193-2010.

Bemis, B. E., H. J. Spero, J. Bijma, and D.W., Lea (1998), Reevaluation of the oxygen isotopic composition of planktonic foraminifera: Experimental results and revised paleotemperature equations: *Paleoceanography* 13, 150–160.

Bemis, B. E., H. J. Spero, and R. C. Thunell (2002), Using species-specific paleotemperature equations with foraminifera: a case study in the Southern California Bight, *Marine Micropaleo.*, 46, 405-430.

Berger, W. H. (1971) Sedimentation of planktonic foraminifera, *Marine Geology*, 11, 325-358.

Biard, T., L. Stemmann, M. Picheral, N. Mayot, P. Vandromme, H. Hauss, G. Gorsky, L. Guidi, R. Kiko, F. Not (2016) *In situ* imaging reveals the biomass of giant protists in the global ocean, *Nature Letter* 532, 504-506, doi:10.1038/nature17652.

Bijma, J., H.J. Spero, and D.W. Lea (1999) Reassessing foraminiferal stable isotope geochemistry: Impact of the oceanic carbonate systems (experimental results). Pp. 489–512 in Use of Proxies in Paleoceanography: Examples from the South Atlantic. G. Fisher and G. Wefer, eds., Springer-Verlag, New York, NY.

Bijma, J., B. Honisch, and R.E. Zeebe (2002) Impact of the ocean carbonate chemistry on living foraminiferal shell weight: Comment on "Carbonate ion concentration in glacial-age deep waters of the Caribbean Sea" by W. S. Broecker and E. Clark, *Geochemistry Geophysics Geosystems*, *3*(11), doi:10.1029/2002GC000388.

Bograd S. and R. J. Lynn (2001) Physical-biological coupling in the California Current during the 1997-99 El Nino-La Nino cycle, *Geophys. Res. Lett.*, 28 (2), 275-278.

Bopp, L., L. Resplandy, J. C. Orr, S. C. Doney, J. P. Dunne, M. Gehlen, P. Halloran, C. Heinze, T. Ilyina, R. Seferian, J. Tjiputra, and M. Vichi (2013) Multiple stressors of ocean ecosystems in the 21st century: projections with CMIP5 models, *Biogeosciences*, 10, 6225-6245, doi:10.5194/bg-10-6225-2013.

Boyle, E. A., and L. D. Keigwin (1985), Comparison of Atlantic and Pacific paleochemical records for the last 215,000 years: Changes in deep ocean circulation and chemical inventories, Earth Planet. Sci. Lett., 76, 135–150, doi:10.1016/0012-821X(85)90154-2.

Branson, O., K. Kaczmarek, S. A. T. Redfern, S. Misra, G. Langer, T. Tyliszczak, J. Bijma, H. Elderfield (2015) The coordination and distribution of B in foraminiferal calcite, *Earth and Planetary Science Letters*, 416, 67-72,

Brewer, P.G. (1997), Ocean chemistry of the fossil fuel CO2 signal: The haline signal of "business as usual": Geophysical Research Letters, v. 24, p. 1367–1369, doi: 10.1029/97GL01179.

Broeker, W. and T-H Peng (1982) Tracers in the Sea, Lamont-Doherty Geological Observatory, Columbia University, Palisades, New York.

Broecker, W., and E. Clark (2001), A dramatic Atlantic dissolution event at the onset of the last glaciation, *Geochem. Geophys. Geosyst.*, 2(11), 1065, doi:10.1029/2001GC000185.

Bruland, K. W., 1974, Pb-210 geochronology in the coastal marine environment [Ph.D. dissert.]:La Jolla, Univ. California, San Diego, 106 p.

Byrne RH, Mecking S, Feely R a and Liu X (2010) Direct observations of basin-wide acidification of the North Pacific Ocean, *Geophys. Res. Lett*. 37 1–5.

Cai, W.-J., X. Hu, W.-J. Huang, L.-Q. Jiang, Y. Wang, T.-H Peng, and X. Zhang (2010) Alkalinity distribution in the western North Atlantic Ocean margins. J. *Geophys. Res.*, 115(C8): C08014.

Carter, M.W. and A.A. Moghissi (1977), Three Decades of Nuclear Testing, *Health Physics.*, 33, 55-71.

Chen, B., W.-J. Cai, and L. Chen (2015), The marine carbonate system of the Arctic Ocean: Assessment of internal consistency and sampling considerations, summer 2010, *Marine Chemistry*, 176, 174-188.

Curry, W, B and R. K. Matthews (1981), Equilibrium $^{18}O$ fractionation in small size fraction planktic foraminifera: Evidence from Recent Indian Ocean sediments, *Mar. Micropaleontol*., 6, 327-337.

Dai, Y., J. Yu, and H. J. H. Johnstone (2016), Distinct responses of planktonic foraminiferal B/Ca to dissolution on seafloor, *Geochem. Geophys. Geosy*st., 17, 1339–1348, doi:10.1002/2015GC006199.

Darling, K.F., Wade, C.M., Kroon, D., Leigh Brown, A.J., Bijma, J., (1999) The diversity and distribution of modern planktonic foraminiferal small subunit ribosomal RNA genotypes and their potential as tracers of present and past ocean circulations. *Paleoceanography* 14, 3–12.

Darling, K.F.,Wade, C.M., Steward, I.A., Kroon, D., Dingle, R., Leigh Brown, A.J., (2000) Molecular evidence for genetic mixing of Arctic and Antarctic subpolar populations of planktonic foraminifers. *Nature* 405, 43–47.

Darling, K.F., Kucera, M.,Wade, C.M., von Langen, P., Pak, D., (2003) Seasonal occurrence of genetic types of planktonic foraminiferal morphospecies in the Santa Barbara Channel, *Paleoceanography* 18, 1032. doi:10.1029/2001PA000723.

Darling, K. F., and C. M. Wade (2008), The genetic diversity of planktic foraminifera and the global distrubtion of ribosomal RNA genotypes, *Marine Micropaleo*, 67, 216-238.

Dittert, N., and R. Henrich (2000), Carbonate dissolution in the South Atlantic Ocean: evidence from ultrastructire breakdown in *Globigerina bulloides*, *Deep-Sea Resrarch, Part I*, 47, 603-620.

de Moel, H., G. M. Ganssen, F. J. C. Peeters, S. J. A. Jung, D. Kroon, G. J. A. Brummer, and R. E. Zeebe (2009) Planktic foraminiferal shell thinning in the Arabian Sea due to anthropogenic ocean acidification? *Biogeosciences*, 6, 1917–1925.

de Villiers, S. (2004), Optimum growth conditions as opposed to calcite saturation as a control on the calcification rate and shell-weight of marine foraminifera, Mar. Biol., 144(1), 45–49, doi:10.1007/s00227-003-1183-8.

De'ath, G., J. M. Lough, K. E. Fabricius (2009), Declining coral calcification on the Great Barrier Reef, *Science* 342 (6158) 599, doi: 10.1126/science.1165283.

Di Lorenzo E, Miller AJ, SchneiderNand McWilliams JC (2005) The warming of the California current system: dynamics and ecosystem implications, *J. Phys. Oceanogr*. 35 336–62.

Dickson, A.G., and F.J. Millero, (1987), A comparison of the equilibrium constants for the dissociation of carbonic acid in seawater media. *Deep-Sea Research* 34, 1733–1743.

Dickson, A.G. (1990), Standard potential of the reaction: AgCl(s) + ½H2(g) = Ag(s) + HCl(aq), and the standard acidity constant of the ion HSO4 in synthetic sea water from 273.15 to 318.15 K, *J. Chem. Thermodyn*. 22: 113–127.

Doney, S. C., M. Ruckelshaus, J. E. Duffy, J. P. Barry, F. Chan, C. A. English, H. M. Galindo, J. M. Grebmeier, A. B. Hollowed, N. Knowlton, J. Polovina, N. N. Rabalais, W. J. Sydeman, L. D. Talley (2012) Climate change impacts on marine ecosystems, Annu. Rev. Mar. Sci. 2012. 4:11–37, 10.1146/annurev-marine-041911-111611.

Etheridge, D.M., L.P. Steele, R.L. Langenfelds, R.J. Francey, J.-M. Barnola, and V.I. Morgan. (1996), Natural and anthropogenic changes in atmospheric CO2 over the last 1000 years from air in Antarctic ice and firn. *Journal of Geophysical Researc*h, 101, 4115-4128.

Fabry, V., Seibel, B., Feely, R., and Orr, J., 2008. Impacys of ocean acidification on marine fauna and ecosystem processes, ICES Journal of Marine Science 65, 414-432.

Fairbanks, R.G., M. Sverdlove, R. Free, P.H. Wiebe, and A.W.H. Bé, (1982), Vertical distribution and isotopic fractionation of living planktonic foraminifera from the Panama Basin, *Nature* 298, 841–844. doi:10.1038/298841a0.

Feely, R. A., Sabine, C. L., Lee, K., Berelson, W., Kleypas, J., Fabry, V. J., Millero, F. J. (2004) Impact of Anthropogenic $CO_2$ on the $CaCO_3$ System in the Oceans. *Science* 305, 362-366.

Feely, R. A., C. L. Sabine, J. M. Hernandez-Ayon, D. Ianson, and B. Hales (2008) Evidence for Upwelling of Corrosive 'Acidified' Water onto the Continental Shelf. *Science* 320 (5882), 1490–92. doi:10.1126/science.1155676.

Feely, R. A, S. R. Alin, J. Newton, C. L. Sabine, M. Warner, A. Devol, C. Krembs, C. Maloy (2010) The combinded effects of ocean acidification, mixing, and respiration on pH and carbonate saturation in an urbanized estuary. *Estuarine, Coastal and Shelf Science* 88 (4), 442-449.

Fehrenbacher, J. S., H. J. Spero and A. D. Russell (2011) Observations of living non-spinose planktic foraminifers *Neogloboquadrina dutertrei* and *N. pachyder*ma from specimens grown in culture, *AGU Fall Meeting 2011,* Abstract #PP41A-1724.

Ferguson, J. E., K. R. Johnson, G. Santos, L. Mayer, A. Tripati (2013) Investigating δ13C and Δ14C within Mytilus californianus shells as proxies of upwelling intensity, *Geochem. Geophys. Geosys.,* 14 (6) 1856-1865, doi:10.1002/ggge.20090.

Field, D., D. Cayan, and F. Chavez (2006) Secular warming in the California Current and North Pacific, *CalCOFI Rep.,* 47.

Foster, G.L. (2008), Seawater pH, $pCO_2$ and $[CO_3^{2-}]$ variations in the Caribbean Sea over the last 130 kyr: a boron isotope and B/Ca study of planktic foraminifera, *Earth and Planetary Science Letters*, 271, 254.

Fassbender, A. J., S. R. Alin, R. A. Feely, A. J. Sutton, J. A. Newton, R. H. Byrne (2016) Estimating total alkalinity in the Washington State Coastal Zone: Complexities and surprising utility for ocean acidification research, *Estuaries and Coasts,* doi:10.1007/s12237-016-0168-z.

Friddell, J. E., R. C. Thunell, T. P. Guilderson, and M. Kashgarian (2003), Increased northeast Pacific climatic variability during the warm middle Holocene, *Geophys. Res. Lett.,* 30, 1560, doi:10.1029/2002GL016834, 11.

Ganssen, G., and M. Sarnthein (1983), Stable isotope composition of foraminifers: The surface and bottom water record of coastal upwelling, in Coastal Upwelling: Its Sedimentary Record, Part A, edited by J. Thiede and E. Suess, pp. 99-121, Plenum, New York.

Ganssen, G. M., F. J. C. Peeters, B. Metcalfe, P. Anand, S. J. A. Jung, D. Kroon, AND G.-J. Brummer (2011) Quantifying sea surface temperature ranges of the Arabian Sea for the past 2000 years, *Climate of the Past,* 7:1337–1349.

Gastrich, M. D. (1987), Ultrastructure of a new intracellular symbiotic alga found within planktonic foraminifera1, J. Phycol., 23(4), 623–632.

Gonzalez-Mora, B., F. J. Sierro, and J. A. Flores (2008), Controls of shell calcification in planktonic foraminifers, Quat. Sci. Rev., 27(9–10), 956–961, doi:10.1016/j.quascirev.2008.01.008.

Gruber, N., C. Hauri, Z. Lachkar, D. Loher, T.L. Frölicher, and G. Plattner (2012) Rapid Progression of Ocean Acidification in the California Current System, *Science* 337, 220-223.

Hauri, C., Gryver, N., Plattner, G., Alin, S., Feely, R. A., Hales, B., Wheeler, P. A., 2009, Ocean acidification in the California Current System, *Oceanography* 22, 60-71.

Hauri, C., N. Gruber, A. M. P. McDonnell, M. Vogt (2013) The intensity duration and severity of low aragonite saturation state events on the California continental shelf *Geophysical Research Letters* 40, 3424-3429, doi:10.1002/grl.50618, 2013.

Hare, S. R. (1996): Low frequency climate variability and salmon production. Ph.D. Dissertation. Univ. of Washington, Seattle, WA, 306 pp.

Hecht, A. D. (1976), An ecologic model for test size variation in recent planktonic foraminifera: Applications to the fossil record, J. Foraminiferal Res., 6(4), 295–311, doi:10.2113/gsjfr.6.4.295.

Hemleben, C., M. Spintiler, and O. R. Anderson, Modern Planktonic Foraminifera, 363 pp., Springer-Verlag, New York, 1989.

Hemming, N.G., Hanson, G.N. (1992), Boron isotopic composition and concentration in modern marine carbonates. *Geochim. Cosmochim. Acta* 56, 537–543.

Hemming, N. G., R. J. Reeder, and G. N. Hanson (1995), Mineral-fluid partitioning and isotopic fractionation of boron in synthetic calcium carbonate, *Geochim. Cosmochim. Acta*, 59(2), 371–379, doi:10.1016/0016-7037(95)00288-B.

Hemming, N. G., R. J. Reeder, S. R. Hart (1998) Growth step selective incorporation of boron on the calcite surface, *Geocim. Cosmochim. Acta*, 62, 2915-2922.

Hendershott, M. and C. Winant (1996), Surface circulation in the Santa Barbara Channel, *Oceanography* 9, 114-121.

Hendy, I. and J. Kennett (1999), Latest Quaternary North Pacific surface-water responses imply atmosphere-driven climate instability, *Geology*, 27(4)291-294.

Hendy, I. L., and J. P. Kennett (2000) Dansgaard-Oeschger cycles and the California Current System: Planktonic foraminiferal response to rapid climate change in Santa Barbara Basin, Ocean Drilling Program hole 893A, *Paleoceanography*, 15, 30– 42.

Henehan, M., J. Rae, G. Foster, J. Erez, K. Prentice, M. Kucera, H. Bostock, J. Milton, P. Wilson, B. Marshall, and T. Elliott (2013) Calibration of the boron isotope proxy in the planktonic foraminifera *Globigerinoides ruber* for use in paleo-$CO_2$ reconstruction, *Earth and Planetary Sciences Letters* 364, 111-122.

Henehan, M.J., Foster, G.L., Rae, J.W.B., Prentice, K.C., Erez, J., Bostock, H.C., Marshall, B.J., Wilson, P.A., (2015) Evaluating the utility of B/Ca ratios in planktic foraminifera as a proxy for the carbonate system: a case study of *Globigerinoides ruber*. *Geochemistry, Geophys. Geosystems* 1–18.doi:10.1002/2014GC005514

Honisch, B., J. Bijma, A. D. Russell, H. J. Spero, M. R. Palmer, R. E. Zeebe, and A. Eisenhauer (2003), The influence of symbiont photosynthesis on the boron isotopic composition of foraminifera shells, *Mar. Micropaleo*ntol., 49(1–2), 87–96, doi:10.1016/S0377-8398(03)00030-6.

Honisch, B., N. G. Hemming, B. Loose (2007) Comment on "A critical evaluation of the boron isotope-pH proxy: the accuracy of ancrient ocean pH estimates" by M. Pagani, D. Lemarchand, A. Spivack and J. Gaillardet, *Geochim. Cosmochim. Acta*, 71, 1636-1641.

Huang, W.-J., Y.Wang, and W.-J. Cai (2012) Assessment of sample storage techniques for total alkalinity and dissolved inorganic carbon in seawater. *Limnol. Oceanogr. Methods* 10: 711-717.

Hut, G., (1987), Stable isotope reference samples for geochemical and hydrological investigations, International Atomic Energy Agency, Vienna.

Jansen, H., R. E. Zeebe, and D. A. Wolf-Gladrow (2002), Modeling the dissolution fo settling $CaCO_3$ in the ocean, *Global Biogeochem. Cycles*, 16(2).

Jørgensen, B. B., J. Erez, N. P. Revsbech and Y. Cohen (1985), Symbiotic photosynthesis in a planktonic foraminiferan, *Globigerinoides sacculifer* (Brady), studied with microelectrodes. *Limnol. Oceanogr.*, 30(6), 1253-1267.

Kaczmarek, K., Nehrke, G., Misra, S., Bijma, J., Elderfield, H., 2016. Investigating the effects of growth rate 910 and temperature on the B/Ca ratio and δ11B during inorganic calcite formation. Chem. Geol. 421, 81–92. doi:10.1016/j.chemgeo.2015.12.002

Keeling, C. D. (1979), The Suess effect: $^{13}$Carbon-$^{14}$Carbon interrelations, *Environ. Int.*, *2*(4–6), 229–300, doi:10.1016/0160-4120(79)90005-9.

Khatiwala, S., Tanhua, T., Mikaloff Fletcher, S., Gerber, M., Doney, S. C., Graven, H. D., Gruber, N., McKinley, G. A., Murata, A., Ríos, A. F., and Sabine, C. L. (2013), Global ocean storage of anthropogenic carbon, *Biogeosciences*, 10, 2169–2191, doi:10.5194/bg-10-2169-2013.

Killingley, J. S., R. F. Johnson, AND W. H. Berger (1981), Oxygen and carbon isotopes of individual shells of planktonic foraminifera from Ontong-Java Plateau, Equatorial Pacific. *Palaeogeography, Palaeoecology, Palaeoclimatology*, 33:193–204.

Kincaid, E., R. Thunell, C. Lange, and A. Weinheimer (2000) Plankton fluxes in the Santa Barbara Basin: response to seasonal and interannual changes, *Deep-Sea Research* 47, 1157-1176.

Kinsey, D. W. and P. J. Davies (1979) Effects of elevated nitrogen and phosphorous on coral reef growth, *Limnol. Oceanog*., 24, 935– 940.

Klaas, C. & Archer, D. (2002) Association of sinking organic matter with various types of mineral ballast in the deep sea: implications for the rain ratio. *Global Biogeochem. Cy.* 16, 63. DOI:10.1029/2001GB001765).

Koide, M., A. Soutar, and E. D. Goldberg (1972), Marine geochronology with Pb-210, *Earth and Planetary Sci. Letters*, 14, 422-446.

Krishnaswami, S., D. Lai, S. Amin, and A. Soutar (1973), Geochronological studies in Santa Barbara Basin: Fe-55 as a unique tracer for particulate settling, *Limnology and Oceanography*, 18, 763-770.

Kroeker, K. J., R. L. Kordas, R. Crim, I. E. Hendriks, L. Ramajo, G. S. Singh, C. M. Duarte, J-P. Gattuso (2013) Impacts of ocean acidification on marine organisms: quantifying sensitivities and interaction with warming, *Global Change Biology* 19 (6) 1884-1896, 10.1111/gcb.12179.

Kroon, D., and G. Ganssen (1988) Northern Indian Ocean upwelling cells and the stable isotope composition of living planktic foraminifers, in Planktonic Foraminifers as Tracers of Ocean-Climate History, edited by G.-J. Brummer and D. Kroon, pp. 299-317, Free University Press, Amsterdam, 1988.

Kučera M. Planktonic Foraminifera as tracers of past oceanic environments. In: Hillaire-Marcel C, de Vernal A, Chamley H, editors. Proxies in late Cenozoic paleoceanography. vol. 1 of Developments in Marine Geology. Amsterdam: Elsevier; 2007. pp. 213–262.

Le Quéré, C., and others (2015) Global Carbon Budget 2015, *Earth Syst. Sci. Data*, 7, 349-396, DOI doi:10.5194/essd-7-349-2015.

Lebrato, M. D. Inglesias-Rodriguez, R. A. Feely, D. Greenley, D. O. Jones, N. Suarez-Bosche, R. S. Lampitt, J. A. Cartes, D. R. H. Green, B. Alker (2010) Global contribution of echinoderms to the marine carbon cycle: $CaCO_3$ budget and benthic compartments, *Ecological Monographs*80 (3), 441-467.

Lee, K., T.-W. Kim, R. H. Byrne, Y.-M. Liu (2010), The universal ratio of boron to chlorinity for the North Pacific and North Atlantic Oceans, *Geochimica et Cosmochimia Acta*, 74(6), 1801-1811.

Lewis, E., and D.W.R. Wallace (1998) Program Developed for CO2 System Calculations, ORNL/CDIAC-105, Carbon dioxide Inf.Anal. Cent. Oak Ridge Nat. Lab., U.S. Dep. of Energy, Oak Ridge, Tenn..

Lin, Y.-P., and P. C. Singer (2006) Inhibition of calcite precipitation by orthophosphate: speciation and thermodynamic considerations, *Geochim. Cosmochim. Ac.*, 70, 2530–2539.

Lombard, F., J. Erez, E. Michel, and L. Labeyrie (2009) Temperature effect on respiration and photosynthesis of the symbiont-bearing planktonic foraminifera *Globigerinoides ruber*, *Orubulina universa*, and *Globigerinella siphonifera*, *Limnol. Oceanogr.*, 54(1), 210-218.

Lombard, F., R. E. da Rocha, J. Bijma, and J. P. Gattuso (2010), Effect of carbonate ion concentration and irradiance on calcification in planktonic foraminifera, *Biogeosciences*, 7(1), 247–255, doi:10.5194/bg-7-247-2010.

McGowan, J., S. Bograd, R. J. Lynn, and A. J. Miller, 2003: The biological response to the 1977 regime shift in the California Current. Deep-Sea Res., 50, 2567–2582.

Manno, C., N. Morata, and R. Bellerby (2012), Effect of ocean acidification and temperature increase on the planktonic foraminifer Neogloboquadrina pachyderma (sinistral), *Polar Bio*l., 35, 1311–1319.

Mantua, N. J. and S. R. Hare (2002) The Pacific decadal oscillation, *J. Oceanogr*. 58 35–44, doi:10.1023/A:1015820616384.

Marshall, B.J., R. Thunell, M. Hennehan, Y.Astor, and K. Wejnert (2013) Planktonic foraminiferal area density as a proxy for carbonate ion concentration: A calibration study using the Cariaco Basin ocean time series, *Paleoceanography* 28, 1-14, doi:10.1002/palo.20034.

Marshall, B. J., R. C. Thunell, H. J. Spero, M. J. Henehan, L. Lorenzoni, and Y. Astor (2015) Morphometric and stable isotopic differentiation of *Orbulina universa* morphotypes from the Cariaco Basin, Venezuela, *Marine Micropaleo.*, 120, 46-64.

Mavromatis, V., Montouillout, V., Noireaux, J., Gaillardet, J., Schott, J., (2015) Characterization of boron incorporation and speciation in calcite and aragonite from co-precipitation experiments under controlled pH, temperature and precipitation rate. *Geochim. Cosmochim. Acta,* 150, 299–313. doi:10.1016/j.gca.2014.10.024

Mehrbach, C., C.H. Culberson, J.E. Hawley, and R.N. Pytkowicz (1973) Measurement of the apparent dissociation constants of carbonic acid in seawater at atmospheric pressure, *Limnology and Oceanography*, 18, 897–907.

Meier, K. J. S., L. Beaufort, S. Heussner, P. Ziveri (2014) The role of ocean acidification in *Emiliania huxleyi* coccolith thinning in the Mediterranean Sea, *Biogeosciences* 11, 2857-2869, doi:10.5194/bg-11-2857-2014.

Mekik, F., and L. Raterink (2008), Effects of surface ocean conditions on deep-sea calcite dissolution proxies in the tropical Pacific, *Paleoceanography*, 23, PA1216, doi:10.1029/2007PA001433.

Milliman, J. D., P. J. Troy, W. M. Balch, A. K. Adams, Y.-H. Li, and F. T. Mackenzie (1999) Biologically mediated dissolution of calcium carbonate above the chemical lysocline? *Deep Sea Res., Part I,* 46, 1653– 1669.

Misra, S., M. Greaves, R. Owen, J. Kerr, A. C. Elmore, and H. Elderfield (2014), Determination of B/Ca of natural carbonates by HR-ICP-MS, *Geochem. Geophys. Geosyst*., 15, doi:10.1002/2013GC005049.

Moore, W. S. (1984), Radium isotope measurements using germanium detectors, Nuclear Instruments & Methods in Physics Research 223 (2-3), 407-411.

Moy, A.D., W.R. Howard, S.G.Bray, and T.W. Trull (2009) Reduced calcification in modern Southern Ocean planktonic foraminifera, *Nature Geoscience* 2, 276–280.

Mucci, A. (1983) The solubility of calcite and aragonite in seawater at various salinities, temperatures and one atmosphere total pressure, *American Journal of Science*, 283, 780-799.

Nam, S., H-J Kim, and U. Send (2011) Amplification of hypoxic and acidic events by La Nina conditions on the continental shelf off California, *Geophys. Res. Lett.*, 38, doi:10.1029/2011GL049549.

Ni, Y., G. L. Foster, T. Bailey, T. Elliott, D. N. Schmidt, P. Pearson, B. Haley, and C. Coath (2007), A core top assessment of proxies for the ocean carbonate system in surface-dwelling foraminifers, Paleoce*a*nography, 22, PA3212, doi:10.1029/2006PA001337.

Orr, James C., Victoria J. Fabry, Olivier Aumont, Laurent Bopp, Scott C. Doney, Richard A. Feely, Anand Gnanadesikan, et al. (2005). Anthropogenic Ocean Acidification over the Twenty-First Century and Its Impact on Calcifying Organisms. *Nature* 437 (7059), 681–86. doi:10.1038/nature04095.

Osborne, E. B., R. C. Thunell, B. J. Marshall, J. A. Holm, E. J. Tappa, C. Benitez-Nelson, W.-J. Cai, and B. Chen(2016), Calcification of the planktonic foraminifera *Globigerina bulloides* and carbonate ion concentration: Results from the Santa Barbara Basin, Paleoceanography, 31, doi:10.1002/2016PA002933.

Pak, D. K., and J. P. Kennett (2002) A Foraminiferal Isotopic Proxy for Upper Water Mass Stratification, *The Journal of Foraminiferal Research* 32 (3), 319–27.

Pak, D. K., D. W. Lea, and J. P. Kennett (2004), Seasonal and interannual variation in Santa Barbara Basin water temperatures observed in sediment trap foraminiferal Mg/Ca, *Geochem. Geophys. Geosyst*., 5, Q12008, doi:10.1029/2004GC000760.

Pak, D. K., D. W. Lea, and J. P. Kennett (2012), Millennial scale changes in sea surface temperature and ocean circulation in the northeast Pacific, 10–60 kyr BP, *Paleoceanography*, 27, PA1212, doi:10.1029/2011PA002238.

Paasche, E. and S. Brubank (1994) Enhanced calcification in the coccolithophorid Emiliania huxleyi (Haptophyceae) under phosphorus limitation, *Phycologia*, 22, 324–330.

Peeters, F., E. Ivanova, S. Conan, G.-J. Brummer, G. Ganssen, S. Troelstra, and J. van Hinte (1999), A size analysis of planktic Foraminifera from the Arabian Sea, *Mar. Micropaleontol*., 36(1),31–61.

Pierrot, D., Lewis, E., Wallace, D.W.R. 2006. MS Excel Program Developed for CO2 System Calculations. ORNL/CDIAC-105a. Carbon Dioxide Information Analysis Center, Oak Ridge National Laboratory, U.S. Department of Energy, Oak Ridge,Tennessee. Prell, W. L., and W. B. Curry, Faunal and isotopic indices of monsoonal upwelling: Western Arabian Sea, Oceanol. Acta, 4, 91-98, 1981.

Prell, W. L., and W. B. Curry (1981) Faunal and isotopic indices of monsoonal upwelling: Western Arabian Sea, *Oceanol. Acta*, 4, 91-98.

Quintana Krupinaski, N. B., A. D. Russell, D. K. Pak and A. Paytan (submitted) Core-top calibration of B/Ca in Pacific Ocean *Neogloboquadrina incompta* and *Globigerina bulloid*es as a surface water carbonate system proxy, *Earth and Planetary Sci. Letters*.

Rae, J. W. B., G. L. Foster, D. N. Schmidt, and T. Elliott (2011) Boron isotopes and B/Ca in benthic foraminifera: proxies for the deep ocean carbonate system, *Earth Planet. Sci. Lett.* 302, 403–413.

Reimers C.E., M. Kastern, and R. E. Garrison (1990) The role of bacteria mats in phosphate mineralization with particular reference to the Monterey Formation, p. 300-311. W. C. Burnett & S. R. Riggs [eds.], Phosphate deposits of the world. V. 3. Cambridge.

Ries, J. B., A. L. Cohen, and D. C. McCorkle (2009), Marine calcifiers exhibit mixed responses to CO2-induced ocean acidification, Geology, 37(12), 1131–1134, doi:10.1130/G30210A.1.

Rink, S., M. Kuhl, J. Bijma, and H. J. Spero (1998) Microsensor studies of photosynthesis and respiration in the symbiotic foraminifer Orbulina universa, *Mar. Biol*., 131, 583–595.

Ritchie, J. C., and J. R. McHenry (1989) Application of radioactive fallout Cesium-137 for measuring soil erosion and sediment accumulations rates and patterns: A review, *J. Environ. Qual.*, 19, 215-233.

Roemmich, D. and J. McGowan (1995) Climatic warming and the decline of zooplankton in the California Current. *Science*, 267, 1324–1326.

Sabine C. L., Feely, R.A., Gruber, N., Key, R. M., Lee, K., Bullister, J. L., Wannikhof, R., Wong, C. S., Wallace, D. W. R., Tilbrook, B., Millero, F. J., Peng, T., Kozyr, A., Ono, T., Rios, A. F. (2004) The Oceanic Sink for Anthropogenic $CO_2$. *Science* 305, 367-371.

Sadekov, A. Y., et al. (2016), Geochemical imprints of genotypic variants of *Globigerina bulloides* in the Arabian Sea, *Paleoceanography*, 31, doi:10.1002/2016PA002947.

Salmon, K. H., P. Anand, P. F. Sexton, M. Conte (2016) Calficaition and groth processes in planktonic foraminifera complicate the use of B/Ca and U/Ca as carbonate chemistry proxies, *Earth and Planetary Sci. Lett.*, 449, 372-381.

Sanyal, A., N. G. Hemming, W. S. Broecker, D. W. Lea, H. J., Spero, G. N. Hanson, (1996) Oceanic pH control on the boron isotopic composition of foraminifera: evidence from culture experiments. *Paleoceanography* 11, 513-517.

Sanyal, A., J. Bijma, H. J. Spero, D. W. Lea (2001) Empirical relationship between pH and the boron isotopic composition of *G. sacculifer*: inplications for the boron isotope paleo-pH proxy, *Paleoceanography*, 16, 515-519.

Sautter, L. R., and R.C. Thunell (1991a), Planktonic foraminiferal response to upwelling and seasonal hydrographic conditions: Sediment trap results from San Pedro Basin, Southern California Bight: J. of Foram. Research, 21(4), 347-363.

Sautter, L. R., and R.C. Thunell (1991b), Seasonal Variability in the $\delta^{18}O$ and $\delta^{13}C$ of planktonic foraminifera from an upwelling environment: Sediment trap results from the San Pedro Basin, Southern California Bight: Paleoceanography, 6(3), 307-334.

Schiebel, R. (2002) Planktonic foraminiferal sedimentation and the marine calcite budget, *Global Biogeochem Cycles* 16(4),13-1–13-21.

Schiffelbein, P., and S. Hills (1984), Direct assessment of stable isotope variability in planktonic foraminifera populations. *Palaeogeography, Palaeoclimatology, Palaeoecology*, 48:197–213.

Schmidt, D. N., S. Renaud, J. Bollmann, R. Schiebel, and H. R. Thierstein (2004), Size distribution of Holocene planktic foraminifer assemblages: Biogeography, ecology and adaptation, *Mar. Micropaleontol*., 50(3-4), 319-338, doi:10.1016/S0377-8398(03)00098-7.

Spero, H.J., J. Bijma, D.W. Lea, and B.E. Bemis (1997), Effect of seawater carbonate concentration on foraminiferal carbon and oxygen isotopes, *Nature* 390(6659), 497–500.

Takahashi, T., R.T. Williams, and D.L. Bos. (1982) Carbonate chemistry. Pp. 77–83 in GEOSECS Pacific Expedition, vol. 3, Hydrographic Data 1973–1974. W.S. Broecker, D.S. Spencer, and H. Craig, eds, National Science Foundation, Washington, DC.

Thiede, J., Skeletal plankton and nekton in upwelling water masses off northwestern South America and northwestern Africa, in Coastal Upwelling: Its Sedimentary Record, Part A, edited by J. Thiede and E. Suess, pp. 183-208, Plenum, New York, 1983.

Thunell, R., R. S. Keir, and S. Honjo (1981), Calcite dissolution: An in situ study from the Panama Basin, *Science* 212 (4495), 659-661.

Thunell, R., E. Tappa, and D. Anderson (1995), Sediment fluxes and varve formation in Santa Barbara Basin, offshore California, *Geology* 23, 1083-1086.

Thunell, R. (1998), Particle fluxes in a coastal upwelling zone: sediment trap results from Santa Barbara Basin, California, *Deep-Sea Research* 45, 1863-1884.

Thunell, R., C. Benitez-Nelson, R. Varela, Y. Astor, and F. Muller-Karger (2007), Particulate Organic Carbon Fluxes Along Upwelling-Dominated Continental Margins: Rates and Mechanisms, *Global Biogeochemical Cycles*, 21, GB1022, doi:1029/2006GB002793.

Thunell, R. C., E. Tappa, C. Pride, and E. Kincaid (1999) Sea-surface temperature anomalies associated with the 1997-1998 El Niño recorded in the oxygen isotope composition of planktonic foraminifera, *Geology*, 27(9), 843-846.

Turi , G., Z. Lachkar, N. Gruber, M. Munnich (2016) Climatic modulation of recent trends in ocean acidification in the California Current System, *Environ. Res. Lett.* 11, doi:10.1088/1748-9326/11/1/014007.

Uchikawa, J., Penman, D.E., Zachos, J.C., Zeebe, R.E., 2015. Experimental evidence for kinetic effects on B/Ca in synthetic calcite: Implications for potential B(OH)4− and B(OH)3 incorporation. Geochim. Cosmochim. Acta 150, 171–191. doi:10.1016/j.gca.2014.11.022

Watson, E.B., (2004) A conceptual model for near-surface kinetic controls on the trace-element and stable isotope composition of abiogenic calcite crystals. *Geochim. Cosmochim. Acta 68*, 1473–1488. doi:10.1016/j.gca.2003.10.003

Weinkauf, M. F. G., T. Moller, M. C. Koch, and M. Kučera (2013), Calcification intensity in planktonic Foraminifera reflects ambient conditions irrespective of environmental stress, Biogeosciences, 10(10), 6639–6655.

Weinkauf, M. F. G., J. G. Kunze, J. J. Waniek, and M. Kučera (2016), Seasonal variation in shell calcification of planktonic Foraminifera in the NE Atlantic reveals species-specific response to temperature, productivity, and optimum growth conditions, PLOS ONE, 11(2), e148363.

Weiss R. F. (1974) Carbon dioxide in water and seawater: the solubility of a non-ideal gas. *Marine Chemistry* 2, 203-215.

Yu, J., J. Day, M. Greaves, and H. Elderfield (2005), Determination of multiple element/calcium ratios in foraminiferal calcite by quadrupole ICP-MS, *Geochem. Geophys. Geos*yst., 6, Q08P01, doi:10.1029/2005GC000964.

Yu, J., H. Elderfield, and B. Honisch (2007) B/Ca in planktonic foraminifera as a proxy for surface seawater pH. *Paleoceanography* 22, 1-17.

Yu, J., G.L. Foster, H. Elderfield, W.S. Broecker, and E. Clark (2010) An evaluation of benthic foraminiferal B/Ca and **δ**11B for deep ocean carbonate ion and pH reconstructions, *Earth Planet. Sci. Lett.*, 293 (1–2), 114–12

Zeebe, R. E. and D. A. Wolf-Gladrow (2001), CO2 in Seawater: Equilibrium, Kinetics, Isotopes. Elsevier Oceanography Series, 65, pp. 346, Amsterdam.

# APPENDIX A – SUPPORTING INFORMATION FOR CHAPTER 1

## Introduction

Supporting text are in-depth descriptions of methodologies and statistical assessments that are referenced and briefly described in the main text. Supporting figures supplement data trends described in the text. Datasets include the sediment trap calibration data, age model radioisotope counts and historic approximation of the marine carbonate system.

**Text S1.** Approximately 2 grams from each sample were freeze dried and used for radioisotope measurements. Wet weights, recorded prior to freeze drying, and dry weights were used to estimate sample porosity and correct for compaction. Freeze dried sediments were ground, loaded into counting vials and sealed with epoxy for 3 weeks prior to counting. Each sample was measured (3-5 days) for $^{210}$Pb, $^{214}$Pb and $^{137}$Cs via gamma decay counting using a high purity germanium well detector [*Moore*, 1984].

The excess $^{210}$Pb ($^{210}Pb_{ex}$), reflective of atmospheric deposition rather than supported $^{210}$Pb ($^{210}Pb_{supp}$) from the decay of $^{226}$Ra, was determined by subtracting the activity of $^{214}$Pb (assumed to be in secular equilibrium with $^{210}Pb_{supp}$; mean 3.7 dpm/gm) from the activity of $^{210}$Pb. The exponential decay of $^{210}Pb_{ex}$ observed in the core sediments (Figure 3) used to determine ages for the core using a combination of Constant Initial Concentration (CIC) and Constant Rate of $^{210}$Pb Supply (CRS) models. An offset of approximately ±1 year between models is used to represent the error on sample age

estimates. Using these age constraints an average sedimentation rate of 0.43 cm $yr^{-1}$; and an average mass accumulation rate of 5.84 g $cm^2$ $yr^{-1}$ was determined for the core. The sedimentation rate determined from the $^{210}Pb_{ex}$ is relatively uniform over the entire 0.5 m core and is also in good agreement with previously determined radioisotope chronologies for the SBB [*Koide et al.*, 1972; *Krishnaswami et al.*, 1973, *Bruland et al.*, 1974]. The increase in $^{137}Cs$ activity at 19 cm (Figure 3) is used as an independent age marker horizon for the year 1964 and represents the peak in radioactive fallout from atmospheric nuclear bomb testing [*Carter and Moghissi*, 1977; *Ritchie and McHenry*, 1989]. The depth of the $^{137}Cs$ spike was shallower than expected using both the CRS and CIC models when assuming a 2012 collection year as the core top age. We therefore conclude that the upper several centimeters of sediments were not preserved when this box-core was collected. As such, we applied a 6 year age correction that anchored the 19 cm $^{137}Cs$ spike to a depositional year of 1964. These age constraints indicate that the 0.5 meter core extends back to ~1895 and the uppermost sediments contained in the core represent the year ~2006.

**Text S2.** Water samples used for TA and DIC analysis were poisoned with $HgCl_2$ and stored in borosilicate glass narrow-neck bottles with ground stopper tops sealed with vacuum grease prior to analysis. TA samples were analyzed using an automated titrator (AS-A2, Apollo Scitech, USA) following the method detailed in *Cai et al.* [2010]. Briefly, a 25- mL seawater sample was used for each titration in an open- cell setting. Variable amounts of 0.1 N HCl were added to the seawater samples until they reached a pH value of 3.8. Then, equal volumes of HCl were added six times to the titration vessel until a final pH value of <3 was reached. The titration end- point was determined by a

linear function, i.e., Gran titration method. Water samples, standards, titrants, and titration vessels were all kept at 22.0°C using water jackets. Each sample was titrated at least twice with an overall precision of better than ±0.1%. DIC was measured using a DIC analyzer (AS-C3, Apollo Scitech, USA) following the method detailed in *Huang et al.* [2012] and *Chen et al.* [2015]. Seawater samples (0.75 mL) were acidified by $H_3PO_4$, and the released $CO_2$ was subsequently quantified by a nondispersive infrared $CO_2$ detector. Two to three duplicates were measured. The method has a precision of better than ±0.1%. Certified Reference Materials (CRMs) from A. Dickson (SIO, UCSD) were used throughout the sample analysis to insure an accuracy of ±0.1% for both TA and DIC data.

**Text S3.** Multicollinearity occurs when two or more predictor variables are inter-related causing difficulty in determining the influence of a single independent variable on the dependent variable response. Collinearity diagnostics such as tolerance and variance inflation factor can be used to identify if bivariate relationships exist between the predictor variables. Tolerance ($1-R^2$) indicates the extent to which the independent variable cannot be predicted by another independent variable. Tolerance values can range from 0 to 1 with values <0.2 indicating that collinearity is an issue. The variance inflation factor or VIF ($(1-R^2)^{-1}$) is another collinearity diagnostic that describes the amount that the standard error of the independent variable will increase due to collinearity. VIF values can range from 0 to 10, with a value of 4 indicating a doubling of the standard error. Tolerance values close to 1 and VIF values less than 2 indicate that collinearity is not an issue.

Results based on collinearity diagnostics from our dataset indicate that [$CO_3^{2-}$] and temperature are highly collinear, while [$CO_3^{2-}$] and [$PO_4^{3-}$] are moderately collinear. By replacing measured values for an independent variable with residual values calculated for that variable, SLR can be used to estimate the significance of relationships after accounting the covariance with another predictor variable. For example, [$CO_3^{2-}$] residuals of [$PO_4^{3-}$] ([$PO_4^{3-}$]$_{Cres}$) were estimated by using the SLR equations relating [$PO_4^{3-}$] to [$CO_3^{2-}$] to determine a predicted [$PO_4^{3-}$] value and then subtracting the predicted value from the measured value of [$PO_4^{3-}$]. This residual represents the variability in [$PO_4^{3-}$] that is unrelated to its covariance with [$CO_3^{2-}$]. By replacing temperature and [$PO_4^{3-}$] measured values with calculated [$CO_3^{2-}$] residuals, collinearity issues are resolved as indicated by tolerance >0.2 and VIF <2. Note that the determination of temperature and [$PO_4^{3-}$] residuals for [$CO_3^{2-}$] and replacing measured [$CO_3^{2-}$] with residual [$CO_3^{2-}$] values yields the same results. Further SLR between temperature$_{Cres}$ and [$PO_4^{3-}$]$_{Cres}$ with area density produce insignificant relationships ($p > 0.05$) with low correlation coefficients (Temperature $R^2 = 0.07$, [$PO_4^{3-}$] $R^2 = 0.01$).

Several hierarchical regression models (HRM) were conducted to determine the influence of each of the predictor variables on area density in a stepwise fashion. Each model lists the predictor variables in order of importance ($X_1$, $X_2$ and $X_3$) and the change in the correlation coefficient ($\Delta R^2$) and change in significance ($p\Delta R^2$) are used to identify the importance of each subsequent variable added to the model. The measured value is used as the input for variable $X_1$ while the $X_2$ and $X_3$ variables are the residuals calculated from variable $X_1$. Model 1 uses [$CO_3^{2-}$], temperature$_{Cres}$ and [$PO_4^{3-}$]$_{Cres}$ as variables $X_1$, $X_2$ and $X_3$, respectively, and indicates no increase in $\Delta R^2$ when

temperature$_{Cres}$ and $[PO_4^{3-}]_{Cres}$ are added to the model, with an insignificant change in $p\Delta R^2$ to both of these additions. Model 2 instead uses temperature as $X_1$ and $[CO_3^{2-}]_{Tres}$ and $[PO_4^{3-}]_{Tres}$ as variables $X_2$ and $X_3$ and indicates more than a 10% increase in $\Delta R^2$ and a highly significant change in $p\Delta R^2$ when $[CO_3^{2-}]_{Tres}$ is added to the model. Models 3 and 4 use $[PO_4^{3-}]$ as $X_1$ and interchange $[CO_3^{2-}]_{Pres}$ and temperature$_{Pres}$ as variables $X_2$ and $X_3$. Model 3 uses $[CO_3^{2-}]_{Pres}$ as $X_2$ and indicates a highly significant 25% increase in $\Delta R^2$ whereas the subsequent addition of temperature$_{Pres}$ $X_3$ results in an nonsignificant change in $p\Delta R^2$ and no change in the $R^2$ for the regression. Model 4 echo results of Model 3 and indicates the addition of $[CO_3^{2-}]_{Pres}$ even as the last variable added to the model results in a considerable and significant increase in regression correlation coefficients.

**Text S4.** A time-series of surface ocean temperature exists in the SBB from the year 1955-present and is used to evaluate how temperature and $[CO_3^{2-}]$ have varied over the last 50 years. Because there is no record of sea surface salinity we use a time-series of surface salinity measurements from the Scripps Pier located just south of the SBB, which is likely representative of salinity conditions in the SBB. We couple these *in situ* measurements with total alkalinity and $pCO_2$ to estimate surface ocean $[CO_3^{2-}]$ over the last 50 years using the CO2Sys program. Due to the fact that alkalinity reflects the charge balance of seawater which is unaffected by increasing seawater $CO_2$ alkalinity should remain relatively unchanged over this interval. We use a constant alkalinity value of 2250 μmol kg$^{-1}$, based on mean surface alkalinity values determined by *in situ* measurements from 2007-2010. We use measurements of atmospheric $CO_2$ from the Mauna Loa Time-series to estimate $pCO_2$ assuming a constant atmospheric pressure of 1 atm and determine a time-specific water vapor pressure according to Henry's Law. Henry's Law constants

($K_0$) were determined using the R package by Jean-Marie Epitalon, Aurelien Proye, and Jean-Pierre Gattuso. The $K_0$ determined as a part of this package follow the formulation of *Weiss* [1974] and account for changes in temperature, salinity and pressure. We evaluate our estimates of $pCO_2$ by comparing our values to measured values from the Hawaii Ocean Time-Series (1988-present), which indicate greater variability but good overall agreement with our $pCO_2$ estimates.

$$pCO2(\mu atm)=XCO_2(ppm)(p\text{Atm}-pH_2O)$$

$XCO_2$= Measured Mauna Loa [$CO_2$]

$p$Atm= 1

$pH_2O$= determined in R according to *Weiss*, [1974]

Weiss R. F., 1974 Carbon dioxide in water and seawater: the solubility of a non-ideal gas. *Marine Chemistry* 2, 203-215.

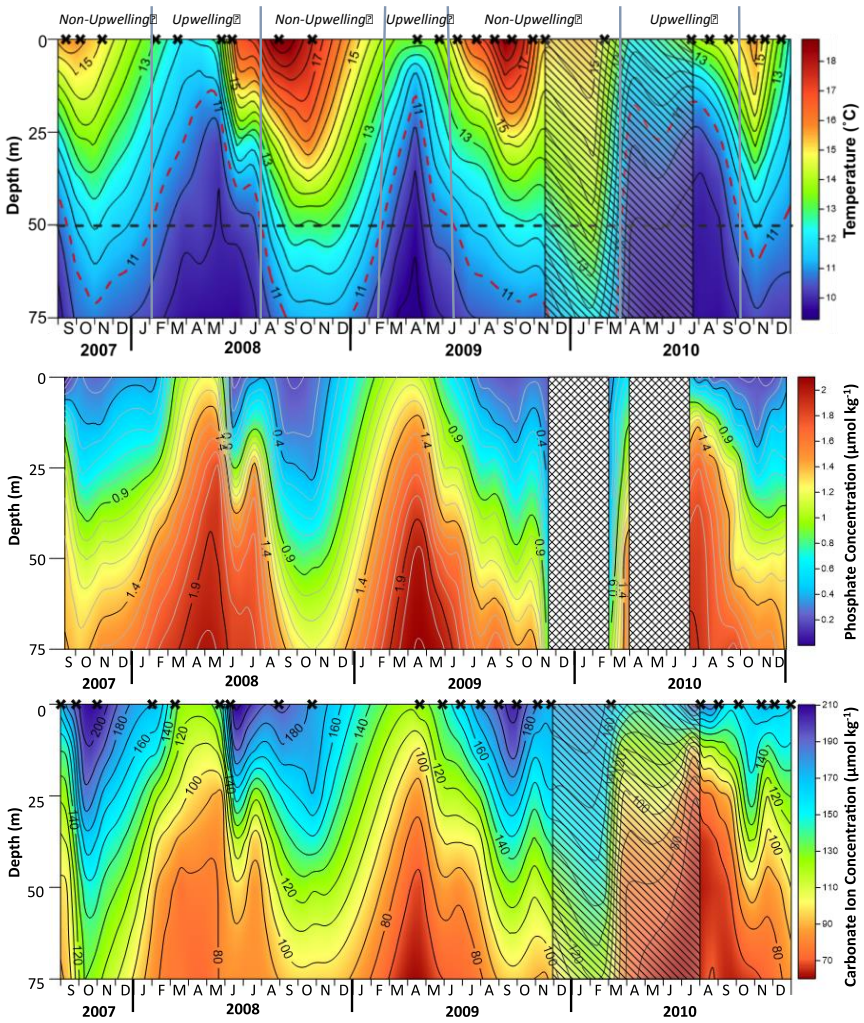


**Figure A.1** Temperature (upper), [$PO_4^{3-}$] (middle) and [$CO_3^{2-}$] (bottom) contour plots from 0-75 meters water depth measured by CTD and from water samples collected by Niskin-bottles for the duration of the study period. Contour plots interpolate 7 water column measurements (0, 5, 10, 20, 30, 50, 75 m) that were generally collected at montly resolution (sampling indicated by X on upper x-axis). Periods of upwelling and non-upwelling are defined by the shoaling of the 11˚C isotherm above 50 meters water depth. Cross-hatched periods represent gaps in sampling that resulted in poor data interpolation for contouring. All data shown here were collected from the Plumes and Blooms Program Station 4 (34˚15.01N, 119˚54.38W) located adjacent to the SBB sediment trap mooring. (Data from: http://www.oceancolor.ucsb.edu/plumes_and_blooms/). *In situ* measurements from the SBB sea surface indicate that temperatures range from 12-19.5 ˚C, total dissolved phosphate concentrations ([$PO_4^{3-}$]) range from 0.13-1.06 µmol $kg^{-1}$, and [$CO_3^{2-}$] ranges from 125-210 µmol $kg^{-1}$ from 2007-2010 when the sediment trap samples used in this study were collected.

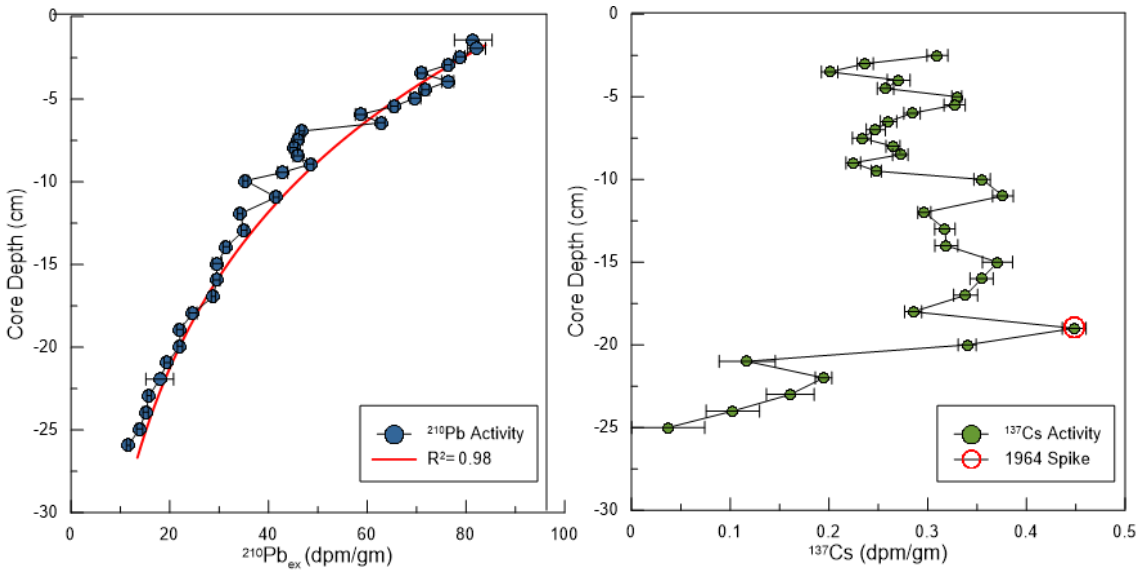


**Figure A.2** The left panel shows the box-core radioisotope counts of $^{210}Pb_{ex}$ relative to core depth. The exponential decay of that $^{210}Pb$ recorded in the upper 30 cm of the core was used to determine a mean sedimentation rate (0.43 cm $yr^{-1}$) for the core. The right panel shows the activities of $^{137}Cs$ with core depth. A notable increase in $^{137}Cs$ observed at 19 cm is used as a even tie point to the year 1964, which represents the peak in atmospheric nuclear bomb testing.

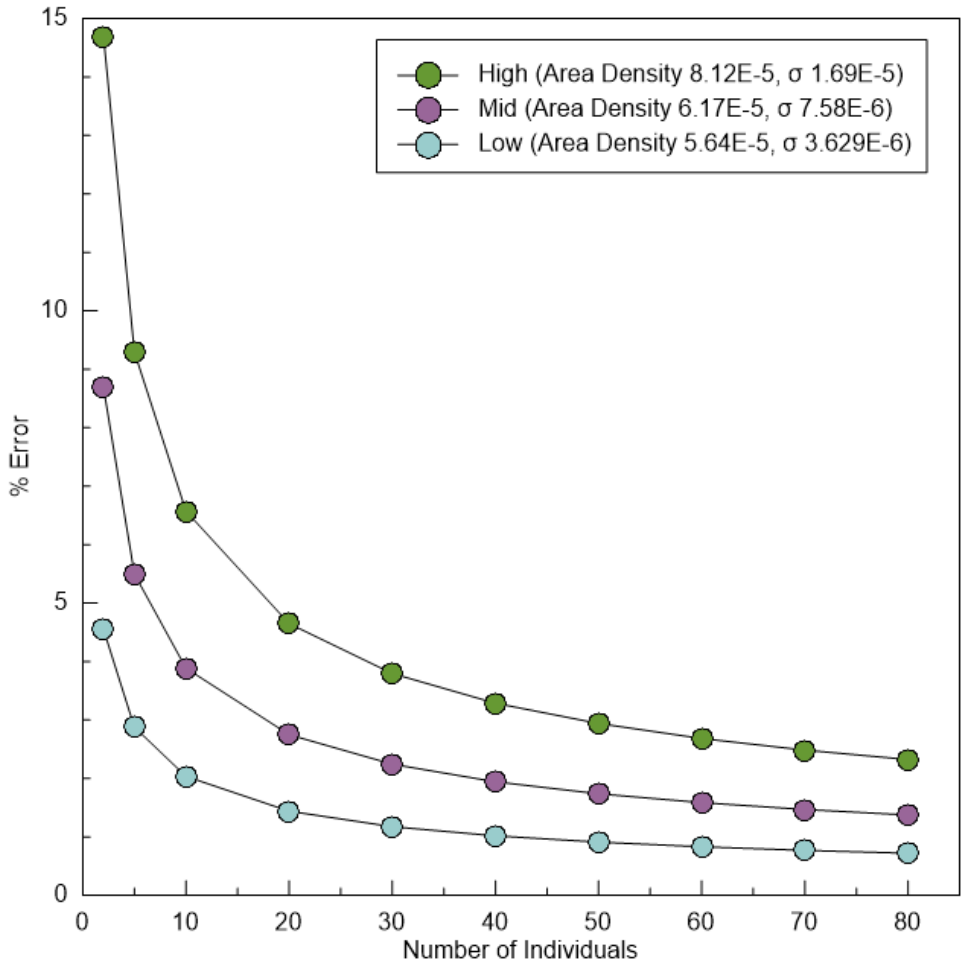


**Figure A.3** The percent error as a function of the number of individuals used to generate a mean area density value. We use actual data from three sediment trap samples that represent a range of area density and standard deviations therefore representing the maximum and minimun range in percent errors associated with our area density measurements. From this test we would suggest that a pool of 30-40 individuals represents a high degree of confidence when using a mean area density value to represent the population mean.

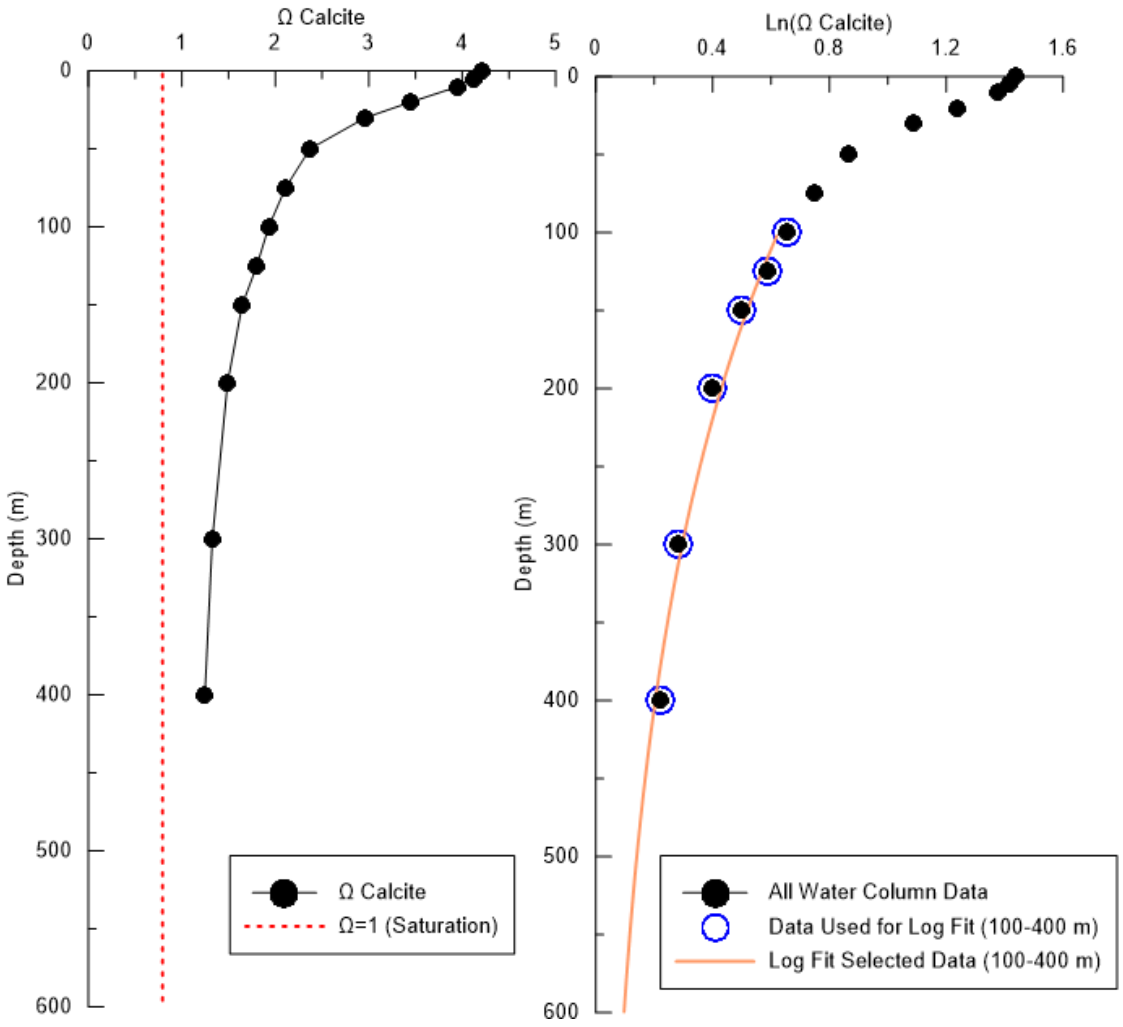


**Figure A.4** We use TA and DIC measurements from the SBB to estimate a mean calcite saturation profile for the SBB using the CO2Sys program. Water column measurements are limited to surface to 400 meters water depth and therefore do not provide information about bottom water saturation. Due to the exponential decline in saturation state that occurs through the water column, we use the natural log of these data and a log fit of the 100-400 meter water depth measurements to project the decline in saturation state below 400 meters. This projection indicates that based on mean conditions within the basin, bottom waters at 600 meters are still supersaturated with respect to calcite in the SBB.

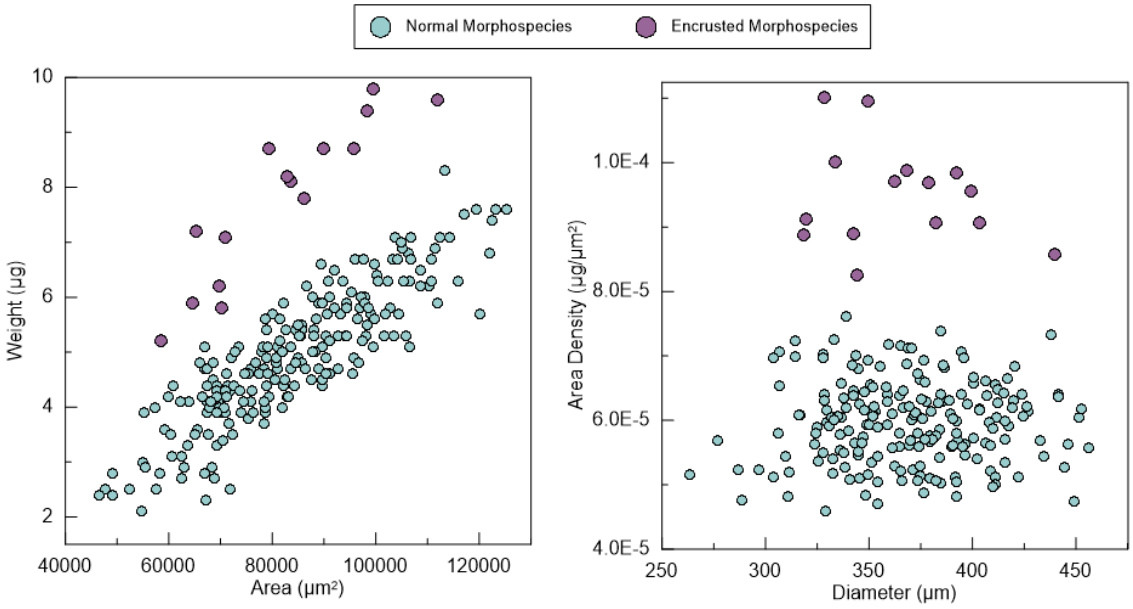


**Figure A.5** A comparison of individual *G. bulloides* morphometric measurements from six consecutive sediment trap samples (*n* =214 individual measurements) that were included in the sediment trap calibration. A total of 15 encrusted individuals were identified from this pool of individuals based on distinct offsets in their morphometric characteristics.

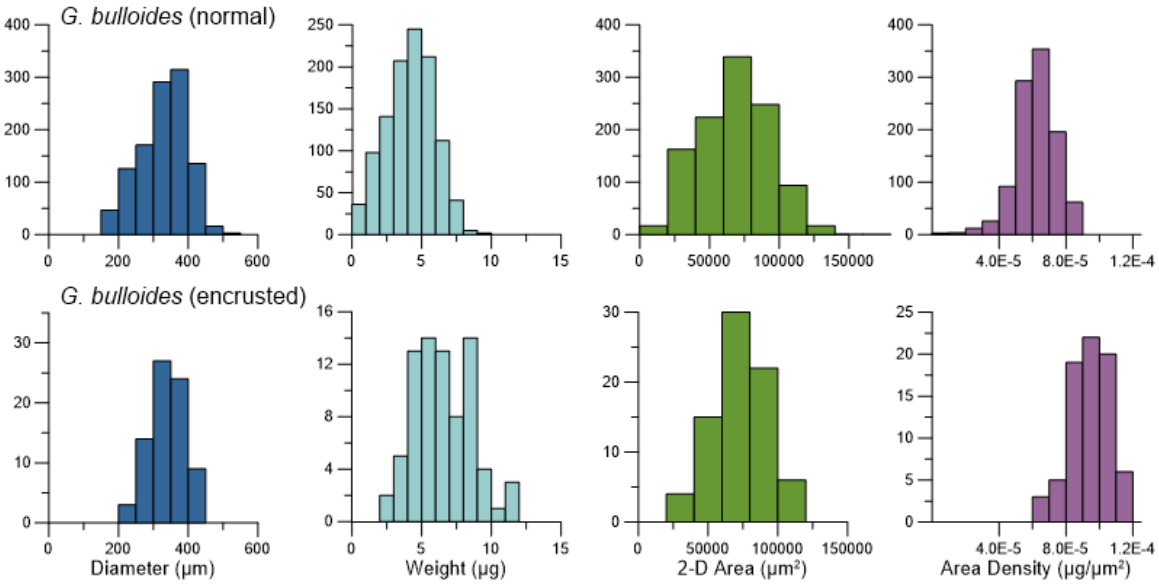


**Figure A.6** Histograms of individual shell diameter, weight, 2-D area and area density measurements of individual normal (upper panels) and encrusted (lower panels) *G. bulloides*. Histograms indicate that the most diagnostic morphologic characteristic to distinguish between the normal and encrusted *G. bulloides* morphospecies is shell area density.

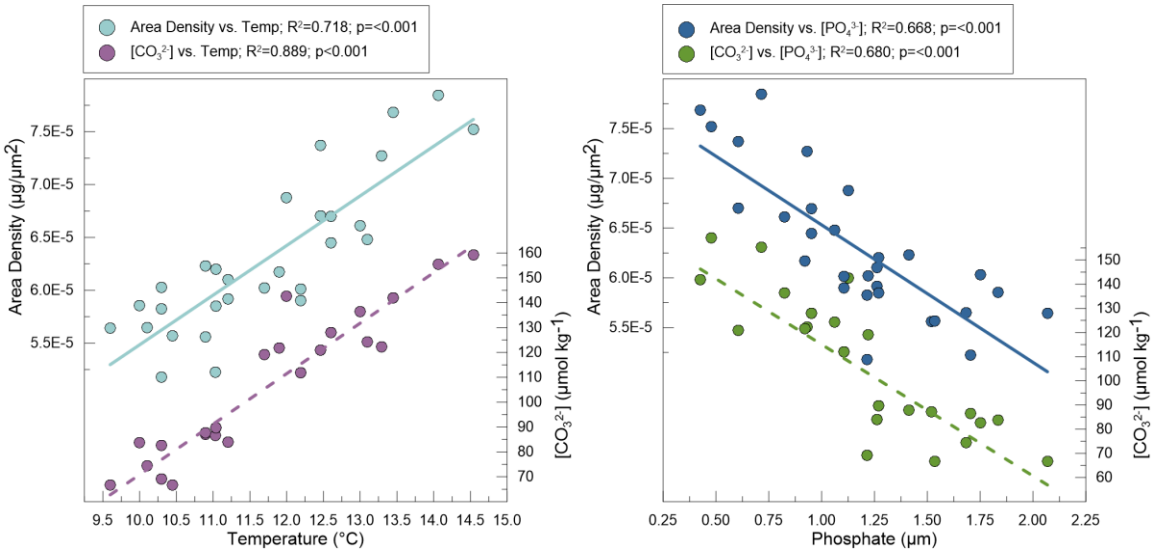


**Figure A.7** Regressions of measured temperature and $[PO_4^{3-}]$ as independent variables showing significant linear relationships with both normal *G. bulloides area* density and measured $[CO_3^{2-}]$ indicating bivariate relationships between the *in situ* predictor variables used in this study. Temperature and $[CO_3^{2-}]$ are positively correlated with area density while phosphate and $[CO_3^{2-}]$ are negatively correlated with area density.

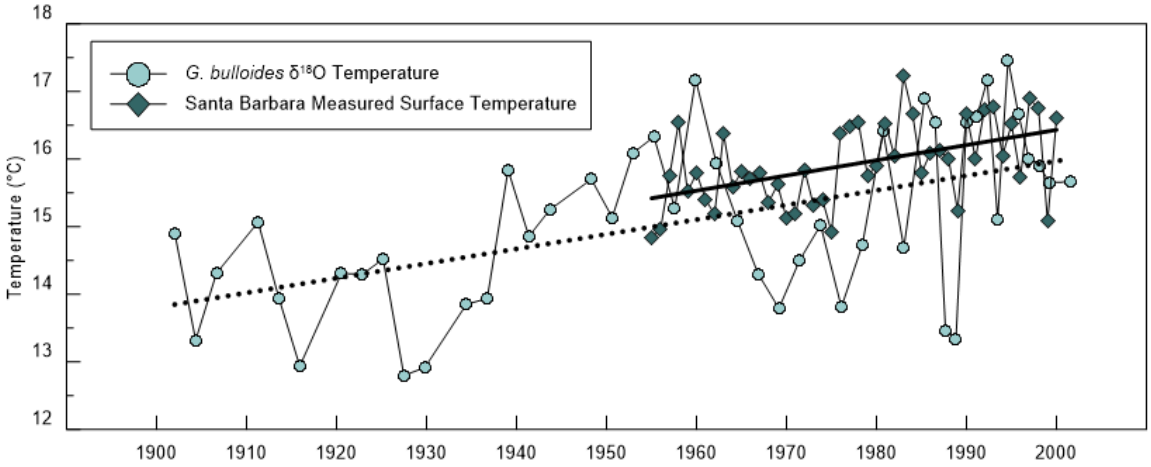


**Figure A.8** Comparison of measured sea surface temperature from the SBB (1955-2000) to temperatures derived from *G. bulloides* $\delta^{18}O$ measurements. The long-term trends of each temperature record are plotted and indicate similar declining trends although surface *in situ* temperatures are warmer than *G. bulloides* derived temperatures. This is likely due to the fact that the temperature relationship used to convert $\delta^{18}O$ to temperature is a culture derived relationship therefore the $\delta^{18}O$ temperatures estimated here represent the calcification, and therefore subsurface, temperature recorded by *G. bulloides.*

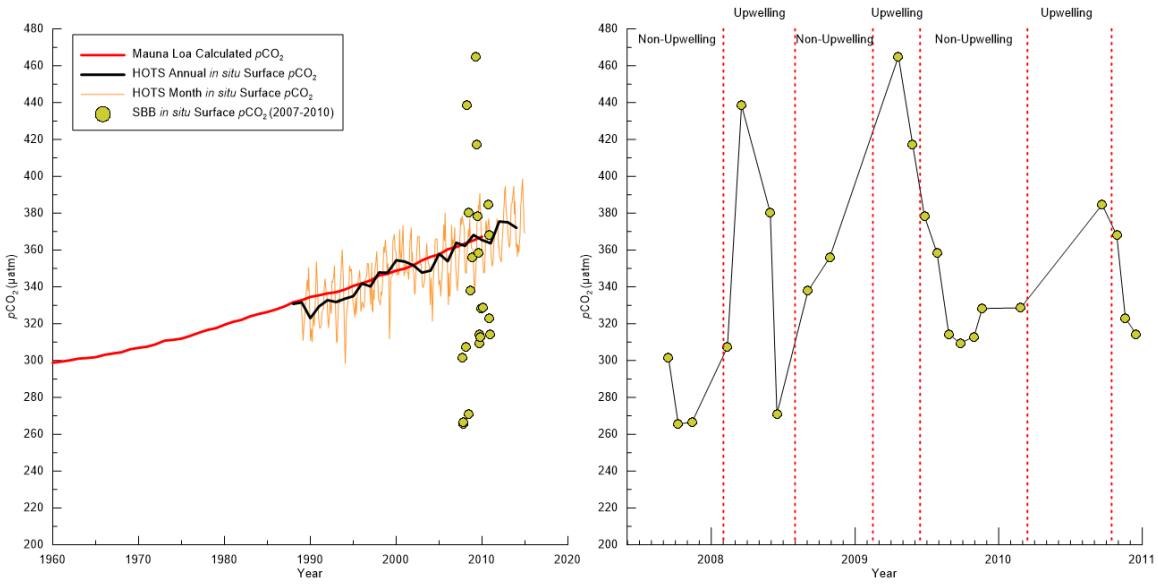


**Figure A.9** The left panel figure compares $pCO_2$ estimates calculated in this study compared to the monthly and annual means of measured surface $pCO_2$ from HOT (1988-Present) and monthly values from the SBB (2007-2010). The right panel illustrates the seasonal shifts in surface ocean $pCO_2$ in the SBB that shifts dramatically in response to upwelling. During periods of non-upwelling $pCO_2$ is lower than atmospheric values while upwelling $pCO_2$ is higher than atmospheric $CO_2$. This variability cannot be captured using mean annual temperature and salinity values for the basin although calculated $pCO_2$ represents integration over the seasonal cycle.

**Table A.1** Simple linear regression results for all of the independent variables examined in this study

Y=a+b(X)

| Y | X | a | b | $R^2$ | F | *p* |
|---|---|---|---|---|---|---|
| Area Density | $[CO_3^{2-}]$ | 4.19E-5 | 1.92E-7 | 0.80 | 121.41 | <0.001 |
| Temperature | $[CO_3^{2-}]$ | 7.57 | 0.04 | 0.86 | 186.85 | <0.001 |
| $[PO_4^{3-}]$ | $[CO_3^{2-}]$ | 2.33 | -0.01 | 0.65 | 55.36 | <0.001 |
| Area Density | Temperature | 1.26E-5 | 4.24E-6 | 0.70 | 69.17 | <0.001 |
| $[CO_3^{2-}]$ | Temperature | -151.50 | 21.95 | 0.86 | 186.85 | <0.001 |
| $[PO_4^{3-}]$ | Temperature | 4.53 | -0.29 | 0.79 | 110.99 | <0.001 |
| Area Density | $[PO_4^{3-}]$ | 7.57E-5 | -1.16E-5 | 0.54 | 35.57 | <0.001 |
| $[CO_3^{2-}]$ | $[PO_4^{3-}]$ | 174.72 | -58.95 | 0.65 | 55.36 | <0.001 |
| Temperature | $[PO_4^{3-}]$ | 14.93 | -2.75 | 0.79 | 110.99 | <0.001 |

.

**Table A.2** Tolerance and VIF values between predictor variables and residual variables.

**Collinearity Statistics**

$Y=a+b_1(X_1)+b_2(X_2)+b_3(X_3)$

| **Y** | **$X_1$** | **$X_2$** | **$X_3$** | **Tolerance $X_1$** | **Tolerance $X_2$** | **Tolerance $X_3$** | **VIF $X_1$** | **VIF $X_2$** | **VIF $X_3$** |
|---|---|---|---|---|---|---|---|---|---|
| Area Density | $[CO_3^{2-}]$ | Temperature | $[PO_4^{3-}]$ | 0.14 | 0.08 | 0.21 | 7.31 | 12.08 | 4.75 |
| Area Density | $[CO_3^{2-}]$ | Temp (*Cres*) | $[PO_4^{3-}]$ (*Cres*) | 0.90 | 0.56 | 0.604 | 1.11 | 1.80 | 1.66 |

**Table A.3** Results from MLR quantifying the redundancy between predictor variables.

**MLR Statistics**

$Y=a+b_1(X_1)+b_2(X_2)$

| **Y** | **$X_1$** | **$X_2$** | ***$R^2$*** | ***p*** |
|---|---|---|---|---|
| Temperature | $[CO_3^{2-}]$ | mean area | 0.86 | <0.001 |
| $[PO_4^{3-}]$ | $[CO_3^{2-}]$ | mean area | 0.65 | <0.001 |
| $[CO_3^{2-}]$ | Temperature | mean area | 0.86 | <0.001 |
| $[CO_3^{2-}]$ | $[PO_4^{3-}]$ | mean area | 0.65 | <0.001 |

**Table A.4** Results from four hierarchical regression models that were used to evaluate the significance of each predictor variable on area density ("ns" indicates a non significant *p* value).

**Hierarchical Regression Models**

$$Y = a + b1(X1) + b2(X2) + b3(X3)$$

| | | | | | | | | | Beta | | |
|---|---|---|---|---|---|---|---|---|---|---|---|
| | **Y** | **X1** | **X2** | **X3** | $R^2$ | $\Delta R^2$ | **F**Δ | $p\ \Delta R^2$ | **Beta 1** | **Beta 2** | **Beta 3** |
| Model 1 | Area Density | $[CO_3^{2-}]$ | | | 0.80 | 0.80 | 121.41 | <0.001 | 0.90 | | |
| | | $[CO_3^{2-}]$ | Temp (*Cres*) | | 0.80 | 0.00 | 0.02 | 0.90 (ns) | 0.90 | 0.01 | |
| | | $[CO_3^{2-}]$ | Temp (*Cres*) | $[PO_4^{3-}]$ (*Cres*) | 0.80 | 0.00 | 0.09 | 0.77 (ns) | 0.90 | -0.01 | -0.01 |
| Model 2 | Area Density | Temperature | | | 0.70 | 0.70 | 69.17 | <0.001 | 0.84 | | |
| | | Temperature | $[CO_3^{2-}]$ (*Tres*) | | 0.80 | 0.10 | 115.22 | 0.001 | 0.77 | 0.33 | |
| | | Temperature | $[CO_3^{2-}]$ (*Tres*) | $[PO_4^{3-}]$ (*Tres*) | 0.80 | 0.00 | 0.06 | 0.81 (ns) | 0.77 | 0.33 | -0.02 |
| Model 3 | Area Density | $[PO_4^{3-}]$ | | | 0.54 | 0.54 | 35.57 | <0.001 | -0.74 | | |
| | | $[PO_4^{3-}]$ | $[CO_3^{2-}]$ (*Pres*) | | 0.80 | 0.26 | 38.19 | <0.001 | -0.68 | 0.51 | |
| | | $[PO_4^{3-}]$ | $[CO_3^{2-}]$ (*Pres*) | Temp (*Pres*) | 0.80 | 0.00 | 0.01 | 0.94 (ns) | -0.68 | 0.52 | -0.01 |
| Model 4 | Area Density | $[PO_4^{3-}]$ | | | 0.54 | 0.54 | 35.57 | <0.001 | -0.74 | | |
| | | $[PO_4^{3-}]$ | Temp (*Pres*) | | 0.70 | 0.16 | 14.86 | 0.001 | -0.73 | 0.39 | |
| | | $[PO_4^{3-}]$ | Temp (*Pres*) | $[CO_3^{2-}]$ (*Pres*) | 0.80 | 0.11 | 14.90 | 0.001 | -0.68 | -0.01 | 0.52 |

# APPENDIX B –COPYRIGHT PERMISSIONS FOR CHAPTER 1

**JOHN WILEY AND SONS LICENSE TERMS AND CONDITIONS**

Nov 09, 2016

This Agreement between Emily B Osborne ("You") and John Wiley and Sons ("John Wiley and Sons") consists of your license details and the terms and conditions provided by John Wiley and Sons and Copyright Clearance Center.

| | |
|---|---|
| License Number | 3985030238690 |
| License date | Nov 09, 2016 |
| Licensed Content Publisher | John Wiley and Sons |
| Licensed Content Publication | Paleoceanography |
| Licensed Content Title | Calcification of the planktonic foraminifera Globigerina bulloides and carbonate ion concentration: Results from the Santa Barbara Basin |
| Licensed Content Author | Emily B. Osborne,Robert C. Thunell,Brittney J. Marshall,Jessica A. Holm,Eric J. Tappa,Claudia Benitez-Nelson,Wei-Jun Cai,Baoshan Chen |
| Licensed Content Date | Aug 17, 2016 |
| Licensed Content Pages | 20 |
| Type of use | Dissertation/Thesis |
| Requestor type | Author of this Wiley article |
| Format | Electronic |
| Portion | Full article |
| Will you be translating? | No |
| Title of your thesis / dissertation | Development and Application of Foraminiferal Carbonate System Proxies to Quantify Ocean Acidification in the California Current |
| Expected completion date | Nov 2016 |